

Functional characterisation of microtubule polyglutamylases in

Trypanosoma brucei

Dissertation

zur Erlangung des akademischen Grades

einer Doktorin der Naturwissenschaften (Dr. rer. nat.)

in der Bayreuther Graduiertenschule für Mathematik und Naturwissenschaften (BayNAT)

der Universität Bayreuth

vorgelegt von **Jana Ritschar (geb. Jentsch)**

geboren in Heidelberg

Bayreuth 2022

Die vorliegende Arbeit wurde von November 2018 bis November 2022 in Bayreuth am Lehrstuhl Genetik in der Arbeitsgruppe molekulare Parasitologie unter Betreuung von Herrn Prof. Dr. Klaus Ersfeld angefertigt.

Vollständiger Abdruck der von der Bayreuther Graduiertenschule für Mathematik und Naturwissenschaften (BayNAT) der Universität Bayreuth genehmigten Dissertation zur Erlangung des akademischen Grades einer Doktorin der Naturwissenschaften (Dr. rer. nat.).

Dissertation eingereicht am: 10.11.2022

Zulassung durch das Leitungsgremium: 22.11.2022

Wissenschaftliches Kolloquium: 20.04.2023

Amtierender Direktor: Prof. Dr. Hans Keppler

Prüfungsausschuss:

Prof. Dr. Klaus Ersfeld (Gutachter)

Prof. Dr. Stefan Geimer (Gutachter/in)

Prof. Dr. Matthias Weiss (Vorsitz)

Prof. Dr. Stefan Heidmann

Die vorliegende Arbeit ist als Monographie verfasst.

Teile der Arbeit sind bereits in der folgenden Publikation erschienen:

Microtubule polyglutamylation is important for regulating cytoskeletal architecture in *Trypanosoma brucei*.

Jentzsch, J., Sabri, A., Speckner, K., Lallinger-Kube, G., Weiss, M., Ersfeld, K., Journal of Cell Science 133 (2020)

DOI:10.1242/jcs.248047

This article has an associated first-person interview with the first author of the paper.

Diese Publikation ist in der vorliegenden Arbeit im Literaturverzeichnis gelistet.

Meinem Papa
Dr. med. Hans-Martin Jentsch

Table of contents

Abbreviations	1
Summary	3
Zusammenfassung.....	4
Introduction.....	5
<i>Trypanosoma brucei and Trypanosomiasis.....</i>	<i>5</i>
<i>The life cycle of T. brucei.....</i>	<i>7</i>
<i>Cell biology of procyclic T. brucei</i>	<i>8</i>
<i>Cell division</i>	<i>11</i>
<i>Tubulin, microtubules and microtubule associated proteins</i>	<i>13</i>
<i>Polyglutamylation.....</i>	<i>18</i>
<i>Aims of the thesis.....</i>	<i>21</i>
Results.....	22
<i>Various TTLLs show in vivo glutamylation activity.....</i>	<i>22</i>
<i>Characterisation of TTLL6A and TTLL12B.....</i>	<i>23</i>
TTLL6A and TTLL12B have in vivo glutamylation activity and are important for the cellular architecture.....	23
TTLL6A or TTLL12B knockdown causes cytokinesis defects.....	27
Increase of newly synthesized microtubules after the depletion of TTLL6A or TTLL12B	28
Impaired binding of microtubule-associated proteins after the depletion of TTLL6A or TTLL12B.....	29
TTLL6A and TTLL12B have glutamylation activity within the flagellum	31
Depletion of TTLL6A or TTLL12B result in motility defects	33
<i>Characterisation of the putative polyglutamylase TTLL1.....</i>	<i>37</i>
TTLL1 has glutamylation activity.....	37
A knockout of <i>ttl1</i> results in abnormal morphology and cytokinesis defects.....	39
Visualisation of newly polymerized microtubules after TTLL1 depletion	43
Binding of MAPs after <i>ttl1</i> knockout.....	43
Effects of a <i>ttl1</i> knockout on the flagellum	45
Add back of TTLL1 leads to a rescue of the knockout.....	49
Overexpression of TTLL1.....	50
Swim velocity of <i>ttl1</i> ^{-/-} and TTLL1-overexpressing cells	53
Discussion.....	54

Materials and methods	64
<i>Materials</i>	64
Hard- and software	64
Chemicals, reagents and kits.....	64
Antibodies.....	65
DNA oligonucleotides	67
Plasmids	69
<i>Microbiological techniques</i>	71
<i>E. coli</i> strains and media	71
Transformation of Plasmid DNA in <i>E. coli</i>	71
<i>Molecular biological methods</i>	71
Polymerase chain reaction.....	71
Isolation of plasmid DNA from <i>E. coli</i>	71
Determination of DNA and RNA concentration	72
Restriction hydrolysis of DNA	72
Separation of DNA fragments by agarose gel electrophoresis	73
Ligation of DNA fragments.....	73
Isolation of RNA	73
Revers transcription of RNA in cDNA	74
Quantitative real time PCR (qPCR).....	74
<i>Protein biochemical methods</i>	75
Denaturing sodium dodecyl sulfate polyacrylamide gel electrophoresis (SDS-PAGE)....	75
Methanol-chloroform precipitation of protein samples.....	76
Immunoblot	77
Microscopy.....	78
Immunofluorescence	78
Ultrastructural expansion microscopy (U-ExM).....	79
Electron microscopy	79
Isolation of flagella from <i>T. brucei</i>	80
<i>Cell biological methods</i>	80
<i>T. brucei</i> cell lines, cultivation and storage	80
Transfection of <i>T. brucei</i>	81
Generation of gene knockout cell lines	82
RNA interference in <i>T. brucei</i>	83
Ectopic expression in <i>T. brucei</i>	85
Growth curves.....	85
Flow cytometry analysis.....	86
Motility analysis of <i>T. brucei</i>	86
<i>Quantification of western blot signal and fluorescence intensities</i>	86
<i>Statistics</i>	87
<i>Editing of images</i>	87
References	88

List of all own publications.....	103
Supplementary figures.....	104
Publication and Licensing Rights for created Figures.....	107
Acknowledgments	115
(Eidesstattliche) Versicherungen und Erklärungen	116

Abbreviations

AIR9	auxin-Induced in Root cultures 9
apoA-I	apolipoprotein A-I
APS	ammonium persulfate
BARP	brucei proline-rich protein
CAP	cytoskeleton associated protein
CCP	cytosolic carboxypeptidase
DAPI	4',6'-diamidino-2-phenylindole
EB1	end binding protein 1
FAZ	flagellum attachment zone
FCS	foetal calf serum
GDP	guanosine-diphosphate
GTP	guanosine-triphosphate
HAT	human African trypanosomiasis
Hpr	haptoglobin-related protein
TbHpHbR	trypanosome haptoglobin (Hp)-Hb receptor
IF	immunofluorescence
Ig	immunglobulin
IPTG	Isopropyl β -D-1-thiogalactopyranoside
MAP	microtubule associated protein
MATCAP	microtubule associated tyrosine carboxypeptidase
MtQ	microtubule quartet
PCR	polymerase chain reaction
PFR	paraflagellar rod
PTM	posttranslational modification
RNAi	RNA interference
SDM	semi-defined-medium
SDS-PAGE	sodium dodecyl sulphate polyacrylamide gel electrophoresis
SMT	subpellicular microtubule
spp.	species
SRA	serum-resistant protein

TAC	tripartite attachment complex
Tb	<i>Trypanosoma brucei</i>
<i>T. brucei</i>	<i>Trypanosoma brucei</i>
TEM	transmission electron microscopy
+TIP	microtubule plus end tracking protein
TTL	tubulin tyrosine ligase
TTL	tubulin tyrosine ligase like protein
TLF	trypanosome lytic factor
U-ExM	ultrastructural expansion microscopy
VASH	vasohibin
VSG	variable surface glycoprotein
WB	western blot
WHO	world health organisation
wks	weeks
XMAP215	<i>Xenopus</i> microtubule associated protein 215

Summary

The shape of kinetoplastids such as *Trypanosoma brucei* is defined by a remarkably stable microtubule-cytoskeleton and is precisely determined during the life cycle stages. This stability has to give room for dynamic properties to allow cell division and morphological rearrangements. How these opposite demands on the cytoskeleton are regulated is poorly understood. One way to alter microtubule properties is via posttranslational modifications (PTMs) of microtubules. Many of these PTMs are present at the C-terminal tails of α - and β -tubulin, such as glutamylation. Defects of enzymes that catalyse the accumulation of glutamate side chains have been shown to lead to ciliopathies and neurodegeneration. *T. brucei* represents a simplified system to study the molecular effects of glutamylation on microtubule-structures like the cytoskeleton and axoneme. This work demonstrated the *in vivo* activity of three *T. brucei* polyglutamylases (TTLL6A, TTLL12B and TTLL1) and their importance to maintain a balance of the glutamylation level. A depletion of the polyglutamylases or the overexpression of TTLL1 resulted in a decreased or increased glutamylation signal and caused the disruption of the cell architecture as well as an aberrant motility. Additionally, it was shown, that the depletion of either enzyme caused a failed localisation of the cytoskeletal-associated proteins EB1, XMAP215 and TbAIR9. Based on the characterisation of these three polyglutamylases this study provides insights that glutamylation is a key regulator in the maintenance of cellular integrity.

Zusammenfassung

Die Form von Kinetoplastiden wie *Trypanosoma brucei* wird durch ein bemerkenswert stabiles Mikrotubuli-Zytoskelett bestimmt und während der Lebenszyklusphasen genau festgelegt. Diese Stabilität muss jedoch auch dynamische Eigenschaften aufweisen, um Zellteilung und morphologische Veränderungen zu ermöglichen. Wie diese gegensätzlichen Anforderungen an das Zytoskelett reguliert werden, ist nicht bekannt. Eine Möglichkeit, die Eigenschaften der Mikrotubuli zu verändern, ist durch posttranslationale Modifikationen (PTM). Viele dieser PTMs befinden sich an den C-terminalen Schwänzen von α - und β -Tubulin, wie etwa die Glutamylierung. Ein Defekt von Enzymen, die das Anhängen von Glutamatseitenketten katalysieren, führt zu Ciliopathien und Neurodegeneration. *T. brucei* stellt ein vereinfachtes System dar, um die molekularen Auswirkungen der Glutamylierung auf Mikrotubuli-Strukturen wie das Zytoskelett und Axoneme zu untersuchen. In dieser Arbeit wurde die in-vivo Aktivität von drei *T. brucei* Polyglutamylasen (TTLL6A, TTLL12B und TTLL1) und ihre Bedeutung für die Aufrechterhaltung des Gleichgewichts des Glutamylierungslevels nachgewiesen. Die Depletion der Polyglutamylasen und die Überexpression von TTLL1 führte zu einem Anstieg oder zu einer Verminderung des Glutamylierungssignals und hatte eine veränderte Zellarchitektur sowie eine gestörte Zellmotilität zur Folge. Darüber hinaus konnte gezeigt werden, dass die Depletion der Enzyme zu einer fehlerhaften Lokalisierung der zytoskelett-assoziierten Proteine EB1, XMAP215 und TbAIR9 führt. Basierend auf der Charakterisierung dieser drei Polyglutamylasen liefert diese Studie Erkenntnisse darüber, dass die Glutamylierung ein wichtiger Regulator bei der Aufrechterhaltung der zellulären Integrität ist.

Introduction

Trypanosoma brucei and Trypanosomiasis

African trypanosomes are the causative agent of the "Human African trypanosomiasis (HAT)". It is a fatal nervous disease whose final stage in humans is called "sleeping sickness"(Brun *et al.*, 2010), due to the occurrence of daytime sleepiness. Those infected often die of heart failure and central nervous disorders (Brun *et al.*, 2010).

The disease is widespread in sub-Saharan Africa wherever the tsetse fly (*Glossina* spp.) is present, because the parasite is transmitted by this blood-feeding arthropode. The clinical pictures differ depending on the infection with different sub-species. An infection with *Trypanosoma brucei gambiense* is responsible for the chronic form of sleeping sickness in West and Central Africa, while *T. brucei rhodesiense* causes the acute form of the disease in East and Central Africa (Odiit, Kansime and Enyaru, 1997; Pepin and Meda, 2001). If left untreated, patients infected with *T. brucei rhodesiense* die within several months, and those infected with *T. brucei gambiense* can be carriers for years, before reaching the lethal stage (Kennedy, 2013). The infection with *T. brucei gambiense* accounts for more than 95 % of the reported cases (Kennedy and Rodgers, 2019)

At the beginning of the 20th century, there were three severe epidemics of sleeping sickness. The first epidemic (1896-1906) killed an estimated 800,000 people (Brun *et al.*, 2010). The catastrophic health and economic impact of the epidemic were so disturbing that strategies were developed to combat the disease and limit subsequent epidemics. Its spread was tracked due to mobile teams and drugs for treatment were developed. However, the diagnosis and the treatment of the disease are complex and require specifically trained staff. Another approach that contributed to a significant reduction in the incidence of infection was the control of the vector, the tsetse fly. The spread of the fly could be reduced by insect traps and by destroying host reservoirs because wild and domestic animals play an important role as parasite reservoirs for human infections with trypanosomes (Brun *et al.*, 2010; Rotureau and Van Den Abbeele, 2013).

In 2009 the number of cases dropped below 10.000 for the first time in 50 years. In 2019 and 2020 only several hundred cases were reported. More and more countries are reporting the elimination of the disease as a public health problem, so that the WHO targeted the

interruption of transmission by 2030 (mondiale de la Santé and World Health Organization, 2021).

Although HAT is now very well controlled, the animal trypanosomiasis “Nagana” (a Zulu expression for “being in low spirit”) is still a problem (Venturelli *et al.*, 2022; <https://www.fao.org/3/ca3887en/ca3887en.pdf>, accessed on 06. November 2022). It is caused by *T. brucei brucei*, *T. brucei congolense* and *T. brucei vivax*, and leads to a drastic decline in livestock. This has a significant impact on the gross domestic product of countries, as African economies are dependent on their agriculture and especially on their livestock (Kargbo *et al.*, 2022).

T. brucei brucei is not human pathogenic, due to the resistance factors TLF1 and TLF2 (trypanosome lytic factors). TLF1 is a high-density lipoprotein that includes apolipoprotein A-I (apoA-I) and haptoglobin-related protein (Hpr). TLF2 is low in lipids and contains immunoglobulin M, apoA-I, and Hpr (Raper *et al.*, 1999). Both TLFs appear to lyse trypanosomes by the same mechanism.

For TLF1, an uptake process could be characterised. In the host bloodstream, hemoglobin (Hb) binds to Hpr and thus to TLF1. This complex binds to the trypanosome haptoglobin (Hp)-Hb receptor (TbHpHbR), whose initial role is to ensure heme uptake via the flagellar pocket for optimal parasite growth (Vanhollebeke *et al.*, 2008). Thus, TLF1 is taken up into the cell in a receptor-mediated manner, and lysis is initiated. While Hpr is involved as a TLF ligand, the lytic activity is due to the pore-forming protein apoA-I (Vanhollebeke and Pays, 2010). It is still unclear whether TLF2 will be taken up via a similar process.

T. brucei gambiense has evolved several mechanisms to escape the lysis of TLFs. First, it reduces the binding of TLF to the TbHpHbR by regulating the mRNA level, and second, this parasite subspecies can make the membrane tolerant to the lytic action of apoA-I by tightening the membrane through TbgGP (*T. brucei gambiense* glycoprotein) (DeJesus *et al.*, 2013; Uzureau *et al.*, 2013).

In contrast, *T. brucei rhodesiense* expresses a serum-resistant protein (SRA) that neutralizes apoA-I (Vanhamme *et al.*, 2003; Stephens and Hajduk, 2011).

Except for the expression of the SRA in *T. brucei rhodesiense*, these trypanosome subspecies are indistinguishable. For this reason, the non-human pathogenic strain *T. brucei brucei* is often used for basic research in laboratories.

The life cycle of *T. brucei*

During its complex life cycle, the parasite alternates between its vertebrate host and the tsetse fly (Figure 1). As an extracellular parasite, *T. brucei* survives in the hosts blood by immune evasion. The constant variation of the surface coat of VSGs (variant surface glycoproteins) protects the parasite from the elimination of the hosts immune response (McCulloch, 2004; Pays, Vanhamme and Pérez-Morga, 2004). This antigenic variation in *T. brucei* is mediated by monoallelic expression of the VSG gene in the active telomeric expression site, with only one of thousands of VSG genes being transcribed. VSG switching is achieved by switching to transcription of a different telomeric expression site or by replacing the VSG in the active expression site (López-Escobar *et al.*, 2022).

Driven by a density-dependent signal (quorum sensing), the slender bloodstream cells (Figure 1A) further develop into stumpy forms (Figure 1B) (Vassella *et al.*, 1997; Matthews, Ellis and Paterou, 2004; Schuster *et al.*, 2021). This change from proliferating slender forms to cell cycle arrested stumpy forms is associated with a series of biochemical and morphological changes (Tyler, Matthews and Gull, 1997; Vassella *et al.*, 1997).

After ingestion of stumpy forms by the blood meal of the tsetse fly, the VSG coat of the cells is replaced by procyclin (Figure 1C). The parasite adapts to the new environment and switches its metabolism from glycolysis to oxidative phosphorylation (Smith *et al.*, 2017). The procyclic trypanosomes, which multiply by binary division in the midgut of the mosquito, afterwards migrate to the salivary glands where they attach as epimastigote forms (Figure 1D).

To colonise the salivary glands, the cells undergo asymmetric division, producing one long and one short daughter epimastigote. Asymmetric division requires multiple coordinated changes in cell shape. Whereas the long daughter cell appears to die, the short epimastigote attach to the salivary gland epithel through an elaboration of the membrane of the flagellum (Tetley and Vickerman, 1985; Sharma *et al.*, 2009). Cells in this stage change their surface coat from procyclin to BARP (brucei alanine-rich proteins) (Fenn and Matthews, 2007; Urwyler *et al.*, 2007).

They further develop to non-proliferative metacyclic cells which are pre-adapted to the new host environment and develop a surface coat of VSGs (Figure 1E) (Vickerman, 1985; Rotureau *et al.*, 2012). After a release from the epithelium the cells are infective for the next host (Sharma *et al.*, 2009).

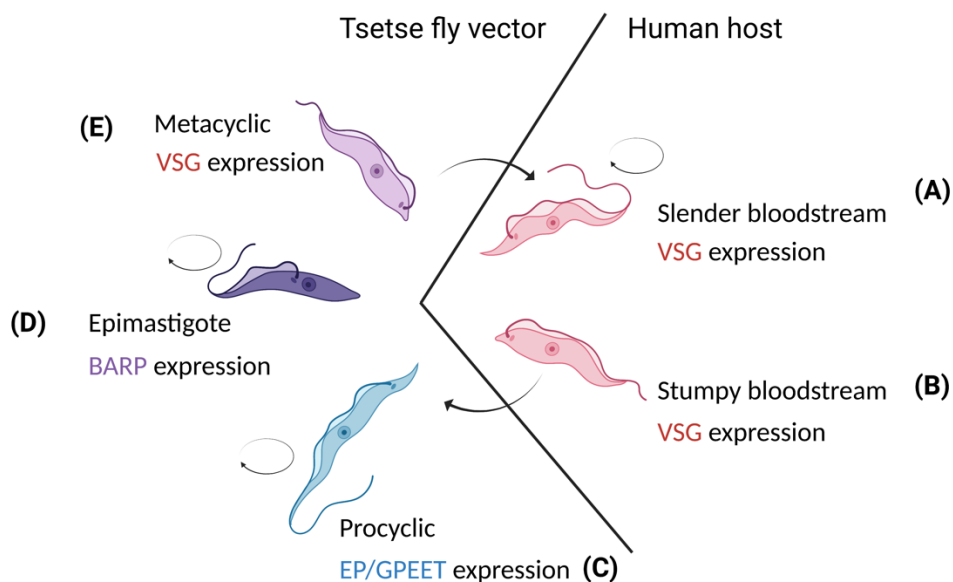


Figure 1: Life cycle of *Trypanosoma brucei*. (A) proliferative slender bloodstream form expressing VSG (variant surface glycoprotein) (B) non-proliferative stumpy bloodstream form expressing VSG (C) proliferative procyclic form expressing EP/GPEET (procyclin) (D) proliferative epimastigote form expressing BARP (brucei alanine-rich protein). (E) non-proliferative metacyclic form. Figure was created based on the inspiration after Schuster *et al.* (2021). Figure was created with BioRender.com.

Cell biology of procyclic *T. brucei*

Procyclic trypanosomes are elongated cells with a size of 15-30 μm . The cell shape is defined by a highly organised microtubule cytoskeleton.

Within the cytoskeleton, single-copy organelles are precisely positioned. They include the mitochondrion, the kinetoplast and nucleus, the flagellar pocket and the single flagellum arising from it (Figure 2) (Gull, 1999).

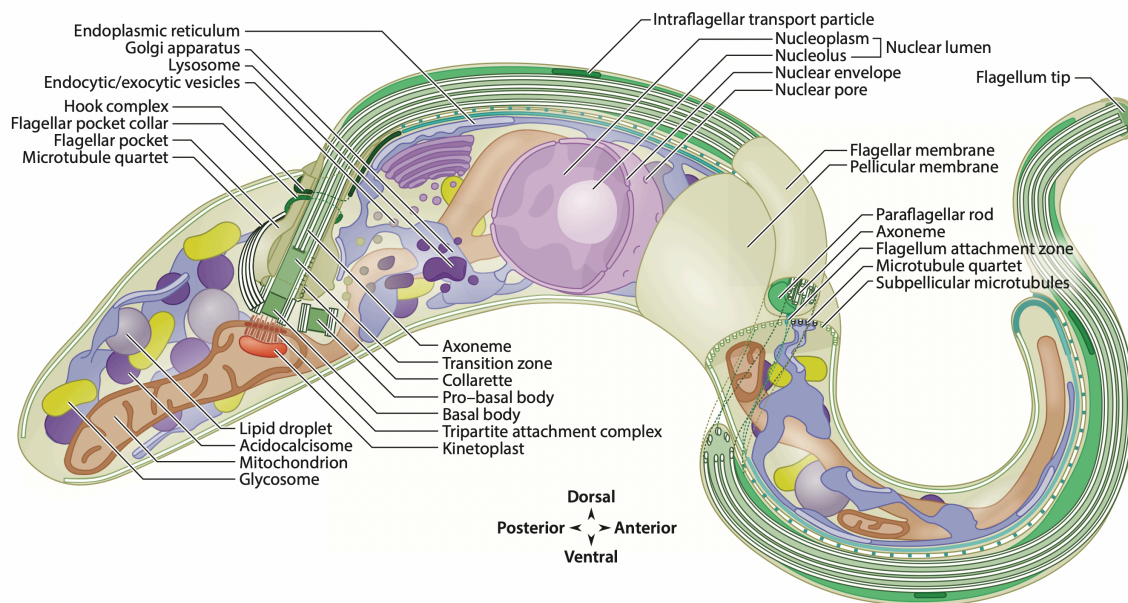


Figure 2: The morphology of an insect stage *T. brucei* cell (Wheeler, Gull and Sunter, 2019).

The mitochondrion of *T. brucei* is unusual among eukaryotes not only because it is formed as a single elongated tubular structure extending the entire length of the cell, but also because the mitochondrial genome is not distributed over this single mitochondrion. It exists as a separate physical structure, the "kinetoplast" (Shapiro and Englund, 1995). Containing thousands of concatenated minicircle DNAs and about 25 maxicircle DNAs it is located at the end of the single mitochondrion adjacent to the basal body of the flagellum (Ryan *et al.*, 1988; Robinson *et al.*, 1991). During the cell cycle, those organelles duplicate and segregate in a highly coordinated manner (McKean, 2003).

The flagellum is essential for the locomotion and viability of the parasite (Rotureau *et al.*, 2014). It is also responsible for the control of cell size and shape, polarity, and cell division, as the anterior end of the flagellum determines the positioning of the cleavage furrow for cytokinesis (Kohl, Robinson and Bastin, 2003). Originating at the posterior end of the cell, it emerges from the basal body. Via the flagellum attachment zone (FAZ, Figure 3) it is connected to the cell body, winds in a left-handed spiral along the cell and protrudes beyond the anterior cell tip (Figure 2). The FAZ includes a FAZ filament and the microtubule quartet (MtQ) which is associated with the endoplasmic reticulum (Figure 3) (Vaughan *et al.*, 2008). The flagellum consists of a canonical 9+2 microtubule axoneme, that contains nine doublet microtubules surrounding a pair of single microtubules in a highly organized manner. Associated with the

axoneme is the paraflagellar rod (PFR; Figure 3) (Ralston *et al.*, 2009). The PFR is a structure found in euglenoids that is indispensable for the parasites' motility and is possibly supporting the efficiency of the flagellar beat (Bastin, Sherwin and Gull, 1998).

The subpellicular cytoskeleton is essential to maintain the structure of the parasite. It consists of non-continuous microtubules that are highly ordered in a parallel manner and are located just below the cell membrane (SMT, Figure 3) (Seebeck *et al.*, 1988).

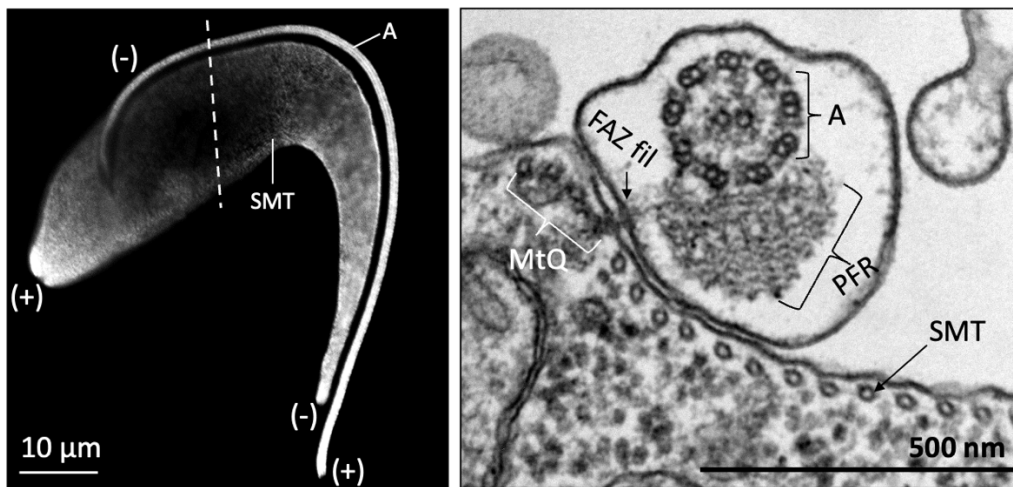


Figure 3: Electron micrograph of a cross-section through a *T. brucei* cell. Left: Expansion microscopy of a cell. Shown is a tubulin staining. Brackets show the polarity of microtubules. Dashed line indicate cross-section. Image was deconvoluted. Right: Transmission electron microscopy of a cross-section of a cell. Axoneme (A), subpellicular microtubules (SMT), paraflagellar rod (PFR), flagellum attachment zone (FAZ) consisting of the microtubule quartet (MtQ) and FAZ filament (FAZ fil). The electron micrograph was taken by Julia Bechthold, a master student under my guidance.

The microtubules of the subpellicular cytoskeleton have a uniform polarity and point with their plus-ends towards the posterior end of the cell (Robinson *et al.*, 1995). The flagellum and the MtQ, which are both emanating from the basal body, show their polarity in the opposite direction with their plus ends directed to the anterior end of the cell (Figure 3) (Robinson *et al.*, 1995). Approximately 100 microtubules are present in an array, whereby the number of microtubules depends on the width of the cell body and varies accordingly (Angelopoulos, 1970; Gull, 1999). The microtubules have a uniform spacing of 18-22 nm, with adjacent microtubules being interconnected by regularly spaced fibrils at intervals of 12-30 nm (Gull, 1999) and are cross-linked with the plasma membrane (Bramblett, Chang and Flavin, 1987; Hemphill, Lawson and Seebeck, 1991). Microtubules of trypanosomes appear to be

remarkably stable, which is very different from the dynamic instability of microtubules in mammalian cells. This is supported by the fact that the microtubules of the parasite are cold and detergent-resistant (Robinson *et al.*, 1991) and do not depolymerize under the influence of microtubule destabilizing drugs (Ploubidou *et al.*, 1999). Even during cell division, the cytoskeleton remains intact.

Cell division

As in other eukaryotes, the cell cycle of *T. brucei* is divided into the phases G1, S, G2 and M. Unique for the parasite is the additional separate cycle of the kinetoplast, which occurs simultaneously but is slightly shifted from that of the nucleus. During the G1 phase, the cell has one kinetoplast (K), one nucleus (N), and one flagellum. This stage is therefore termed 1K1N (Figure 4A) (Robinson *et al.*, 1995).

The S phases of the kinetoplast and nucleus begin synchronously, but the S phase of the kinetoplast is completed faster (Woodward and Gull, 1990). The initial morphological event occurs during the transition of the kinetoplast G1-S phase. First a new basal and pro-basal body and a new MtQ are formed (Lacomble *et al.*, 2010). As the pro-basal body grows, a new flagellum nucleates (Figure 4B) (Sherwin and Gull, 1989). Located in the same flagellar pocket, the newly growing flagellum binds with its distal tip to the old flagellum (Lacomble *et al.*, 2010). It is connected to the old flagellum via the flagellar connector until cytokinesis (Figure 4B-E) (Moreira-Leite *et al.*, 2001; Briggs *et al.*, 2004; Lacomble *et al.*, 2010). It was shown that at the early stages of flagellar growth, the now mature basal body rotates around the new flagellum in a counterclockwise direction (Lacomble *et al.*, 2010; Gluenz *et al.*, 2011). This leads to a repositioning of the basal body and the new growing flagellum from an anterior to a posterior position. During S phase, the kinetoplast elongates, and the DNA content of the nucleus increases (Figure 4C) (Siegel, Hekstra and Cross, 2008).

During the nuclear G2 phase, the newly formed basal bodies separate in a microtubule-mediated manner (Robinson and Gull, 1991). Since they are connected to the kinetoplast via the tripartite attachment complex (TAC), the kinetoplast also divides (Ogbadoyi, Robinson and Gull, 2003), producing a 2K1N cell (Figure 4D) (Robinson *et al.*, 1995).

After the segregation of kinetoplasts is complete, 'closed mitosis' begins. In this process an intranuclear spindle is formed without disrupting the nuclear envelope (Ogbadoyi *et al.*, 2000). The new nucleus is placed between the kinetoplasts, resulting in a 2K2N cell (Figure 4E)

(Robinson *et al.*, 1995). The distal tip of the new flagellum now defines the point at which cytokinesis starts. The cell divides helically towards the posterior end, with each cell having one kinetoplast, one nucleus, and one flagellum in the end (Figure 4F) (Kohl, Robinson and Bastin, 2003). Defects in cytokinesis have serious consequences for the cell since the correct distribution of single-copy organelles is disturbed (LaCount, Barrett and Donelson, 2002; Hammarton *et al.*, 2003).

Trypanosomes have evolved a unique cytokinetic mechanism that ensures the reliability of cytoskeletal array duplication and segregation. The cytoskeleton of the cells does not break down during cell division, instead, new microtubules are formed between the existing microtubules. Thus, at the end of cytokinesis, each daughter cell has a so-called semiconservative cytoskeleton, which consists of both old and new microtubules (Sherwin and Gull, 1989).

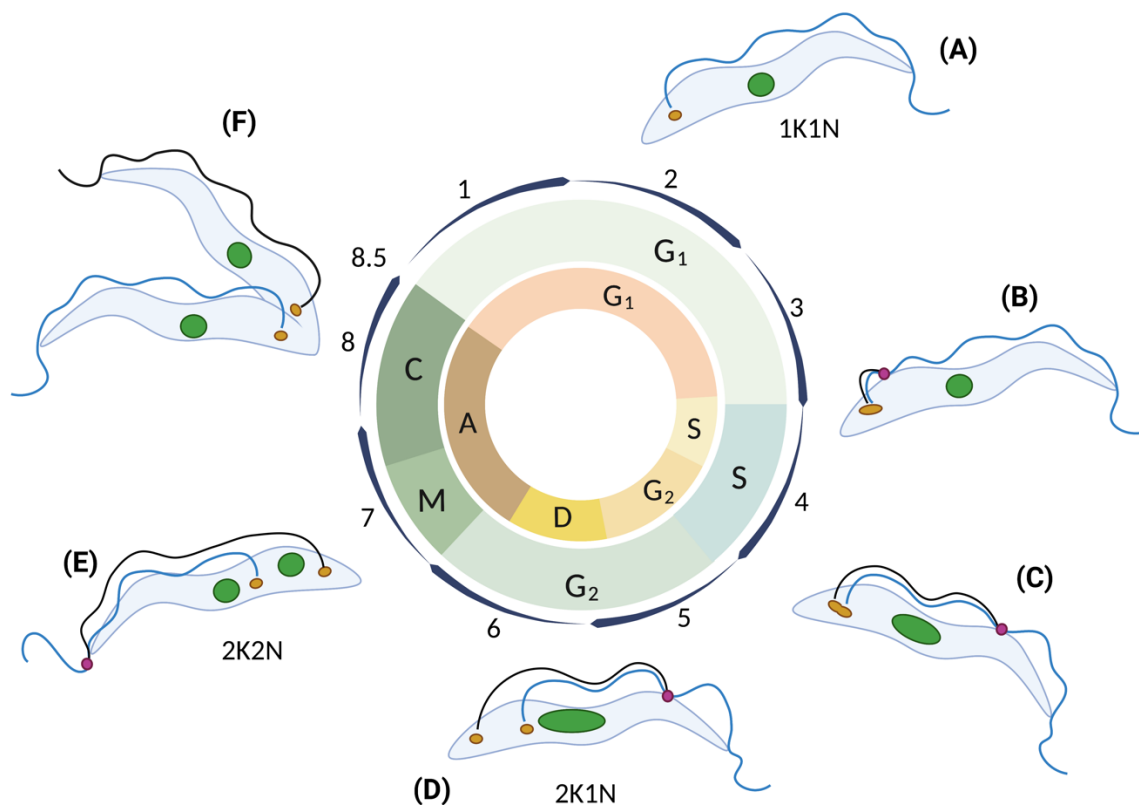


Figure 4: Cell cycle of *T. brucei*. Schematic representation of the cell division cycle of *T. brucei* cells. (A)-(F) show the cell cycle stages. Circle diagrams show the cycle events of the nucleus (green) and the events of kinetoplast DNA (yellow). A= segregation of the kinetoplasts, C= cytokinesis, D= division of the kinetoplasts, K= kinetoplast, N= nucleus/nuclei. Blue flagellum corresponds to the old flagellum, black flagellum corresponds to the new growing flagellum. Indicated in red is the flagellar connector. Numbers represent the time scale in hours. The figure was created based on the inspiration after Ploubidou *et al.* (1999) and McKean (2003). Figure was created with BioRender.com.

Tubulin, microtubules and microtubule associated proteins

Microtubules have essential functions in cells and are involved in cell structure, cell division and intracellular transport processes (Ishikawa, 2012; Guedes-Dias and Holzbaaur, 2019; Kelliher, Saunders and Wildonger, 2019; Nachury and Mick, 2019; Redemann *et al.*, 2019; Vicente and Wordeman, 2019). They are tube-like structures built from a protein complex consisting of α - and β -tubulin dimers.

In a head-to-tail formation, the dimers form individual protofilaments. 13 of these filaments assemble laterally and form a microtubule (Gudimchuk and McIntosh, 2021). This organization causes a functional polarity of the filaments and thus leads to the division of the microtubules into a structurally and biochemically distinct plus- and a minus-end. Thereby, α -tubulin is directed to the minus and β -tubulin to the plus end.

A special property is their dynamic instability. This is the constant formation and degradation of a microtubule (Figure 5). Dynamic instability is driven by the hydrolysis of GTP (guanosine triphosphate) (Mitchison and Kirschner, 1984; Desai and Mitchison, 1997; Gudimchuk and McIntosh, 2021).

Both tubulin subunits can bind GTP. The association of GTP to the E-site (exchangeable) of β -tubulin leads to the hydrolysis of GTP to GDP (guanosine diphosphate), whereby a binding of GTP to the N-site (non-exchangeable) of α -tubulin results in no hydrolysis (Figure 5) (Nogales, Wolf and Downing, 1998; Alushin *et al.*, 2014). Heterodimers that have GTP bound to β -units form stable and straight-growing protofilaments, but hydrolysis of GTP to GDP causes a slight conformational change in tubulin, causing protofilaments to lose stability and disassemble (Howard and Timasheff, 1986; Alushin *et al.*, 2014).

Tubulin dimers on rapidly growing microtubules form a GTP cap, which maintains filament stability until the cap is lost and the microtubules depolymerize (Mitchison and Kirschner, 1984).

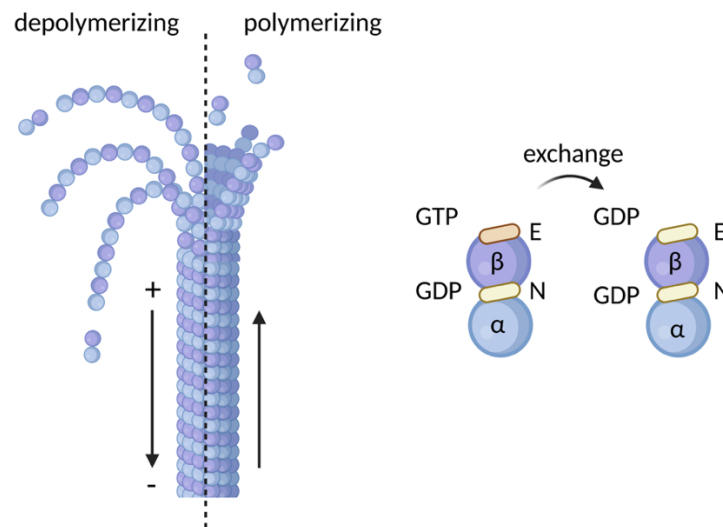


Figure 5: Microtubule dynamic instability. Left: Shown is a microtubule consisting of α - and β -tubulin. Dimers polymerize in a head-to-tail formation growing at the plus (+) ends. A microtubule consists of 13 protofilaments formed of α - and β -tubulin heterodimers. Dynamic instability occurs mainly at the plus-end of the microtubule, with cycles of polymerization and depolymerization. β -tubulin is located on the plus-ends and α -tubulin at the minus-ends. Right: both α - and β -tubulin dimer subunits bind GTP. α -Tubulin binds GTP in the N-site (non-exchangeable), where it is not hydrolysable; β -Tubulin binds GTP in the E-site (exchangeable), where it can be hydrolysed. Figure was created based on the inspiration after Alushin et al. (2014). Figure was created with BioRender.com.

In cells, a large microtubule diversity is provided to achieve certain physiological goals. Thus, microtubules consist of several tubulin isoforms and are endowed with different evolutionarily conserved posttranslational modifications (PTMs). This provides a large tubulin diversity and alters the intrinsic properties of microtubules, such as their dynamics and mechanics, as well as the recruitment and activity of motors and microtubule-associated proteins (Westermann and Weber, 2003; Janke and Magiera, 2020).

This combination of differential isotype expression and PTMs is termed the ‘tubulin code’ (Janke, 2014). As described above, the microtubule cytoskeleton of trypanosomes has unique properties. It is extremely robust, which naturally raises the question of how this stability is achieved. One could assume that the parasites regulate this stability by providing a variety of tubulin isoforms. However, this is not an option, as *T. brucei* has no tubulin isoforms. The unicellular organism only has one variant of α - and β -tubulin. Several copies of these are present in the genome arranged as tandem repeats (Thomashow et al., 1983; Ersfeld, Asbeck and Gull, 1998). This leaves the cell with two options for regulating microtubule properties:

Posttranslational modifications of microtubules (PTMs) and the recruitment of microtubule-associated proteins (MAPs).

MAPs can be divided into different categories depending on their function. These include motile proteins that can generate forces and motion (Hirokawa *et al.*, 2009; Bhabha *et al.*, 2016), proteins that have a depolymerizing effect on microtubules (McNally and Roll-Mecak, 2018), MAPs that nucleate microtubules (Roostalu and Surrey, 2017), end-binding proteins that specifically bind plus- or minus-ends of microtubules (Akhmanova, 2015) and structural MAPs.

Several cytoskeleton-associated proteins have been identified in *T. brucei*, but what their roles in the regulation of microtubule dynamics are still unclear. Most of cytoskeleton-associated proteins appear to be essential for the maintenance of the cell morphology and for a successful cytokinesis (Sinclair and de Graffenried, 2019). Also, the recently identified proteins CAP50, CAP52 and CAP42 seem to be important for cellular integrity (Schock, Schmidt and Ersfeld, 2021). It is also proposed that some of those proteins have a stabilizing function and cross-link microtubules to each other (Sinclair and de Graffenried, 2019).

In mammalian cells, the end-binding protein 1 (EB1) is a plus-end-binding protein (+TIP) that accumulates at growing microtubule ends and plays a central role in regulating microtubule dynamics (Akhmanova, 2015; Nehlig *et al.*, 2017). EB1 binds elongated tubulin GTP/GDP-Pi structures at growing microtubule ends and acts as a molecular platform that recruits other regulatory +TIP proteins (Akhmanova and Steinmetz, 2008; Zanic *et al.*, 2009; Galjart, 2010). EB1 is one of the few conserved microtubule-binding proteins in *T. brucei*. The functions of EB1 in the parasite have not yet been fully understood. An in-house laboratory study has shown that depletion of EB1 leads to severe cytokinesis and growth defects. It is assumed that EB1 plays a role during microtubule polymerization (Lallinger-Kube, 2017).

Another well-studied plus-end binding protein is the microtubule polymerase XMAP215. This microtubule-associated protein was first identified in *Xenopus laevis* extracts. It can increase the growth rate of a microtubule up to 10-fold (Gard and Kirschner, 1987). It has been shown that the interplay between EB1 and XMAP215 has an even higher effect on microtubule growth (up to 33-fold), suggesting that both proteins act synergistically together (Zanic *et al.*, 2013).

The microtubule-associated protein Air9 (Auxin-Induced in Root cultures 9) was first identified in *Arabidopsis thaliana* (Neuteboom *et al.*, 1999). This MAP was shown to be essential and has homologs in excavate protists like trypanosomatids (Buschmann *et al.*, 2007). The homologous TbAir9 in *T. brucei* is expressed throughout the subpellicular array except for the flagellum. Depletion of TbAir9 resulted in the formation of elongated posterior ends of procyclic cells, nuclear malposition and cytokinesis defects (May *et al.*, 2012). It was also shown to play a role in organizing other MAPs such as PAVE1, Tb927.9.10790, and Tb927.11.1840. Depletion of TbAIR9 resulted in altered localization of these MAPs (Sinclair *et al.*, 2021).

Also, well-characterised regulators of microtubule dynamics in mammalian cells are posttranslational modifications (PTMs) of tubulin. Many of these modifications occur simultaneously, resulting in a considerable diversity of cellular microtubules. We know today that posttranslational modifications of tubulin affect not only microtubule dynamics but also their organization and interplay with other cellular components (Song and Brady, 2015). Some of the known PTMs are also identified in trypanosomatids. Except for polyglycylation, modifications such as acetylation (Sasse and Gull, 1988), detyrosination/tyrosination (Sherwin *et al.*, 1987), phosphorylation (Nett *et al.*, 2009) and polyglutamylolation (Schneider, Plessmann and Weber, 1997; Casanova *et al.*, 2015) were identified in *T. brucei* (Figure 6). This was enabled by analyses based on mass spectrometry and specific antibodies, that target such modifications. Except for acetylation, which is in the lumen of a microtubule, most PTMs are located at the exposed C-terminal tails of alpha and beta tubulin.

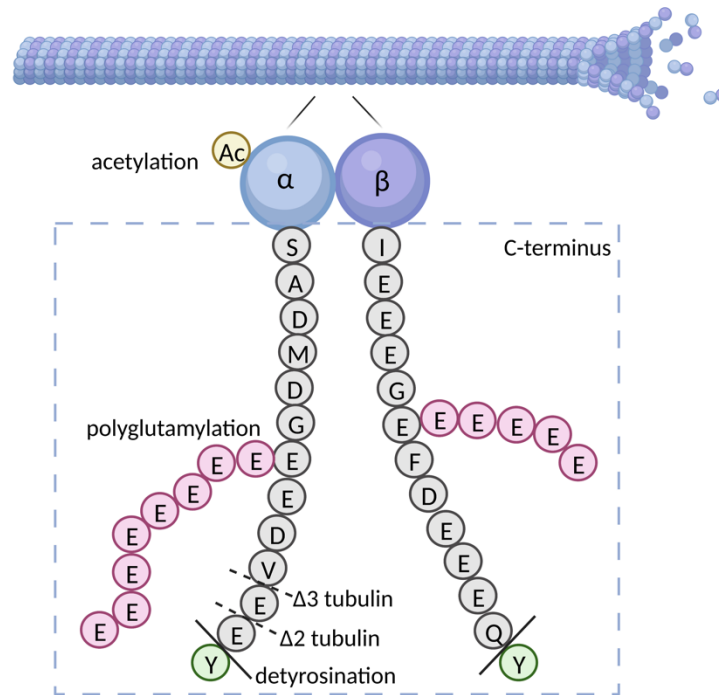


Figure 6: Posttranslational modifications of microtubules in *T. brucei*. Shown is a microtubule composed of α - and β -tubulin heterodimers (blue and purple, respectively). Both α - and β -tubulin subunits have long, intrinsically disordered and highly negatively charged C-terminal tails, that can be modified posttranslationally. In contrast to other organisms, in *T. brucei* both the α - and β -tubulin subunits contain a tyrosine residue, that are removed by a tubulin carboxypeptidase. Carboxypeptidases can also cleave both terminal glutamic acid residues resulting in $\Delta 2$ -tubulin and $\Delta 3$ -tubulin. Free tubulin dimers can be retyrosinated by a tubulin tyrosine ligase. In contrast to most posttranslational tubulin modifications, acetylation does not occur at the c-terminal tails, but at an inwardly directed site of the α -tubulin subunit. Represented is the amino acid sequence from *T. brucei*. Figure was modified after Sinclair *et al.* (2019). Figure was created with BioRender.com.

The most prominent site for acetylation is on lysine 40 (K40) at α -tubulin (Janke, 2014). However, other sites can also be acetylated (Choudhary *et al.*, 2009; Chu *et al.*, 2011). Acetylation occurs at polymerized microtubules, increases their flexibility and protects them from mechanical stress by weakening the interaction of interprotofilaments (Portran *et al.*, 2017). Therefore, acetylated tubulin is often used as a marker for long-lived microtubules. In contrast, tyrosinated α -tubulin serves as a marker for newly synthesized microtubules. The gene for α -tubulin encodes a C-terminal tyrosine, thus newly synthesized α -tubulin is already tyrosinated (Gadadhar *et al.*, 2017). Once tubulin dimers polymerize into a microtubule, the terminal tyrosine is rapidly removed by the recently identified carboxypeptidases VASH1 and VASH2 (vasohibin-1 and 2) (Aillaud *et al.*, 2017), and MATCAP (microtubule associated tyrosine carboxypeptidase) (Landskron *et al.*, 2022). After depolymerization of a microtubule, free tubulin dimers can be retyrosinated in the cytoplasm by another enzyme, the tyrosine ligase

(TTL) (Ersfeld *et al.*, 1993). These two processes of constant detyrosination and tyrosination are referred to as the tubulin detyrosination cycle (Nieuwenhuis and Brummelkamp, 2019). In *T. brucei*, tyrosinated microtubules are found at the posterior end of the cell, within the growing flagellum, at the basal bodies and at the mitotic spindle (Sasse and Gull, 1988). A comparison of the amino acid sequences of α - and β -tubulin shows that, unlike in mammals, in *T. brucei* both α - and β -tubulin have a terminal tyrosine (Table 1) (Sinclair and de Graffenried, 2019). A study has shown that both tyrosine residues in *T. brucei* are cleaved by the single carboxypeptidase homologue VASH (van der Laan *et al.*, 2019).

Table 1: Amino acid sequences of the C-terminal tails of alpha and beta tubulin. The sequences of *T. brucei* and *Homo sapiens* are shown. In bold letters, the C-terminal tyrosine is highlighted. Figure was modified after Sinclair *et al.* (2019).

species	alpha tubulin	beta tubulin
<i>T. brucei</i>	439 SADMDGEED V EEY 451	430 IEEEGEFDEEE Q Y 442
<i>H. sapiens</i>	439 SVEGEGEEEGEE Y 451	430 AEEEEDFGEEAEEEA 444

Polyglutamylatation

Unlike monomodifications, such as acetylation and phosphorylation, glutamylatation is a polymodification, i.e., the attachment of side chains with variable lengths that contain glutamate residues. Thus, polymodifications do not have the typical on/off effect, like phosphorylation, but generate a series of signals by varying the length of the side chains (van Dijk *et al.*, 2007).

Side chains are formed by adding glutamates to internal glutamate residues on the intrinsically disordered C-terminal tails of α - and β -tubulin on polymerized microtubules (Westermann and Weber, 2003). Responsible for the formation of such side chains are a series of polyglutamylases, the tubulin tyrosine ligase-like proteins (TTLL). They all belong to the group of the tubulin ligase (TTL) since they all share a homologous domain (TTL domain) (Janke *et al.*, 2005; van Dijk *et al.*, 2007).

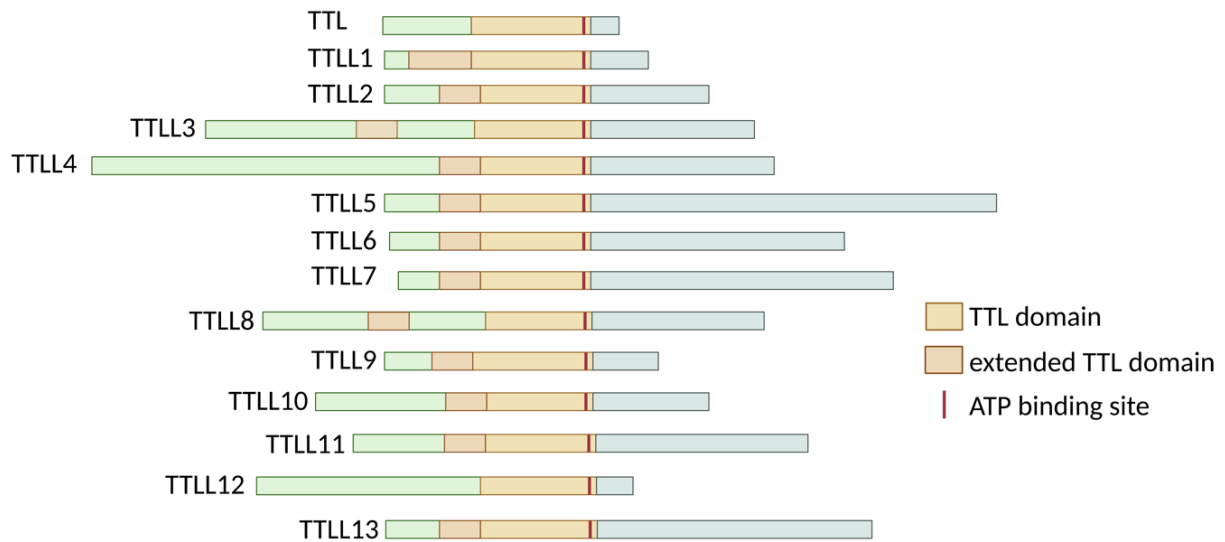


Figure 7: The Group of TTLL proteins. Schematic representation of TTL and 13 TTLL in mouse with conserved homology domains. The core domain is the TTL domain, which all proteins have in common. Figure was modified after van Dijk et al. (2007). Figure was created with BioRender.com.

Within the group of polyglutamylases, there are enzymes with different functions (Figure 8). On the one hand, there are enzymes with an initiating function, i.e., they attach the initial glutamate rest to the C-terminal tail (TTLL4, 5 and 7). On the other hand, there are enzymes that have an elongating function, i.e., they serially link further glutamate residues to the initial residue (TTLL1, 6, 11 and 13) (van Dijk *et al.*, 2007). Specifically, during branch initiation, the first glutamate is added by the formation of an isopeptide bond between the γ -carboxyl group of a glutamate within the C-terminal tail and the amino group of the incoming glutamate. From this initial branching point, additional glutamates are then added to form a polyglutamate chain. In this extension step, the glutamates within the chain can be linked either via a peptide bond to α -carboxyl groups (α -linked extension) or an isopeptide bond using the γ -carboxyl group (γ -linked extension) of the receiving glutamate (Mahalingan *et al.*, 2020).

Since glutamylation also belongs to the reversible modifications, deglutamylases were described within a novel family of cytosolic carboxypeptidases (CCPs) (Kimura *et al.*, 2010; Rogowski *et al.*, 2010). Currently, six CCPs have been identified, of which three enzymes are shown to cleave C-terminal glutamate residues within the side chain, or even remove terminal glutamate residues within the tail. Cleavage of gene-encoded glutamate within the tail generates $\Delta 2$ -tubulin and $\Delta 3$ -tubulin (Figure 6) (Rogowski *et al.*, 2010; Berezniuk *et al.*, 2012). $\Delta 2$ -tubulin is an irreversible modification and cannot be retyrosinated by the tyrosine ligase

(TTL) because of structural limitations (Prota *et al.*, 2013). Thus, a balance of the glutamylation level can be maintained in polymerized microtubules. Manipulating this balance can have serious consequences. It was demonstrated that a hyperglutamylation due to the lack of CCP1 in mice is directly linked to neuronal degeneration (Rogowski *et al.*, 2010; Shashi *et al.*, 2018). Also, mice lacking the deglutamylase CCP5 do not form functional sperm and are therefore sterile (Giordano *et al.*, 2019). The opposite way was shown that a knockout of the polyglutamylase TTL1 in mice resulted in respiratory problems because of an abnormal beating of airway cilia (Ikegami *et al.*, 2010). Interestingly a hyperglutamylation due to the knockout of the deglutamylase CCP1 can be fully rescued by a knockout of the counteracting polyglutamylase TTL1 (Magiera *et al.*, 2018a). Furthermore, an altered balance of glutamylation could possibly have structural consequences, since polyglutamylation adds a significant negative charge to the C-terminal tails (Wall *et al.*, 2020).

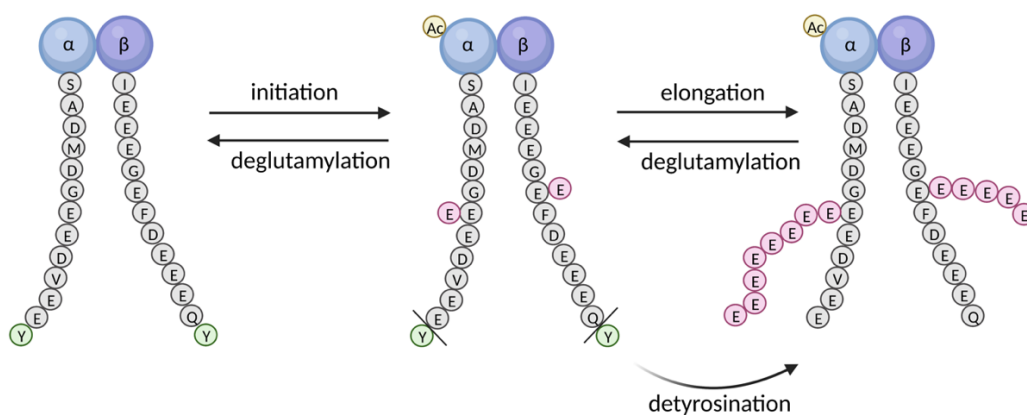


Figure 8: Schematic representation of the catalysis of glutamate side chains. Shown are α - and β -tubulin dimers with the C-terminal tails (grey). Acetylation is shown in yellow and the terminal tyrosine residues in green. Initiating glutamylases attach a glutamate residue to a glutamate residue within the C-terminus (dark grey). Elongating glutamylases then extend the glutamate chain by adding further glutamate residues to the initial glutamate. Deglutamylases remove individual glutamate residues. Figure was created based on the inspiration after Janke and Bulinski (2011). Figure was created with BioRender.com.

In *T. brucei* the cytoskeleton as well as the flagellum are highly glutamylated (Schneider, Plessmann and Weber, 1997). Glutamyl side chains vary in their lengths, of up to 15 amino acid residues on α - tubulin and six residues on β -tubulin (Schneider, Plessmann and Weber, 1997; Casanova *et al.*, 2015).

Using sequence homologies, nine genes encoding putative polyglutamylases were identified in trypanosomes (Table 2) (Casanova *et al.*, 2018). The occurrence of multiple TTLs can be

explained based their localisation in different cellular compartments, and thus presumably assume different functions. For example, TTLL4A is strongly localised in the nucleus and flagellum, whereas TTLL4B is localised in the mitochondrion. Others are predominantly found in the cytoplasm and also in the flagellum (<http://www.tryptag.org>). The presence of several proteins of this family can also be explained by their specific catalytic activity, which is divided into an initiating and an elongating function (Mahalingan *et al.*, 2020). TTLL7 has been shown to be active as both an initiase and an elongase (Mukai *et al.*, 2009).

Until today only two studies have published initial insights into the function of polyglutamylation in *T. brucei*. It could be shown that the depletion of TTLL4B leads to a reduction of polyglutamylation and is an important factor for correct cytokinesis (Casanova *et al.*, 2018). In a second study, which is also part of the present work and was published in the “journal of cell science”, it was shown that two other enzymes, namely TTLL6A and TTLL12B are important for the maintenance of a normal cell morphology and cell motility and lead to cytokinesis defects when depleted (Jentzsch *et al.*, 2020).

Table 2: Nomenclature of all putative polyglutamylases identified in *T. brucei* and the tubulin tyrosine ligase. TTLL = Tubulin tyrosine ligase-like proteins. Annotation after TritypDB. TTLL1, TTLL6A and TTLL12B were further characterised in this thesis. Figure was modified after Casanova *et al.* (2015).

Abbreviation	Annotation	Function	Addressed in this thesis
TTL	Tb927.2.5250	tubulin tyrosin ligase	
TTLL1	Tb927.5.3860	putative polyglutamylases	TTLL1
TTLL4A	Tb927.9.9580		
TTLL4B	Tb927.6.3570		
TTLL4C	Tb927.1.1550		
TTLL6A	Tb927.3.5380		TTLL6A
TTLL6B	Tb927.11.6810		
TTLL9	Tb927.10.13870		
TTLL12A	Tb927.11.2390		
TTLL12B	Tb927.11.2420		TTLL12B

Aims of the thesis

Posttranslational modifications contribute significantly to the regulation and functionality of microtubules in eukaryotes. The protozoan parasite *T. brucei* represents a suitable model-organism to study some of these evolutionary highly conserved PTMs. It possesses a well

characterised subpellicular microtubule-based cytoskeleton and a canonical axonemal structure within the flagellum. The absence of a variety of tubulin isoforms, which complicate such analysis in higher eukaryotes, in conjunction with a range of molecular and cell biological tools to analyse protein function make *T. brucei* an ideal system to study tubulin PTMs. Therefore, the aim of this thesis was the cell biological characterisation of three putative *T. brucei* tubulin polyglutamylases (TTLL6A, TTLL12B and TTLL1) in order to gain insights into the significance of the tubulin code for cellular organisation and dynamics.

Results

Various TTLLs show in vivo glutamylation activity

The aim of this thesis was to investigate whether the putative *T. brucei* TTLLs show polyglutamylase activity and which benefit the respective proteins might have for the cell. For this purpose, a series of RNAi (RNA interference) constructs were created to deplete the TTLL homologs of *T. brucei*, which were previously identified by Casanova *et al.* (2015). The analysis of the putative polyglutamylase TTLL4C was not addressed in this work, because it is subject to another project.

In a first experiment, cell extracts of the corresponding RNAi-depleted cell lines were analysed at protein level. For this purpose, the monoclonal antibody GT335 was used to detect short glutamate side chains, as it recognizes the branching point of the side chain, and the polyclonal antibody PolyE was used to detect long side chains with at least four glutamate residues (Figure 9A).

After one day depletion of individual TTLLs, almost all cell lines showed a significant decrease in the glutamylation signal. Only the depletion of TTLL6A resulted in a lower decrease of signal with a reduction of approximately 30 % for GT335 and 20 % for PolyE (Figure 9B and C).

Although a knockdown of TTLL4B, 6B and 9 showed a strong loss of the glutamylation signal, no obvious phenotypic changes of the cells could be observed.

Only the depletion of TTLL1, TTLL6A, and TTLL12B resulted in morphological changes of the cells (Figure 9D).

Based on these initial observations, these last three mentioned proteins were further characterised.

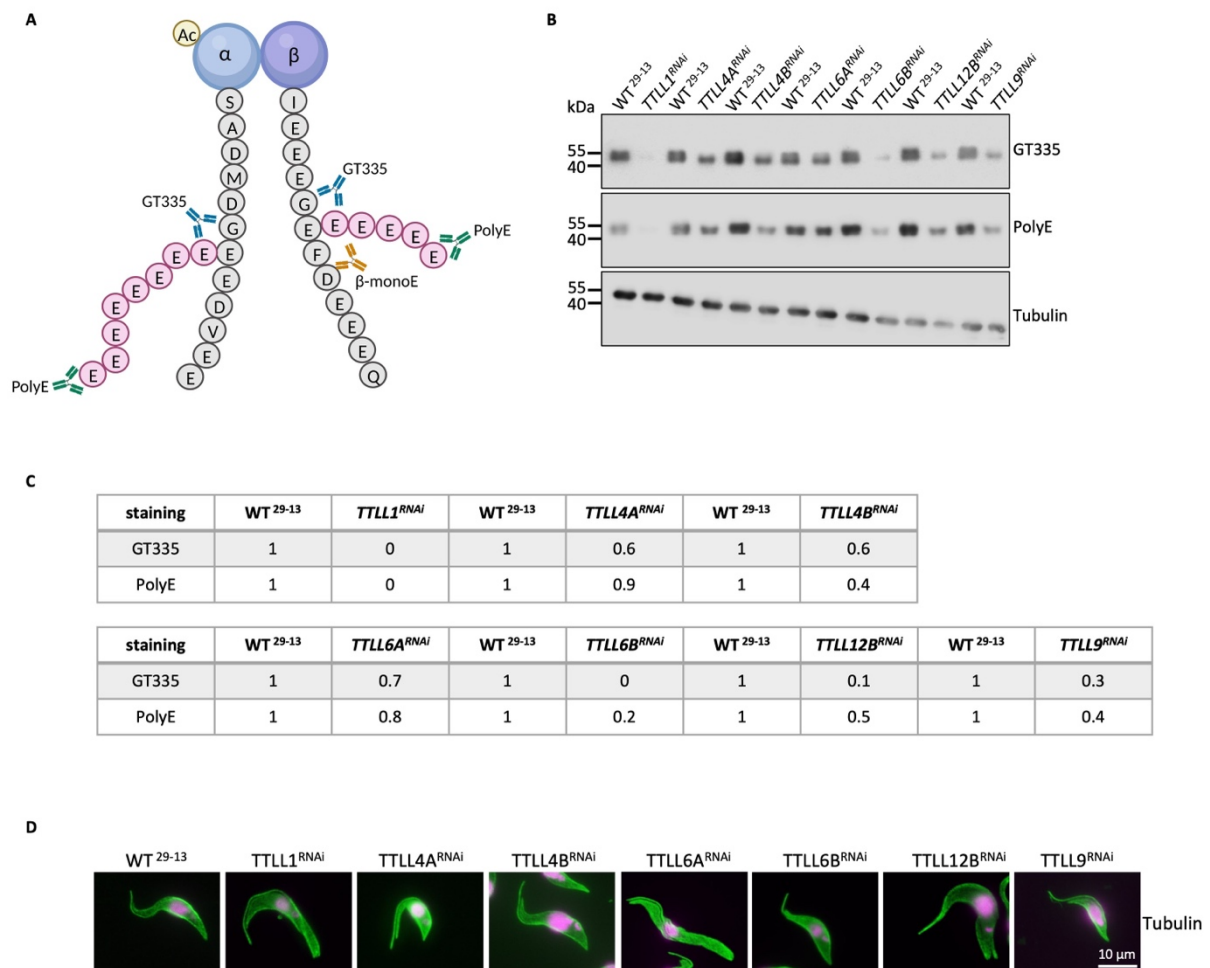


Figure 9: Initial analysis of the TLL-depleted cell lines. (A) The monoclonal antibody GT335 detects the branching point of the glutamate side chain; the polyclonal antibody PolyE detects long side chains with at least four glutamyl residues. **(B)** Whole-cell extracts of WT²⁹⁻¹³ cells and RNAi cells after induction with doxycycline for two days. Tubulin served as a loading control. **(C)** Densitometric evaluation of the protein bands from the western analysis (B). WT²⁹⁻¹³ samples were compared with the samples of the respective RNAi cell line to the right. Tubulin was used for normalisation. **(D)** Immunofluorescence of cytoskeletal preparations of WT²⁹⁻¹³ cells and cells after depletion of the respective TLLs. Cells were stained with an anti-tubulin antibody (green). DNA was stained with DAPI (magenta). Figure (A) was created with BioRender.com.

Characterisation of TLL6A and TLL12B

TLL6A and TLL12B have in vivo glutamylation activity and are important for the cellular architecture

To further investigate the glutamylase activity of TLL6A and TLL12B, the degree of mRNA depletion was analysed using RT-qPCR.

The mRNA levels of both cell lines were reduced by approximately 60-70 % (Figure 38). After RNAi induction over a period of three days samples were analysed by western blotting.

The western blot results showed that the glutamylation signal decreased after the depletion of the two proteins (Figure 10A, results have partially been published and were later modified (Jentzsch *et al.*, 2020)). The immunoblots were replicated three times and then evaluated densitometrically. The result of the evaluation is shown as the mean values of the replicates (Figure 10B, results have been published and were modified after (Jentzsch *et al.*, 2020)). After three days induction of both RNAi cell lines a significant reduction of 60-70 % of the short chains (GT335) can be observed. The signal of long chains (PolyE) was decreased by 80 % after depletion of TLL12B. However, the PolyE signal after the depletion of TLL6A decreased only by 40 % (Figure 10B, results have been published and were later modified (Jentzsch *et al.*, 2020)). Depletion of TLL12B and TLL6A appears to cause a decrease in signal for both alpha and beta tubulin.

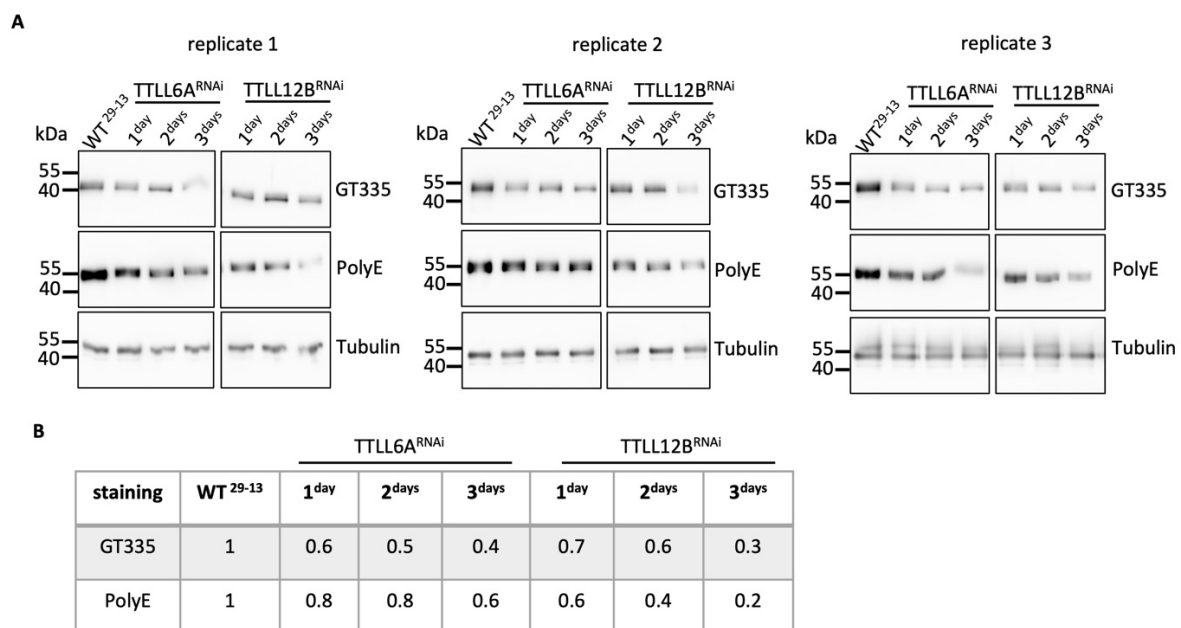


Figure 10: TLL6A and TLL12B have in vivo glutamylation activity. (A) Shown are three replicates of a western blot analysis of cytoskeletal preparations of WT²⁹⁻¹³ cells and cells depleted of either TLL6A or TLL12B. RNAi was induced over a period of three days. Samples were probed with the glutamyl-specific antibodies GT335 and PolyE. Tubulin served as a loading control. (B) Densitometric evaluation of the reduction of the signal. WT²⁹⁻¹³ samples were compared with the samples of the respective RNAi cell line. Tubulin was used for normalisation. Represented is the mean value of the three replicated western blots. (Results have partially been published and were later modified (Jentzsch *et al.*, 2020)).

The TLL6A and TLL12B depleted cells exhibit the recently described ‘glove phenotype’ (Jentzsch *et al.*, 2020). Normally, *T. brucei* cells have a highly ordered cytoskeleton with microtubules clustered into a pointed tip at the posterior end of the cell. In glove cells, this

end is split into several fingers (Figure 11A, results have partially been published and were later modified (Jentzsch *et al.*, 2020)). This extreme phenotype occurred in approximately 40 % of $TTL6A^{RNAi}$ cells and in 20 % of $TTL12B^{RNAi}$ cells of the population. The glove phenotype was also found in a smaller proportion of the non-induced RNAi cells (Figure 11B, results have been published (Jentzsch *et al.*, 2020)).

The remaining 60 % ($TTL6A^{RNAi}$) and 80 % ($TTL12B^{RNAi}$) of the cell population appeared to have a normal morphology.

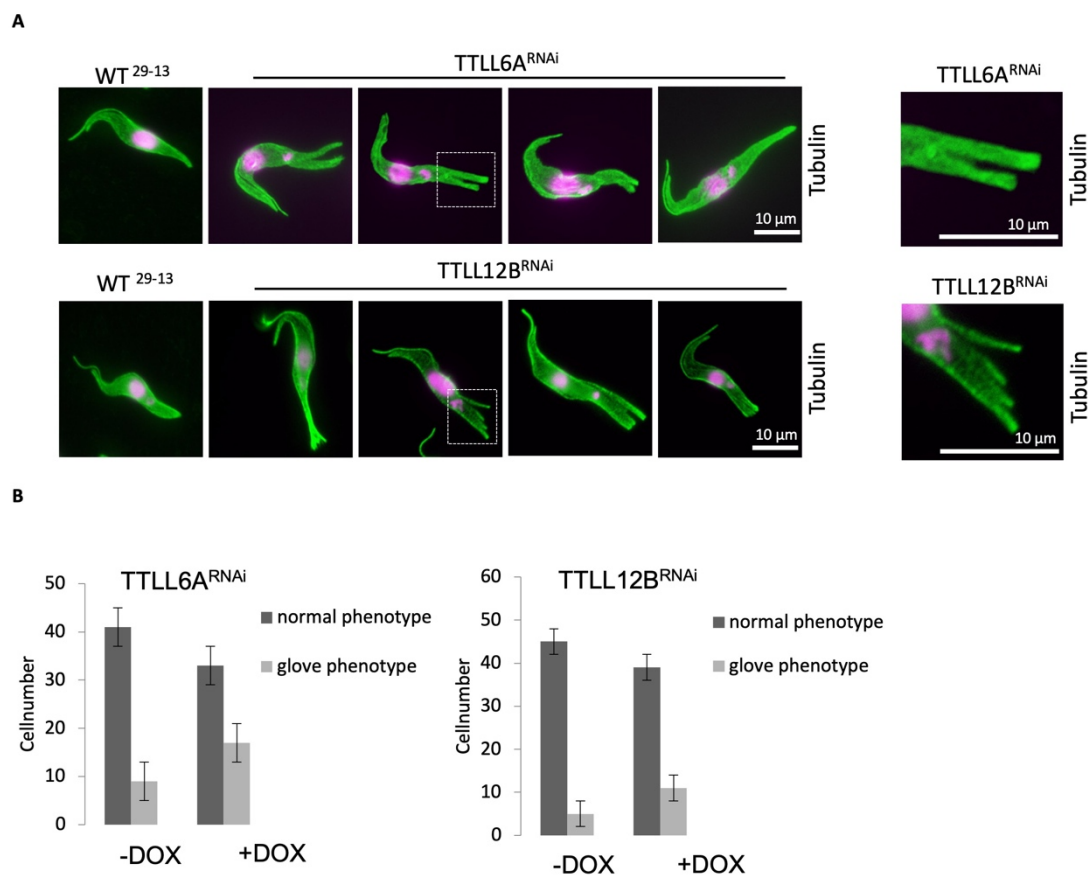


Figure 11: Depletion of $TTL6A$ and $TTL12B$ results in the appearance of the ‘glove phenotype’. (A) Immunofluorescence of WT^{29-13} and $TTL6A^{RNAi}$ or $TTL12B^{RNAi}$ cells after two days depletion. Cytoskeletons were stained with an anti-tubulin antibody (green). DNA was stained with DAPI (magenta). Depletion of either protein leads to a disruption of the posterior ends of the cells. A detailed view is shown on the right (zoom of indicated white squares). (B) Count of cells that have glove phenotype. Error bars represent the standard error. (Results of (A) and (B) have partially been published and were later modified (Jentzsch *et al.*, 2020)).

Electron microscopy was used to study the ultrastructural organisation of the posterior tip of the cells. In WT^{29-13} cells, the microtubules could be seen to be clustered into a pointed end. After a knockdown of $TTL6A$ or $TTL12B$, the microtubule structures are not bundled, but

individual microtubules are fanned out (results have partially been published and were later modified (Jentzsch *et al.*, 2020)).

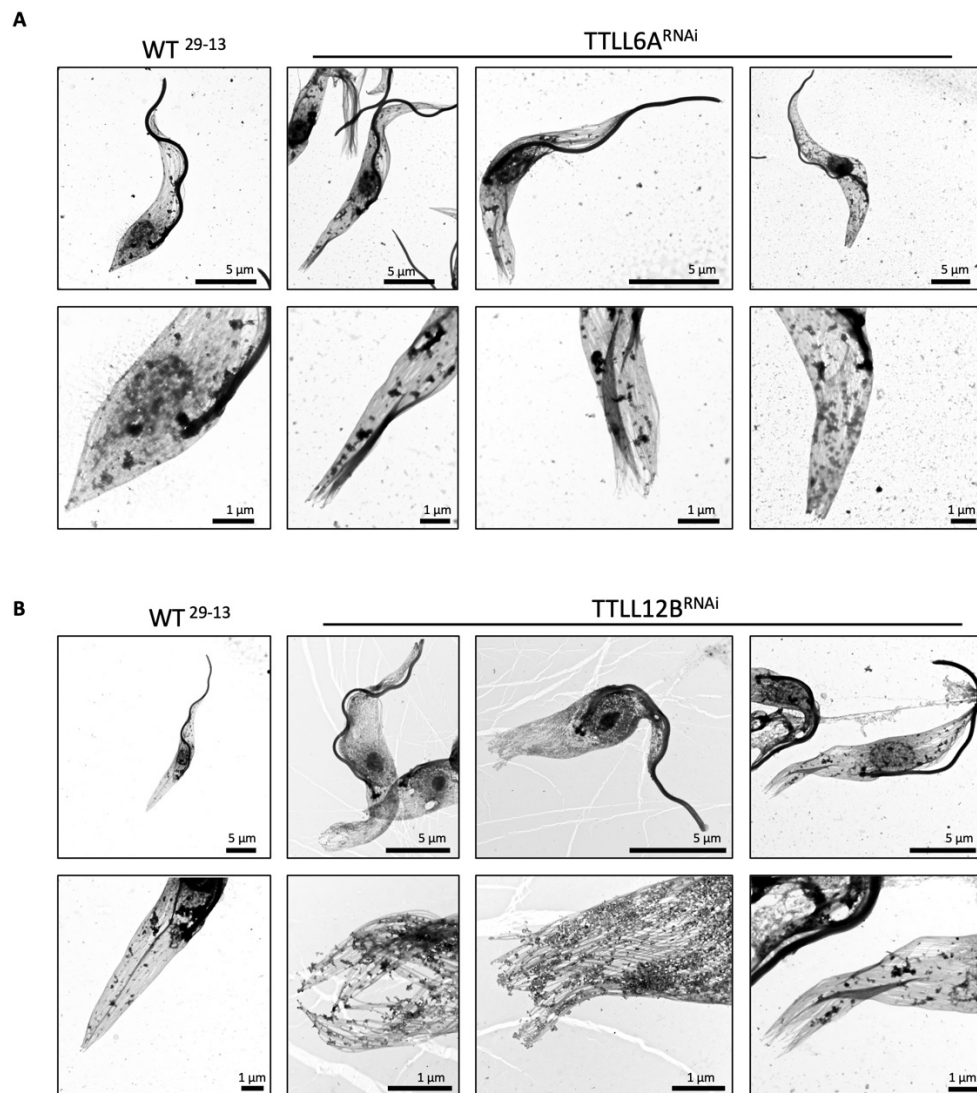


Figure 12: Ultrastructure of the posterior ends of *TLL6A*^{RNAi} and *TLL12B*^{RNAi} cells. Whole mount electron microscopy of cytoskeletons of *WT*²⁹⁻¹³ and *TLL6A*^{RNAi} (A) or *TLL12B*^{RNAi} (B) cells. **Upper panels** show an overview of the cells; **lower panels** show a more detailed view of the posterior ends of the cells. (Results have partially been published and were later modified (Jentzsch *et al.*, 2020)).

In a next step, the glutamylation pattern was analysed in a more detailed manner. For this purpose, cytoskeletons were stained with the antibodies GT335 and PolyE. *WT*²⁹⁻¹³ cells show a homogeneous staining when probed with both antibodies (Figure 13). In *TLL6A* and *TLL12B* depleted cells, it was observed that the staining with GT335 decreased strongly, especially at the posterior ends of the cells, or even disappeared completely. In contrast, the signal of a PolyE staining was weaker over the entire cell body (Figure 13, results have partially been published and were later modified (Jentzsch *et al.*, 2020)).

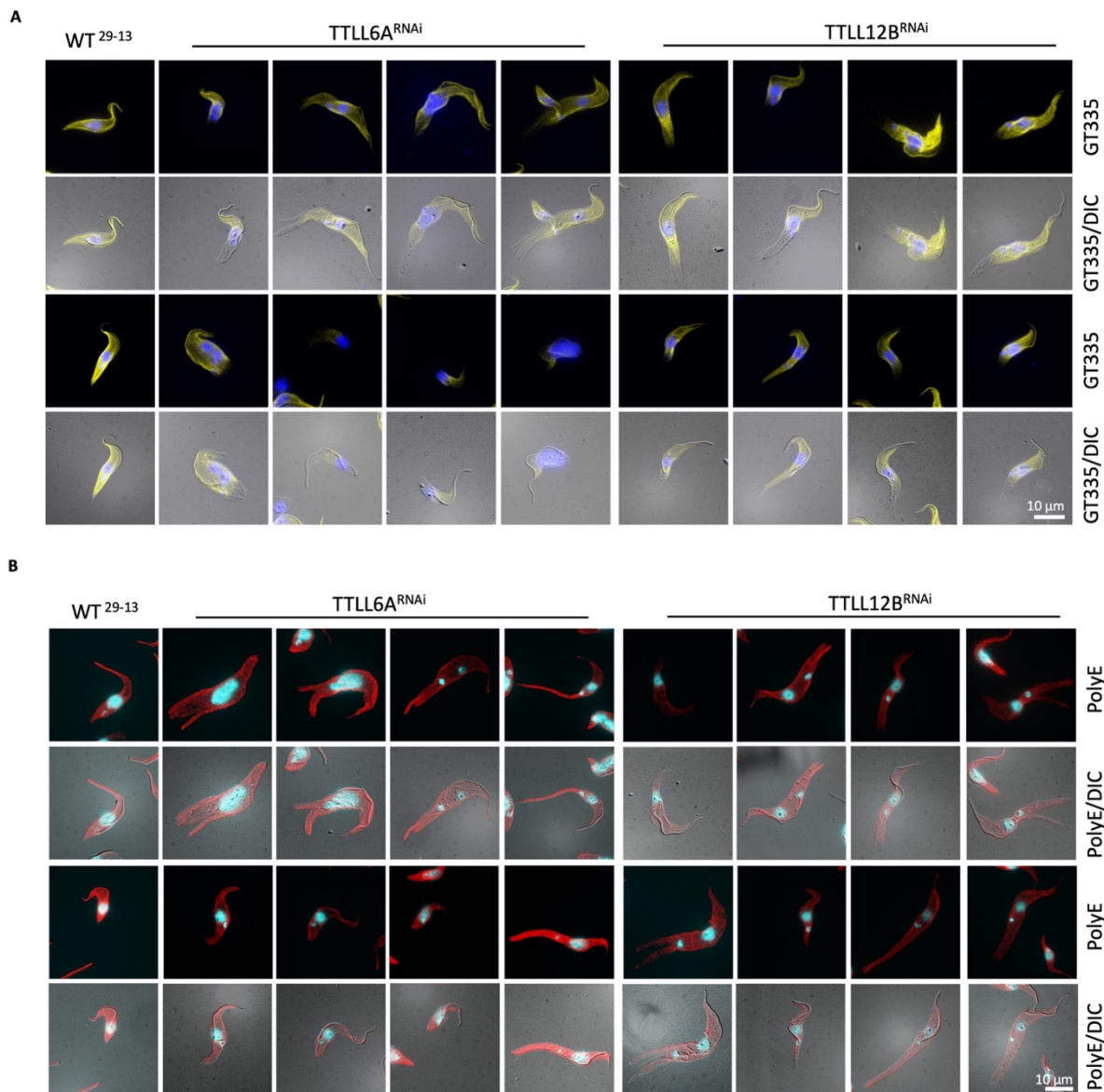


Figure 13: Loss of glutamylation at the posterior ends of cells depleted of either TTLL6A or TTLL12B. (A) Cytoskeletons of WT²⁹⁻¹³ and TTLL6A^{RNAi} or TTLL12B^{RNAi} cells after two days depletion. Cytoskeletons were stained with GT335 (yellow) and DAPI (blue). (B) Cytoskeletons were stained with PolyE (red) and DAPI (light blue). (Results have partially been published and were later modified (Jentzsch et al., 2020)).

TTLL6A or TTLL12B knockdown causes cytokinesis defects

The knockdown of either TTLL6A or TTLL12B resulted in inhibited cell growth and associated cytokinesis defects. To analyse growth, three biological replicates of the respective cell lines were cultivated for four days, and samples were taken. The cell density of each sample was measured three times. The mean values of the biological and technical replicates were

represented in cumulative growth curves. The results show an inhibition of the division rates after three days of depletion of either TLL (Figure 14A, results have been published and were later modified (Jentzsch *et al.*, 2020)). It is reasonable to expect that impaired growth is due to disturbances in cell division. Disturbances during cell division lead to an incorrect distribution of the nuclei and kinetoplasts among the daughter cells. Such defects are reflected in an increase of multinucleated cells, or cells that have missing nuclei (zoids) (Figure 14B, results have been published and were later modified (Jentzsch *et al.*, 2020)).

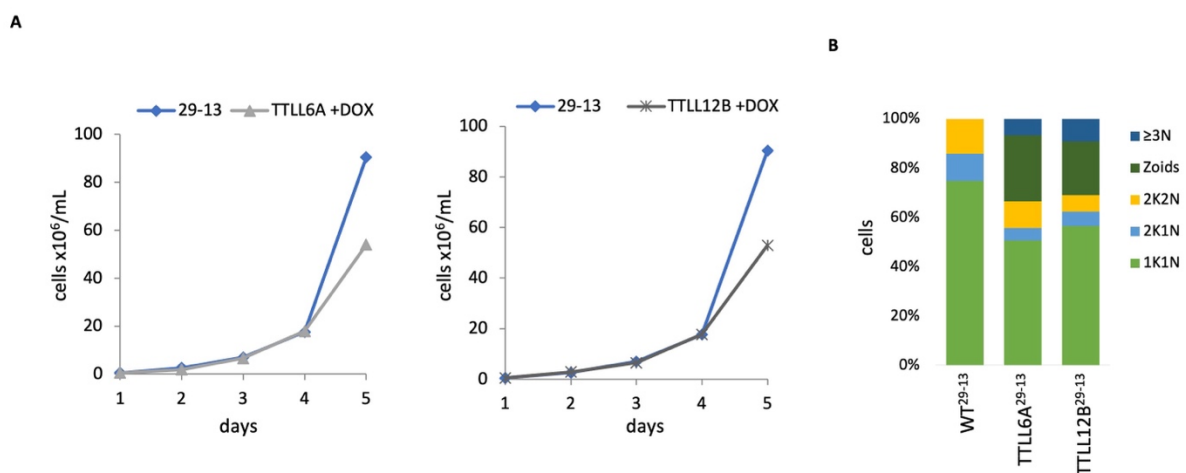


Figure 14: TLL6A or TLL12B knockdown causes growth and cytokinesis defects. (A) Cumulative growth curves of WT²⁹⁻¹³ and TLL6A^{RNAi} or TLL12B^{RNAi} cells. Each data point corresponds to the mean of three biological replicates, that were measured three times. **(B)** Representation of a count of karyotypes of WT²⁹⁻¹³ cells and RNAi cells after two days of induction. Zoids correspond to cells without nuclei (N) or kinetoplast DNA (K), ≥3N corresponds to cells with more than two nuclei or kinetoplasts. n=120 cells. (Results have been published and were later modified (Jentzsch *et al.*, 2020)).

Increase of newly synthesized microtubules after the depletion of TLL6A or TLL12B

Tyrosination serves as a marker for newly synthesized microtubules. In long-lived, stable microtubules, this tyrosine is rapidly removed by a carboxypeptidase. For a detection of newly polymerized microtubules, the antibody YL1/2 can be used, because it recognizes tyrosinated α -tubulin.

Microtubules of *T. brucei* are extremely stable, which is why YL1/2 only shows a signal at the basal bodies and a weak staining of the posterior end as well as the newly developing flagellum (Sasse and Gull, 1988). For this experiment a very high dilution of YL1/2 was used, which is why only basal body staining was seen in WT²⁹⁻¹³ cells. After the knockdown of TLL6A or

TLL12B, a strong increase in the staining at the posterior ends was observed (Figure 15, results have partially been published and were later modified (Jentzsch *et al.*, 2020)). This was especially the case for cells exhibiting the glove phenotype.

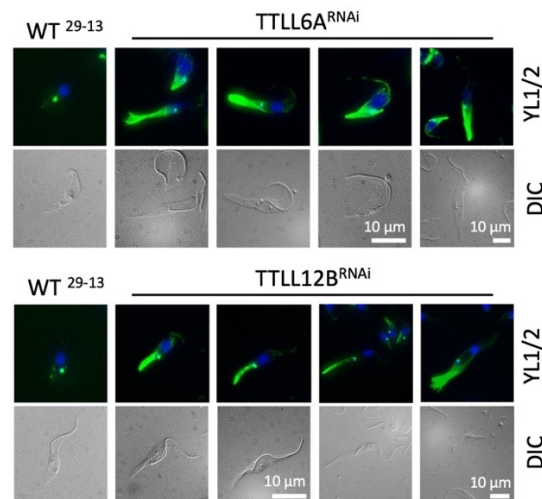


Figure 15: Increase of newly synthesized microtubules in TLL6A or TLL12B depleted cells. Immunofluorescence of cytoskeletons of WT²⁹⁻¹³ cells and cells after RNAi induction for two days. Cells were stained with YL1/2 (green) which detects tyrosination on α -tubulin. DNA was stained with DAPI (blue). (Results have partially been published and were later modified (Jentzsch *et al.*, 2020)).

Impaired binding of microtubule-associated proteins after the depletion of TLL6A or TLL12B

As a marker for a correctly organised posterior end, the localisation of the end-binding protein 1 (EB1) was examined, because it binds to the plus-ends of microtubules and is thus localised at the posterior ends of the cells.

In TLL6A and TLL12B depleted cells, the signal was absent (Figure 16A, results have partially been published and were later modified (Jentzsch *et al.*, 2020)). This was also the case for cells with an apparently normal cell architecture. This observation is consistent with EB1 being in the soluble fraction in the Western blot after depletion of TLL6A and TLL12B. After two days of depletion, the EB1 signal in the cytoskeletal fraction is 70-80% lower (Figure 16B, results have partially been published and were later modified (Jentzsch *et al.*, 2020)).

The binding of a second microtubule-associated protein, XMAP215, was investigated (Figure 16C, modified (Master thesis of Marinus Thein, Molecular Parasitology, University of Bayreuth, 2022)). It also binds to the plus-ends of microtubules and is located at the posterior

ends of the cells. This analysis was done by Marinus Thein, a master student of mine. He generated a TTLL6A-RNAi cell line that expressed an endogenously tagged XMAP215 (the required RNAi-construct targeting TTLL6A corresponded to the same used in this thesis). The results showed, that XMAP215 was lost in 65 % of the cell population after a depletion of TTLL6A, while it was absent in 30 % of the population of non-induced cells (Figure 42, supplements) (Master thesis of Marinus Thein, Molecular Parasitology, University of Bayreuth, 2022).

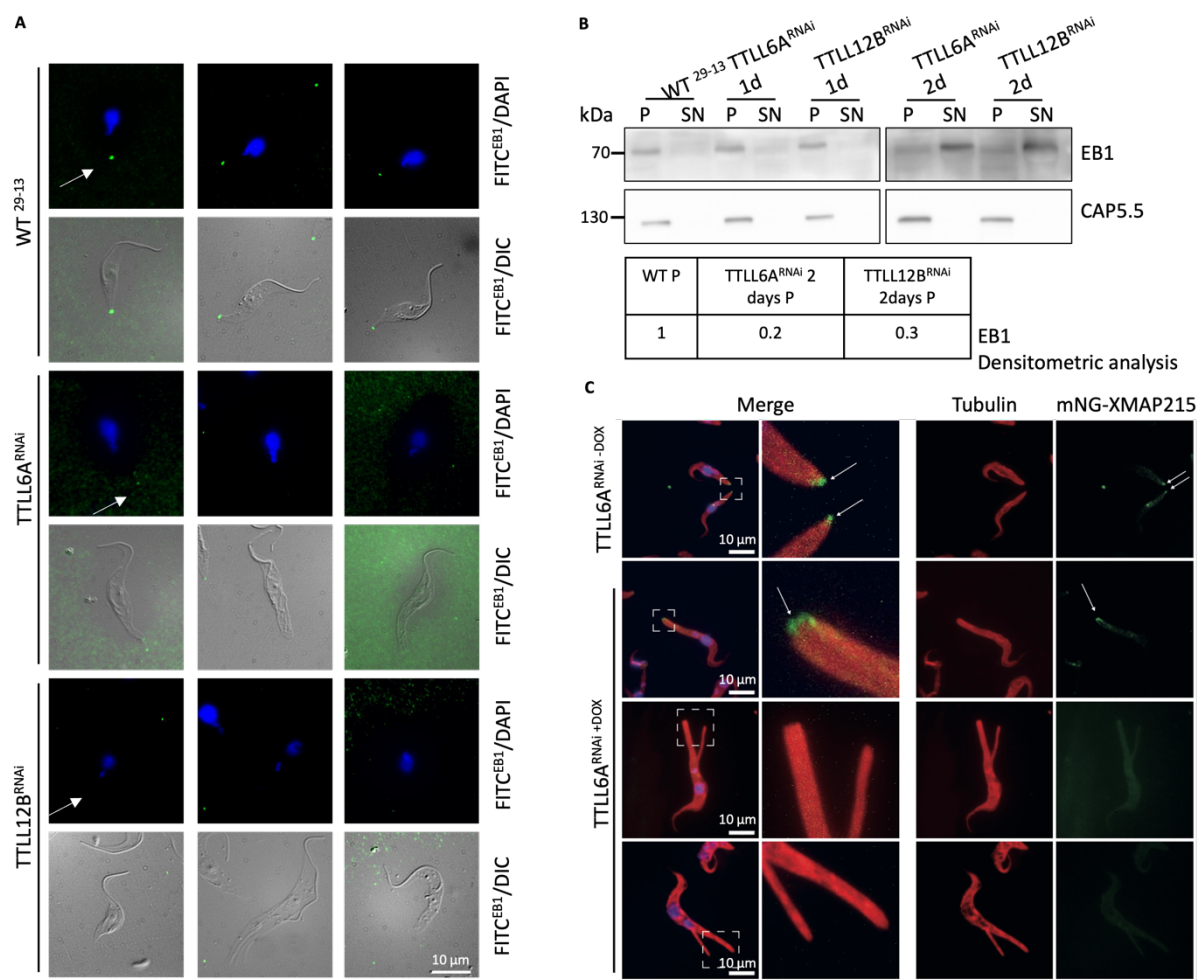


Figure 16: Failed localisation of the end binding Protein 1 (EB1) and the microtubule-associated protein XMAP215. (A) Immunofluorescence of WT²⁹⁻¹³ and TTLL6A^{RNAi} or TTLL12B^{RNAi} cells after depletion for two days. Cytoskeletons were stained with an anti-EB1 monoclonal antibody (green), DNA was stained with DAPI (blue). The appearance of an EB1 signal or the absence of the signal is indicated with a white arrow. **(B)** Western blot of soluble (SN) and cytoskeletal (P) fractions of WT²⁹⁻¹³ and RNAi cells. Samples over a period of two days of RNAi induction were analysed. They were probed with an anti-EB1 antibody. CAP5.5 served as a loading control for the insoluble fraction. For the densitometric analysis of the western blot, the signal of the cytoskeletal fraction of wildtype cells was compared to that of the RNAi cells. CAP5.5 was used for normalisation. **(C)** Shown are cytoskeletons of TTLL6A^{RNAi} cells with and without RNAi induction. The endogenously tagged mNG-XMAP215 is shown in green, tubulin in red and DNA in blue. Figure **(C)** was obtained from Marinus Thein and was later modified (Master thesis of Marinus Thein, Molecular Parasitology, University of Bayreuth, 2022). (Results of **(A)** and **(B)** have partially been published and were later modified (Jentzsch et al., 2020)).

The investigation of a third MAP, TbAIR9, was also carried out by Marinus Thein (Figure 17, modified (Master thesis of Marinus Thein, Molecular Parasitology, University of Bayreuth, 2022)). Therefore, he created a TLL6A-RNAi cell line, that expressed an endogenously tagged TbAIR9-mNG. TLL6A^{RNAi} cells that were not induced showed a uniform mNeon green signal throughout the cell body. After a knockdown of TLL6A, the signal was lost in the posterior protrusions of the cells that had a glove phenotype (Master thesis of Marinus Thein, Molecular Parasitology, University of Bayreuth, 2022).

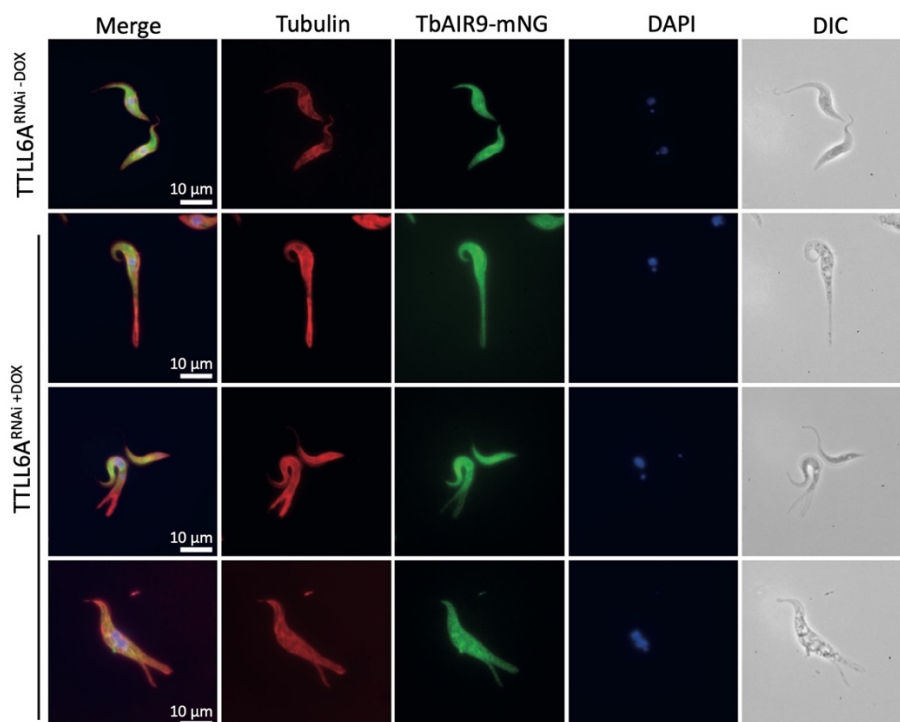


Figure 17: Loss of TbAIR9 in posterior gloves after depletion of TLL6A. Shown are the non-induced and induced TLL6A^{RNAi} cells, that expressed an endogenously tagged TbAIR9-mNG (green). Tubulin is shown in red and DNA in blue. The figure was obtained from Marinus Thein and was later modified (Master thesis of Marinus Thein, Molecular Parasitology, University of Bayreuth, 2022).

TLL6A and TLL12B have glutamylation activity within the flagellum

Since the flagellum of *T. brucei* is known to be highly glutamylated (Schneider, Plessmann and Weber, 1997), it was also of interest to investigate possible effects of a knockdown of TLL6A and TLL12B on the axoneme function.

For this purpose, the glutamylation pattern within the flagellum was examined. Cytoskeletons were stained with an anti-tubulin antibody, GT335 and PolyE. Their signal intensities were measured within a region of the flagellum, just behind the anterior end of the cell body (Figure

18A, results have been published (Jentzsch *et al.*, 2020)). The obtained data of GT335 and PolyE intensities were normalised against the signal of tubulin.

The results showed a significant decrease in the glutamylation level within the flagellum after depleting TLL6A or TLL12B (** $P < 0.001$, t-test). Only the PolyE signal of TLL6A^{RNAi} cells did not show a statistically significant decrease (Figure 18B, results have been published and were later modified (Jentzsch *et al.*, 2020)). When isolated flagella fractions were tested at the protein level, a reduction in the signal of GT335 and PolyE was confirmed (Figure 18C, results have been published and were later modified (Jentzsch *et al.*, 2020)).

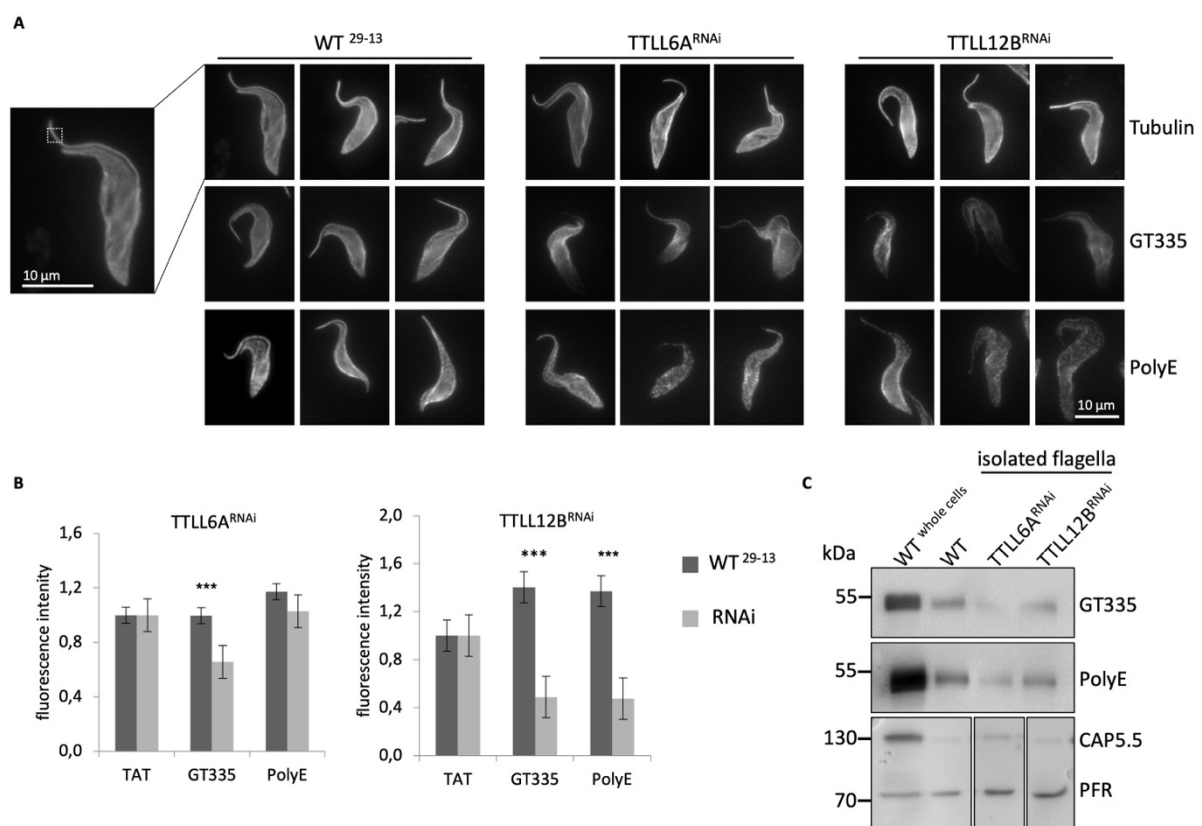


Figure 18: Decrease of glutamylation levels within the flagellum after the depletion of TLL6A or TLL12B. (A) Immunofluorescence of WT²⁹⁻¹³, TLL6A^{RNAi} and TLL12B^{RNAi} cells after two days induction. Cytoskeletons were stained with an anti-tubulin antibody, GT335 and PolyE. The fluorescence intensity of the flagellum was measured in all three staining, within the indicated region (box). (B) Quantification of the mean \pm s.e.m. fluorescence intensity. $n=16$ for WT²⁹⁻¹³ and RNAi cells. *** $P < 0.001$ (t-test). Error bars represent the standard error. Tubulin (TAT) served for normalisation. (C) Western blot of flagellar fractions of WT²⁹⁻¹³ and RNAi cells after two days induction. CAP5.5 and PFR served as controls. (Results have been published and were later modified (Jentzsch *et al.*, 2020)).

Depletion of TLL6A or TLL12B result in motility defects

To investigate the biological effects of a reduced glutamylation within the flagellum, the swimming behaviour of RNAi cells was analysed. For this purpose, living cells were monitored using bright field microscopy and individual cells were tracked resulting in single trajectories. These experiments were carried out in collaboration with Prof. Dr. Matthias Weiss, Dr. Adal Sabri and Konstantin Speckner (Experimental Physics I, University of Bayreuth).

First, a proof of principle experiment was conducted. For this purpose, procyclic cells were placed on untreated and on poly-L-lysine-treated coverslips and the swimming distance of the cells was recorded for a few minutes. According to the expectations, the cells on the treated coverslips should attach to them due to their surface charge. At first glance, the cells on untreated coverslips moved freely and in a straight line, whereas cells on the treated coverslips were attached to the surface as expected (Figure 19A).

The Mean square displacement (MSD) analysis is a method to determine the type of migration of particles that were tracked over time. It determines whether a particle is actively moving in a free space (super-diffusive), whether it is randomly moving and therefore freely diffusing (normal-diffusive), or whether it is restricted in its motion (sub-diffusive) (Figure 19B). The MSD is defined as $MSD = \langle \Delta r^2(\tau) \rangle = 2 * n * K_{\alpha} * \tau^{\alpha}$, with n being the dimension, K_{α} representing the diffusion coefficient and τ as the time scale over which the process is viewed. The movement patterns can be described by the anomaly parameter α , that represents the slope of the MSD in a logarithmically representation. Values of $\alpha = 1$ describe the normal-diffusive motion, $\alpha > 1$ describe an increase of the MSD-growth at large time scales (super-diffusive), $\alpha < 1$ describe a decrease of the MSD-growth at large time scales (sub-diffusive).

Evaluating an example as shown in Figure 19A, a movement pattern for WT²⁹⁻¹³ cells results in 73 % super-diffusive, 24 % normal-diffusive and 3 % sub-diffusive moving cells. In comparison, more than 50 % of the cells placed on the treated coverslips showed a sub-diffusive locomotion and 23 % of the cells did not migrate at all (confined).

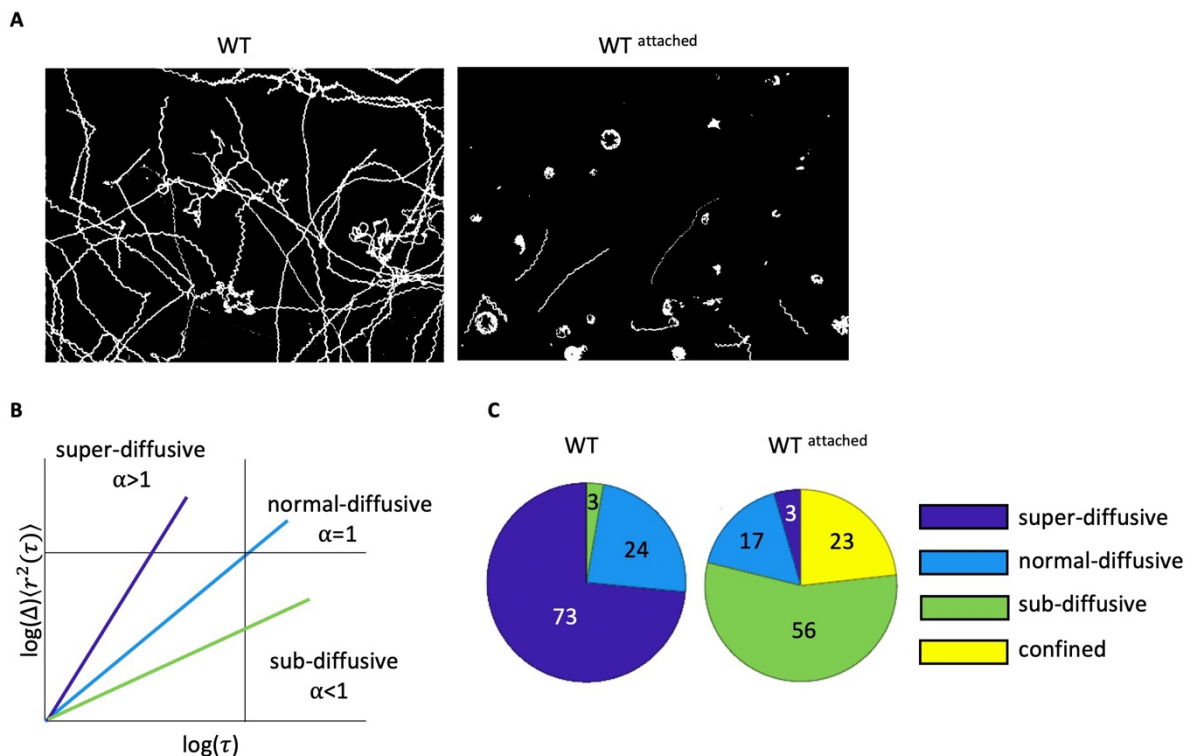


Figure 19: Principle of the analysis of the swimming behaviour of *T. brucei* cells. (A) Example of trajectories of WT^{29-13} cells and cells, that were attached to lysine-coated coverslips ($WT^{attached}$). (B) Schematic representation of the mean square displacement (MSD (Δ)) with α being the anomaly parameter. If $\alpha=1$ it describes the ordinary normal diffusion. If $\alpha>1$ the MSD-growth is increasing (super-diffusive). If $\alpha<1$ the MSD-growth is decreasing (sub-diffusive). (C) An example of an evaluation of the MSD of the experiment shown in (A). Numbers within the pie-charts show percentages.

With the aim of showing quantitative differences after a knockdown of TLL6A or TLL12B, the scaling exponent α of the mean square displacement was extracted for each of the recorded trajectories and all α -values of the respective cell lines were combined into a normalised histogram ($P(\alpha)$, i.e., probability density function (PDF)) (Figure 20A, D, G, results have been published (Jentzsch *et al.*, 2020)). For the parent cell line (Figure 20A, black bars, results have been published (Jentzsch *et al.*, 2020)), a PDF with a value of $\langle \alpha \rangle \approx 1.5$, was observed, clearly indicating a super-diffusive motion.

Consistent with the expectations, cells that had been attached to lysine-coated coverslips showed a highly significant shift of $P(\alpha)$ to smaller values around a mean $\langle \alpha \rangle \approx 0.5$ (Figure 20A, red bars, results have been published (Jentzsch *et al.*, 2020)). TLL6A and TLL12B RNAi cells without induction, resulted in only minor changes in $P(\alpha)$ compared with the parental cell line (Figure 20D, G, blue bars, results have been published (Jentzsch *et al.*, 2020)).

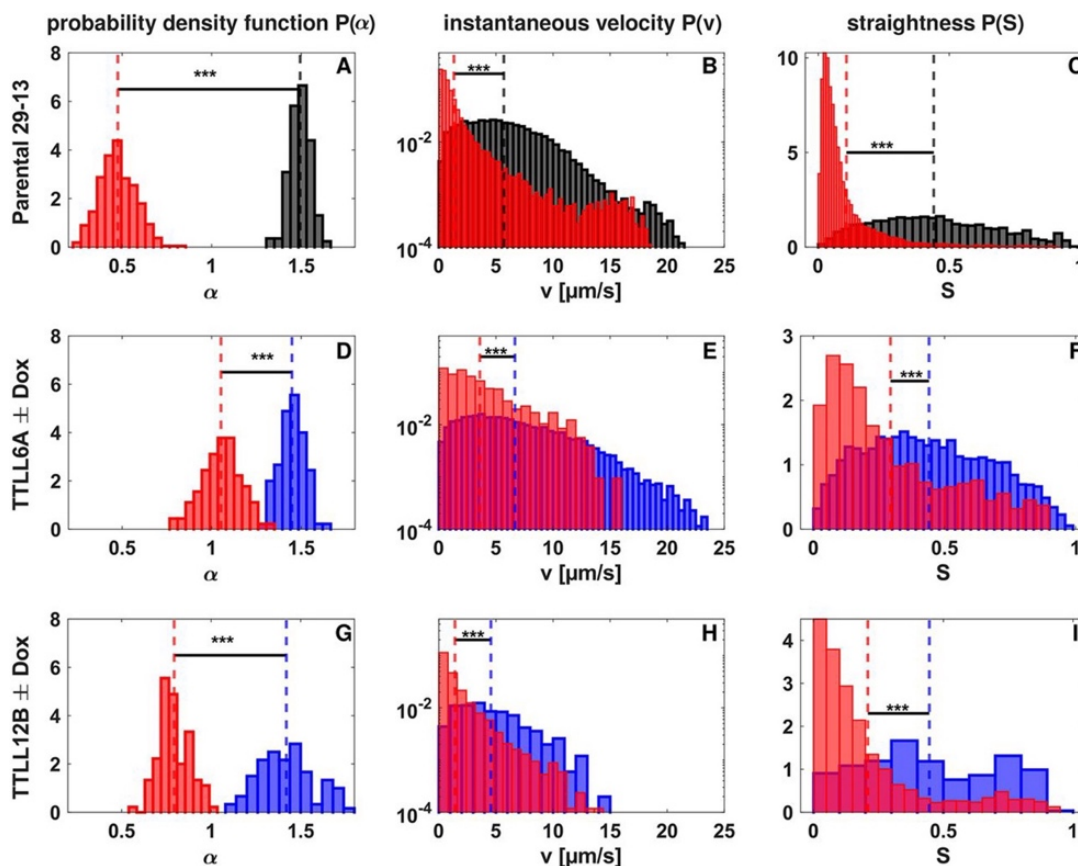


Figure 20: Motility defects after depletion of TLL6A or TLL12B. Probability density functions (PDF) of the mean square displacement of the trajectories, $P(\alpha)$ (left column), the velocity, $P(v)$ (middle column), and the straightness of the trajectories, $P(S)$ (right column). For cells of the parental cell line (A-C), highly significant changes were documented between freely moving cells (black histograms) and attached cells (red histograms). $TLL6A^{RNAi}$ (D-F) and $TLL12B^{RNAi}$ (G-I) cells without induction showed no changes in $P(\alpha)$ (blue histograms) compared to parental cells. After induction (red histograms), highly significant changes were observed. Similar changes were also observed for $P(v)$ and $P(S)$. The dashed vertical lines indicate the average value. *** $P < 0.001$ (Kolmogorov-Smirnov two-sample test). (Results have been published (Jentzsch et al., 2020)).

However, after RNAi induction, highly significant shifts to smaller α -values were observed. Depletion of TLL6A resulted in a pattern of cell movement close to normal diffusion ($\alpha = 1$), whereas TLL12B depleted cells even exhibited a significant sub-diffusive movement with an $\langle \alpha \rangle \approx 0.8$ (Figure 20D, G, red bars, results have been published (Jentzsch et al., 2020)). Thus, highly significant changes in the type of movement were observed after a depletion of TLL6A or TLL12B.

As a second parameter, the velocities $P(v)$ were plotted for the corresponding cell lines. As expected, a drastic change in $P(v)$ was observed when cells were placed on lysine-coated coverslips (Figure 20B, results have been published (Jentzsch et al., 2020)). As before, non-induced RNAi cells showed only minor changes, but when induced, depletion of TLL6A and

TLL12B resulted in highly significant changes in $P(v)$ (Figure 20E, H, results have been published (Jentsch *et al.*, 2020)).

The direction of movement of the cells was also analysed in more detail. This was measured by the straightness (S) of the trajectories. While unattached cells of the parental cell line showed movement with large values for straightness, $P(S)$ shifted to much smaller values after the attachment of cells to lysine-coated coverslips (Figure 20C, results have been published (Jentsch *et al.*, 2020)). The non-induced RNAi cell lines showed little difference from the parental cells, whereas induction resulted in a highly significant decrease in straightness values (Figure 20F, I, results have been published (Jentsch *et al.*, 2020)). Thus, depletion of TLL6A or TLL12B resulted not only in a decreased velocity of the cells and a decreased MSD-growth, but also resulted in fewer straight trajectories.

Characterisation of the putative polyglutamylase TTLL1

TTLL1 has glutamylation activity

In the second part of this work, it was investigated whether the putative polyglutamylase TTLL1 also functions similarly to TTLL6A and TTLL12B. Although an RNAi cell line against TTLL1 (knockdown of approximately 65 %, Figure 39) was already available, a cell line was generated in which TTLL1 was 100 % depleted. Therefore, a gene knockout was performed via the mechanism of homologous recombination.

The knockout was verified at DNA level via PCR. Therefore, primer pairs that bind in the homologous region of the 5'UTR (forward) and downstream of the 3'UTR (reverse) were used to confirm the correct localisation of the inserted knockout cassettes.

Both *ttl1* alleles have been successfully replaced by the knockout constructs. Since the two constructs differed in size by 100 bp, the cassettes appeared as one thick band (Figure 21A). To verify the knockout on the expression level, qPCR was performed. A full depletion could be detected as well (Figure 21B).

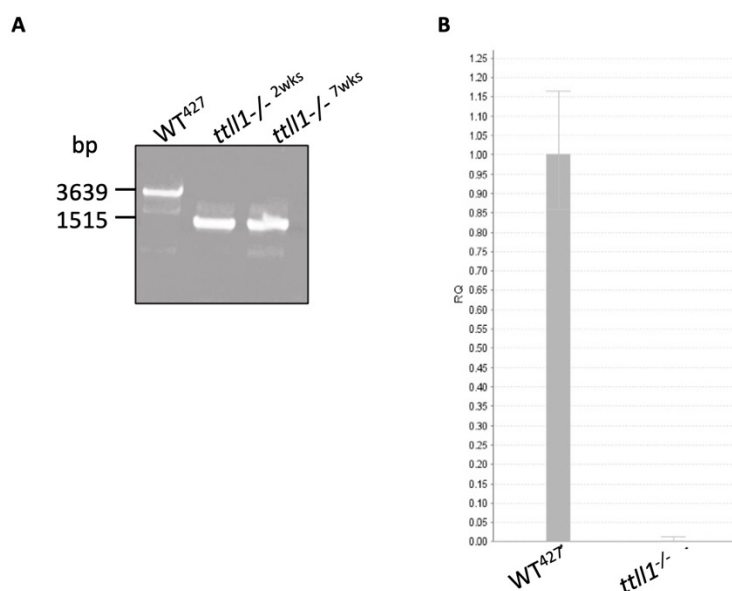


Figure 21: Gene knockout of *ttl1*. (A) PCR analysis of WT⁴²⁷ *ttl1* and knockout of both *ttl1* alleles. Cells after two weeks and seven weeks of TTLL1-depletion were analysed. wks=weeks (B) qPCR of the expression levels of WT⁴²⁷ TTLL1 and knockout cells. Error bars represent the standard deviation.

Consistent with the initial analyses for TLL6A and TLL12B, it was first examined at protein level whether TLL1 exhibited glutamylase activity.

It was shown that after the knockout of *ttl1*, the signals of GT335 and PolyE had become significantly weaker. For GT335 there was an average reduction of 50 % detected and for PolyE even an average reduction of 60 %. Analysis of the samples over several weeks showed that the reduction remained stable (Figure 22A and B). The antibody β -monoE can be used to specifically detect glutamate chains on β -tubulin (Figure 9A). However, after a knockout of *ttl1* no difference was seen in the glutamylation level of β -tubulin (Figure 22C).

Immunofluorescence confirmed the reduction in glutamate levels that were observed in the western blot analysis. To better illustrate the reduction, 20 % WT⁴²⁷ cells were mixed into the *ttl1*^{-/-} sample. It was clearly shown that *ttl1*^{-/-} cells have a weak staining (Figure 22D).

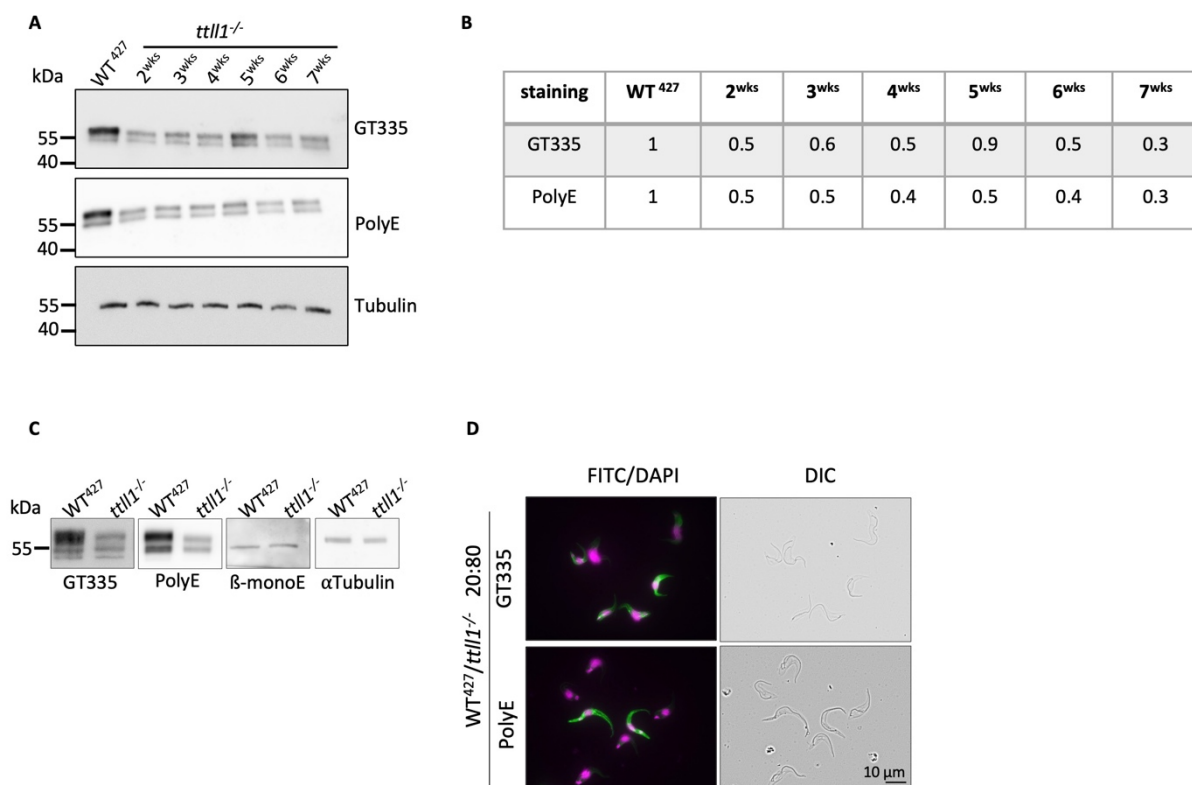


Figure 22: Reduced glutamylation signal after knockout of *ttl1*. (A) Western blot analysis of cytoskeletal fractions of WT⁴²⁷ and *ttl1*^{-/-} cells. Samples were taken over a period of seven weeks and probed with GT335 and PolyE. Tubulin served as a loading control. wks=weeks (B) Densitometric evaluation of (A). (C) Western blots of WT⁴²⁷ and *ttl1*^{-/-} cells. Cytoskeletons were additionally probed with β -monoE; an antibody that detects glutamylation specifically on β -tubulin. (D) Immunofluorescence of a mixture of WT⁴²⁷ and *ttl1*^{-/-} cells (20^{WT}: 80^{-/-}). Cytoskeletons were stained with either GT335 or PolyE (green). DNA was stained with DAPI (magenta).

Expansion microscopy was used to get a more detailed view of the glutamylation pattern and of cellular structures. It allowed a magnification of the cells of about four times. This made it possible to visualise structures like microtubules, basal bodies and even pro-basal bodies (Figure 23 and Figure 27).

After a double staining with the antibodies GT335 and PolyE, a reduction in each signal was visible, with a much greater reduction of PolyE. Additionally, different phenotypes of *TLL1*-depleted cells were observed (Figure 23).

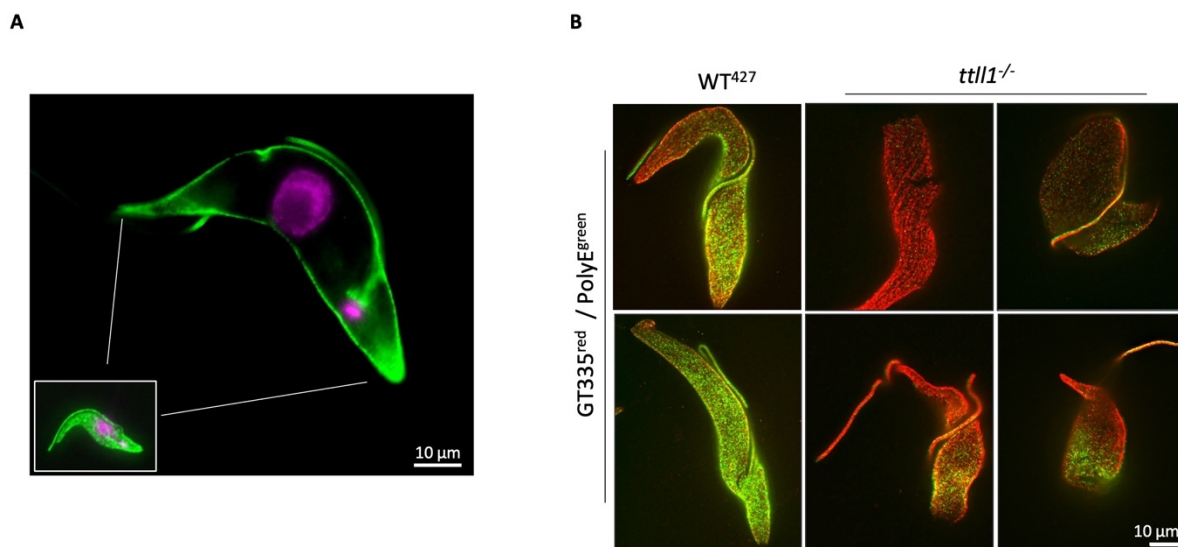


Figure 23: Expansion microscopy of *T. brucei*. (A) Example of a normal cell (bottom left) and an expanded cell. The scale is identical for both cells. Cells were stained with an anti-tubulin antibody (green) and DNA was stained with DAPI (magenta). (B) Expansion microscopy of WT⁴²⁷ and *ttl1*^{-/-} cells. Cells were stained with GT335 (red) and PolyE (green). Images of (A) and (B) were 2D-deconvoluted.

A knockout of *ttl1* results in abnormal morphology and cytokinesis defects

A knockout of *ttl1* also influenced the cell morphology. Cells with a truncated posterior tip were observed and occurred in more than 95 % of the *ttl1*^{-/-} cell population.

Since this phenotype was not observed in previous publications, it was termed in this work as 'blunt cells' and was classified as cells with a posterior end that is wider than 0.8 μm (Figure 24A and B).

The tip width of *ttl1*^{-/-} cells was measured over a period of seven weeks. Most cells had a tip that was wider than 0.8 μm with an average width of approximately 1.3 μm (Figure 24B). In addition, the *ttl1*^{-/-} cells were smaller in average size (Figure 24C).

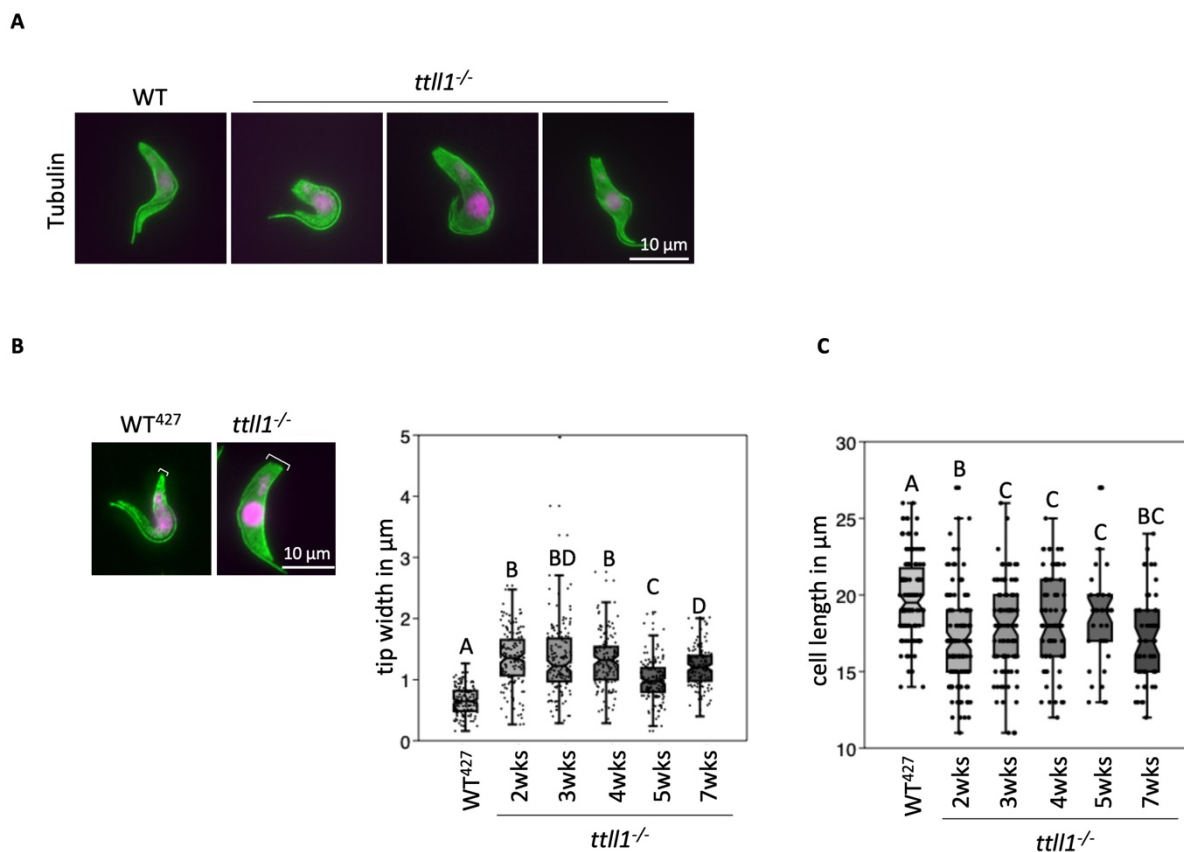


Figure 24: A knockout of *ttl1* causes a truncated posterior tip. (A) Immunofluorescence of WT⁴²⁷ and *ttl1*^{-/-} cells. Cytoskeletons were stained with an anti-tubulin antibody (green). DNA was stained with DAPI (magenta). (B) Measured tip width of WT⁴²⁷ and *ttl1*^{-/-} cells. The posterior tip width of G1 cells was measured as indicated in the figure to the left. The cells were analysed over a period of seven weeks. Box and jitter plots show mean values and single data points respectively. Statistical significance between groups is indicated by different letters ($P < 0.05$). Error bars represent the standard deviation. wks=weeks (C) Measured cell length of WT⁴²⁷ and *ttl1*^{-/-} cells. The length of G1 cells was measured from the posterior cell tip to the anterior cell end through the nucleus. Cells were analysed over a period of seven weeks. Box and jitter plot shows single data points. Notches represent the mean values. Statistical significance between groups is indicated by different letters. Error bars represent the standard deviation. wks=weeks.

For the ultrastructural investigation of the posterior tip of *ttl1*^{-/-} cells, electron microscopy was performed. The images show that the microtubules of the posterior end, although still highly ordered, were not clustered in a pointed tip (Figure 25A). This is different from the frazzled cell tip that was observed in TLL6A and TLL12B RNAi-depleted cells.

Normally, the posterior end of the cells is a slightly open structure, the so-called 'open-pipe' (Hemphill, Lawson and Seebeck, 1991). Cells that had a blunt tip appeared to have an open-pipe structure with a larger diameter (Figure 25B).

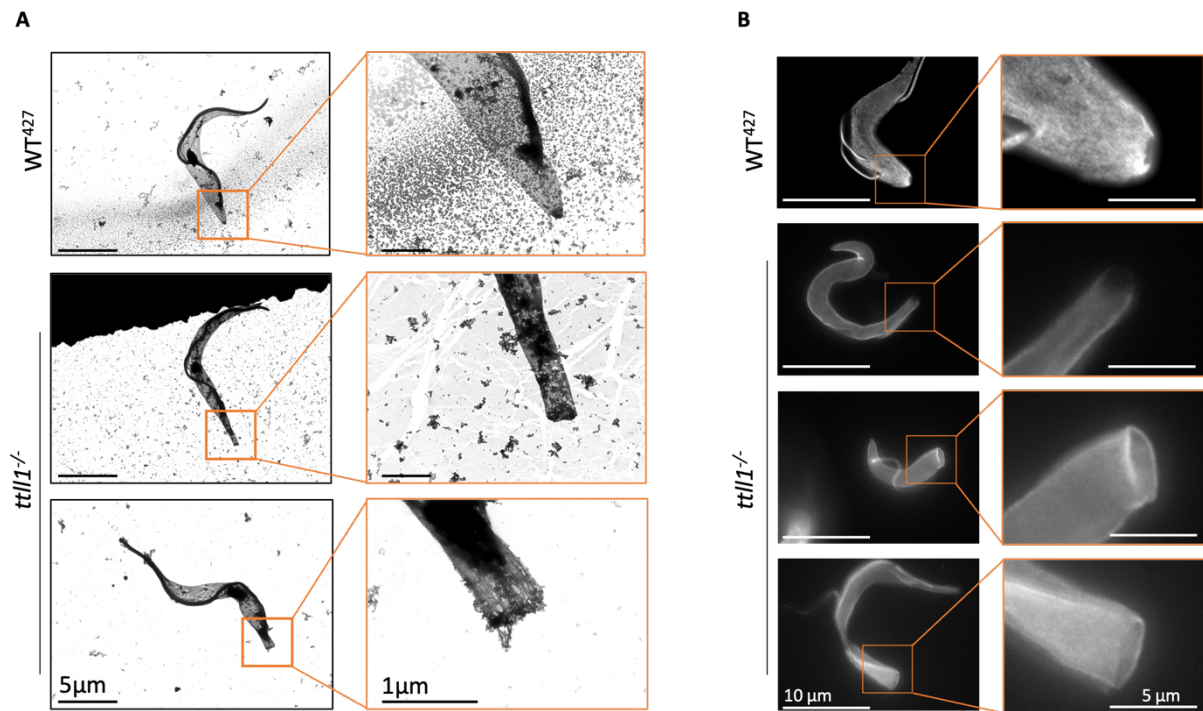


Figure 25: Ultrastructure of posterior cell tips. (A) Electron microscopy of whole mount cytoskeletons and (B) Expansion microscopy of WT⁴²⁷ and ttll1^{-/-} cells. Cells for immunofluorescence were stained with an anti-tubulin antibody. Images were 2D-deconvoluted.

Furthermore, a knockout inhibited the growth of the cells (Figure 26A). Therefore, growth curves were generated. Three biological replicates of the respective cell lines were cultivated for six days, and samples were taken. Each sample was measured three times. The mean values of the biological and technical replicates were represented in cumulative growth curves that were plotted logarithmically.

Additionally, cytokinesis defects could be observed, that were reflected in an increase of anucleate (zoids) and multinucleate cells ($\geq 3N$) (Figure 26B). This was also confirmed by flow cytometry (Figure 26C). Cells which had been three weeks depleted of TTLL1 showed a strong peak in zoids and an increase of multinucleated cells. Defects in cytokinesis were also evident in immunofluorescence by the appearance of cells with multiple flagella and cells with multiple basal bodies (Figure 26D, E, F).

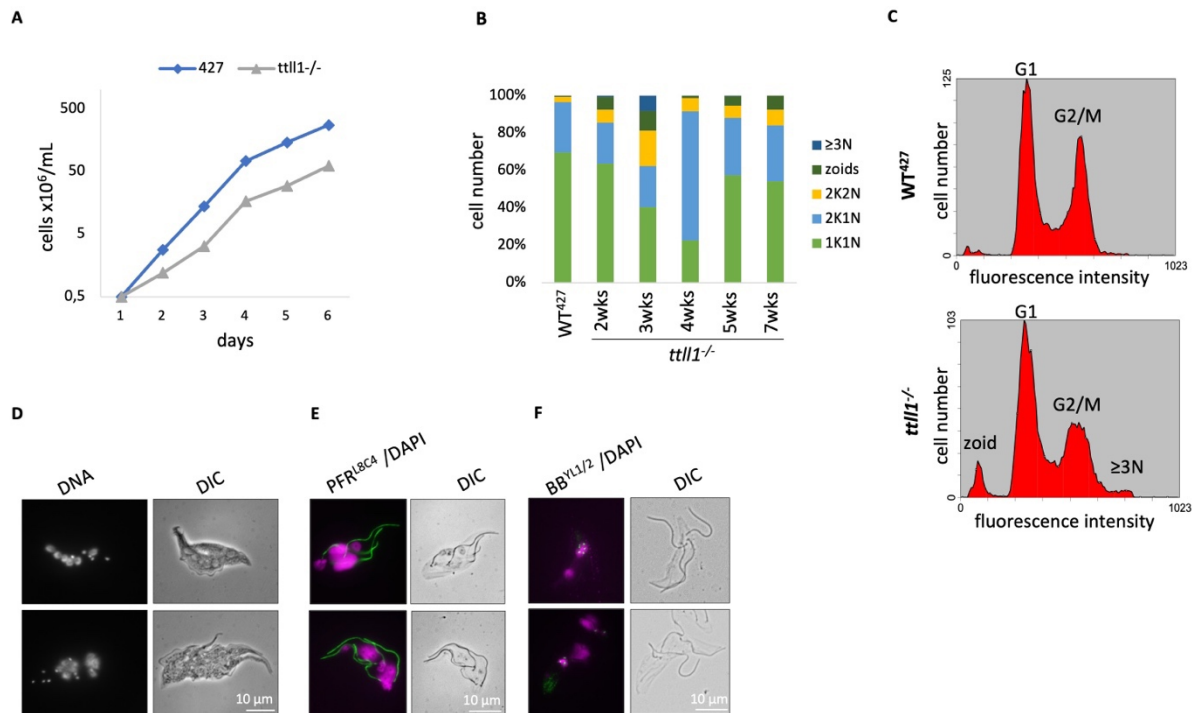


Figure 26: Growth and cytokinesis defects after a knockout of *ttll1*. (A) Cumulative growth curves of WT⁴²⁷ and *ttll1*^{-/-} cells. Each data point corresponds to the mean of three biological replicates, that were measured three times each. The data were plotted logarithmically (B) Percentages of WT⁴²⁷ and *ttll1*^{-/-} cells with different cell cycle stages. wks=weeks. Zoids correspond to cells without nuclei (N) or kinetoplast DNA (K) and ≥3N corresponds to cells with more than two nuclei or kinetoplasts. WT(n)=250 cells; 2wks(n)=250 cells; 3wks(n)=265 cells; 4wks(n)=305 cells, 5wks(n)=457 cells, 7wks(n)=288 cells. (C) Flow cytometry of WT⁴²⁷ and *ttll1*^{-/-} cells after three weeks depletion of TLL1. Cells were stained with propidium iodide. (D) Example of *ttll1*^{-/-} cells with multiple nuclei. DNA was stained with DAPI. (E) Immunofluorescence of *ttll1*^{-/-} cells. Cytoskeletons were stained with L8C4 (green), an antibody that detects the paraflagellar rod (PFR). DNA was stained with DAPI (magenta). (F) Immunofluorescence of *ttll1*^{-/-} cells. Cytoskeletons were stained with YL1/2 (green), an antibody that detects the basal bodies (BB). DNA was stained with DAPI (magenta).

Visualisation of newly polymerized microtubules after TTLL1 depletion

To investigate whether the depletion of TTLL1 has similar effects on the microtubule polymerization like the RNAi-mediated depletion of TTLL6A and TTLL12B, *ttl1*^{-/-} cells were stained with YL1/2 and visualised by immunofluorescence.

This experiment was performed on expanded cells. In contrast to TTLL6A- and TTLL12B-depleted cells, which showed a significant increase of the YL1/2 signal, TTLL1-depleted cells only had a slight increase in the signal compared to the WT⁴²⁷ (Figure 27). However, the expansion of the cells made it possible to visualise single microtubules at the posterior end of *ttl1*^{-/-} cells.

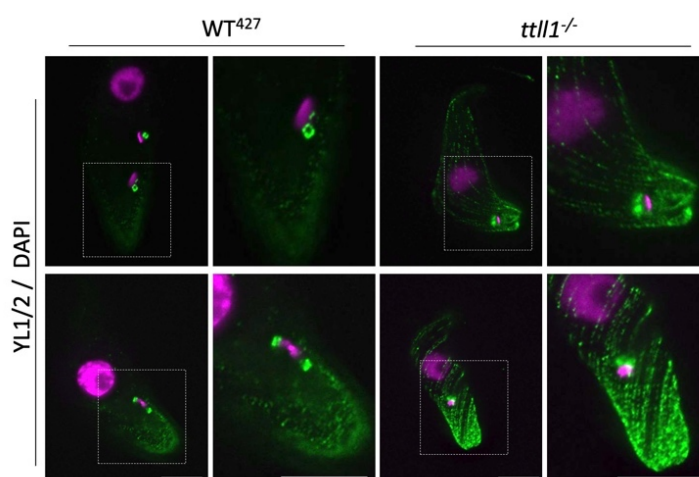


Figure 27: Increase of newly polymerized microtubules in *ttl1*^{-/-} cells. Expansion microscopy of WT⁴²⁷ and *ttl1*^{-/-} cells. Cells were stained with YL1/2 (detects tyrosinated α -tubulin, green). DNA was stained with DAPI (magenta). Images were 2D-deconvoluted. Scale bar=10 μ m.

Binding of MAPs after *ttl1* knockout

Similar to the experiments that were performed with TTLL6A and TTLL12B RNAi-depleted cells, the binding of MAPs in cells that were depleted of TTLL1 was investigated. For this purpose, the plus-end binding proteins EB1 and XMAP215 were analysed. The analysis of the endogenously tagged mNG-XMAP in *ttl1*^{-/-} cells was carried out by Marinus Thein (the corresponding *ttl1*^{-/-} cell line was the same as that generated in this thesis).

EB1 was still present at the posterior end of *ttl1*^{-/-} cells. But it was distributed across the blunt tip (Figure 28A). TTL1-depleted cells that expressed an endogenously tagged mNG-XMAP215 showed no loss of the signal.

Like EB1, mNG-XMAP215 appeared in an elongated signal compared to the WT⁴²⁷ (Figure 28A lower panels, results were obtained from Marinus Thein, Molecular Parasitology, University of Bayreuth, 2022).

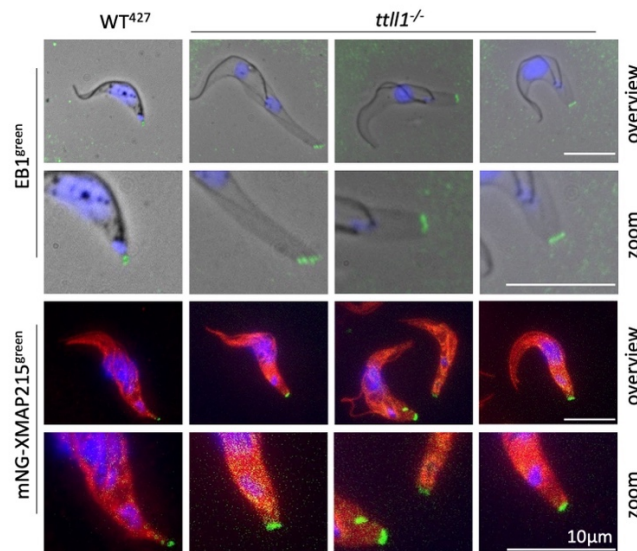


Figure 28: Binding of EB1 and mNG-XMAP215 in *ttl1*^{-/-} cells. Immunofluorescence of cytoskeletons of WT⁴²⁷ and *ttl1*^{-/-} cells. Upper two panels: *ttl1*^{-/-} cells were stained with anti-EB1 (green). DNA was stained with DAPI (blue). Lower panels: *ttl1*^{-/-} cells express an endogenously tagged mNG-XMAP215 (green). Cells were stained with anti-tubulin (red). DNA was stained with DAPI (blue). Images of the endogenously tagged cell line were obtained from Marinus Thein and modified (Marinus Thein, Molecular Parasitology, University of Bayreuth, 2022).

Effects of a *ttl1* knockout on the flagellum

It was noticed that the flagellum of the *ttl1*^{-/-} cells seemed to be longer than the WT⁴²⁷ flagella. After measuring the length of the single flagellum of 1K1N cells, this observation could be confirmed (Figure 29A).

After two and three weeks of TTL1-depletion the flagella had an average length of 20 µm in comparison to the WT flagella, which had an average length of approximately 18 µm.

To determine possible changes in the glutamylation level of the axoneme, flagella were isolated and subsequently analysed by western blot. The success of the isolation was demonstrated via SDS-PAGE and western blot using PFR as a control (Figure 29B I and II).

The analysis of the flagellar fractions with the antibodies GT335 and PolyE showed a reduction of both signal in TTL1-depleted cells (Figure 29B, on the left).

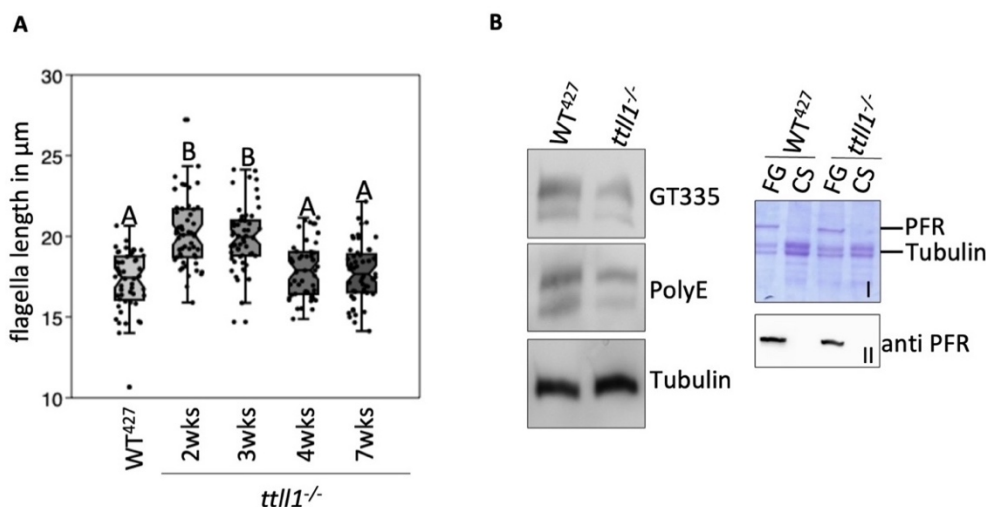


Figure 29: A knockout of *ttl1* affects the length of the flagellum and the degree of glutamylation within the flagellum. (A) Analysis of the length of the single flagellum of G1 WT⁴²⁷ and *ttl1*^{-/-} cells. Cells over a period of seven weeks were analysed. Box and jitter plots show mean values and single data points respectively. Statistical significance between groups is indicated by different letters ($P < 0.05$). Error bars represent the standard deviation. wks=weeks **(B)** Western blot of isolated flagella. Samples were probed with the antibodies GT335 and PolyE. Tubulin served as a loading control. I= Coomassie gel to show the success of the flagella isolation. II= western blot of the samples probed with PFR to verify flagellar fractions.

In a next step the glutamylation pattern within the flagellum was analysed. For this purpose, expanded cells were co-stained with GT335 and PolyE. In WT⁴²⁷ cells, the axoneme was uniformly stained with both antibodies. After a knockout of *ttl1*, the polyE signal was much more concentrated on one side of the axoneme, while the opposite side was almost lacking signal. (Figure 30A). This was also seen in cells, that were co-stained with an anti-tubulin antibody (Figure 30B).

To better visualise this altered distribution, the signal intensities were evaluated. Therefore, a rectangle with a length of 10 μm and a width of 3 μm was placed on a straight area of the flagellum and the signal intensity within this rectangle was plotted (Figure 30A and B, analysed area is indicated with white rectangles, analysis was done by Hannes Wunderlich, collaboration with Experimental Physics I, University of Bayreuth).

For WT⁴²⁷ cells it was shown, that GT335 was distributed over approximately 2 μm (Figure 30A I and II). In cells depleted of TLL1 the signal is enriched to one site of the flagellum (Figure 30A III and IV). This was also seen for the PolyE signal, but to a weaker extent (Figure 30A III and IV).

However, the shift of the PolyE signal was clearly visible when the cells were co-stained with an anti-tubulin antibody (Figure 30B I-IV).

To localise on which side of the axoneme the PolyE signal was accumulated, an additional staining of the PFR was performed.

This co-staining of PolyE and PFR showed, that PolyE is located directly adjacent to the PFR signal (Figure 30C, left). This indicates an accumulation of long glutamate chains between the microtubule duplets 4-7 in *ttl1*^{-/-} cells (Figure 30C and D).

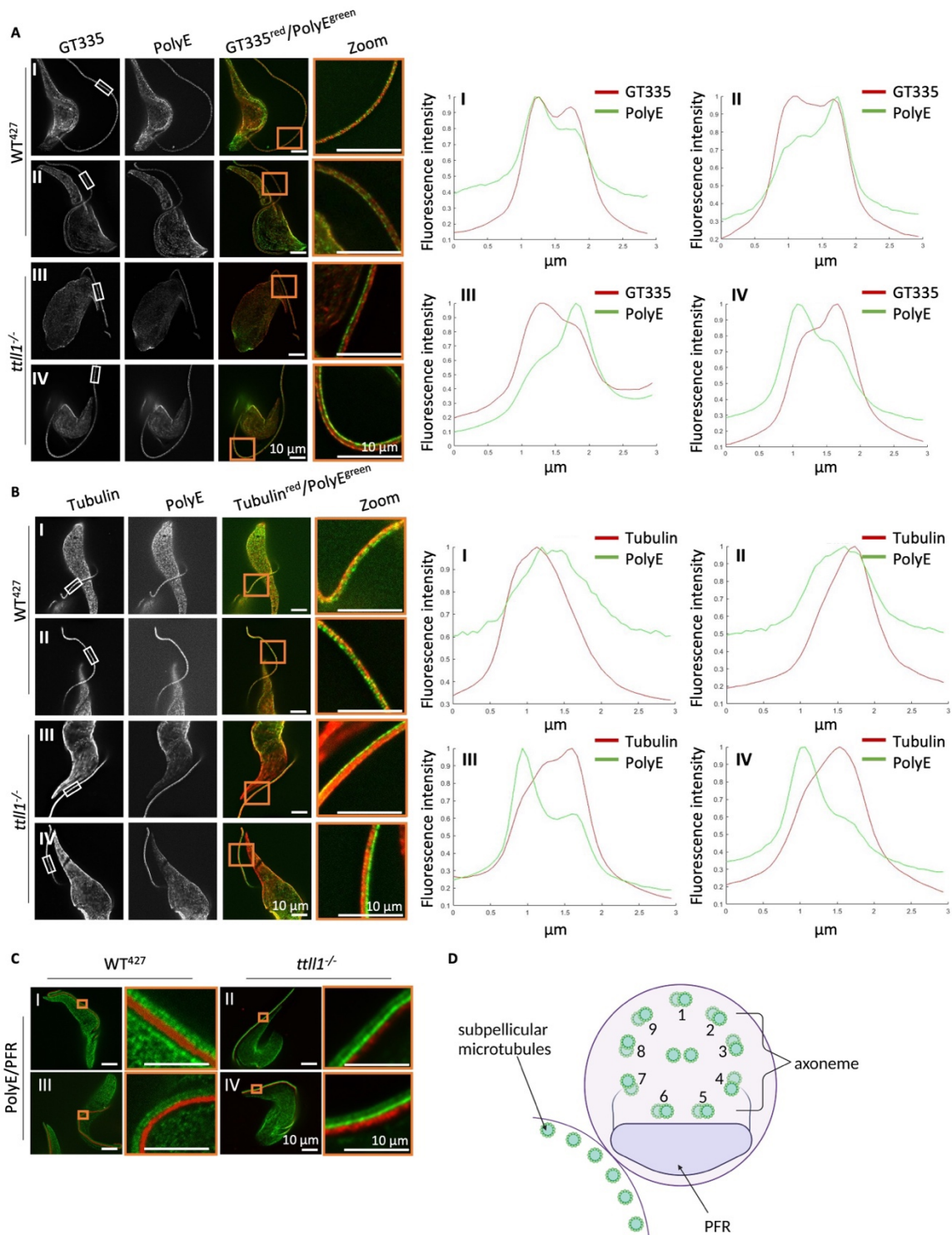


Figure 30: Accumulation of long glutamyl chains on one side within the flagellum after depletion of *TLL1*. Expansion microscopy of WT^{427} and $ttl1^{-/-}$ cells after staining with **(A)** GT335 (red) and PolyE (green), **(B)** anti-tubulin (red) and PolyE (green) and **(C)** PFR (red) and PolyE (green). Orange rectangles show a detailed view of flagellar regions. **(I)-(IV)** Quantification of signal intensities in areas indicated with white rectangles of the corresponding staining. **(D)** Schematic representation of a cross-section of *T. brucei*. Figure **(D)** was created with BioRender.com.

Based on these observations, it was further analysed if there were any abnormalities within the ultrastructure of the flagellum in *ttl1*^{-/-} cells. Therefore, cross-sections of the cells were examined by electron microscopy.

This was done by Julia Bechthold, a master student of mine. Apparently, there was no evidence of any abnormalities within the axoneme or the cytoskeletal microtubules (Figure 31) (results obtained from Julia Bechthold, Molecular Parasitology, University of Bayreuth, 2022).

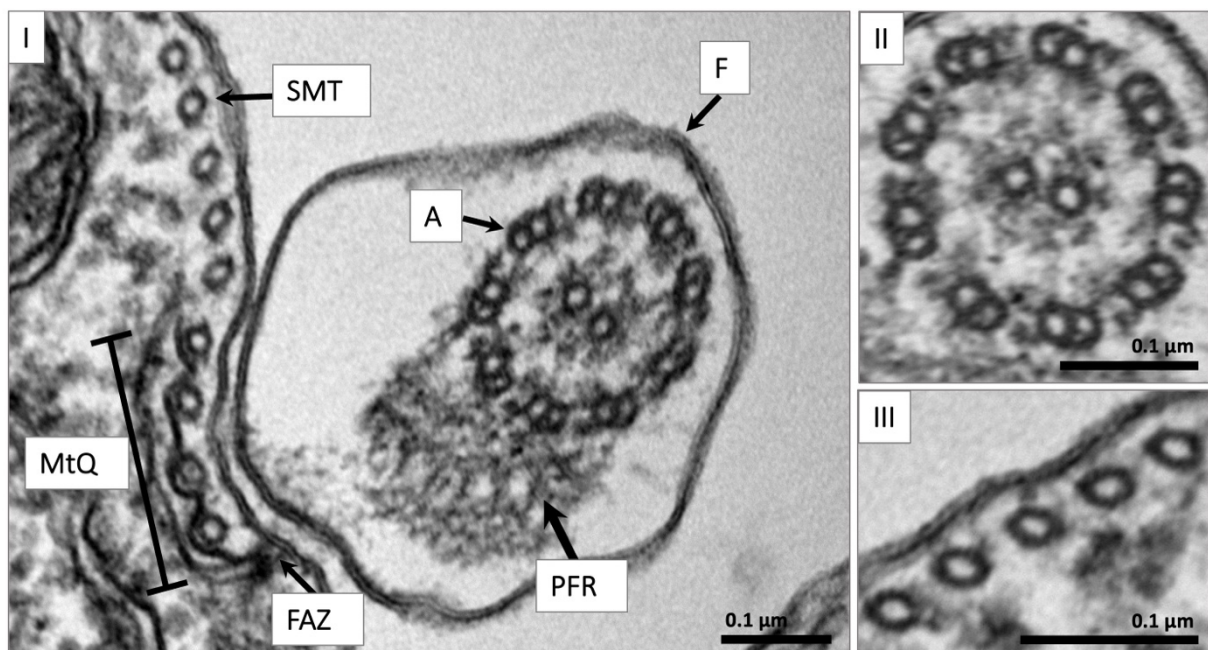


Figure 31: Ultrastructure of the flagellum of *ttl1*^{-/-} cells. (I) Electron micrograph of a cross-section of a *ttl1*^{-/-} cell showing the flagellum (F), subpellicular microtubules (SMT), axoneme (Ai), paraflagellar rod (PFR), flagellar attachment zone (FAZ) and the microtubule quartet (MtQ). (II) and (III) show the axoneme and SMT structure in detail. Results were obtained from Julia Bechthold (Molecular Parasitology, University of Bayreuth, 2022).

Add back of TTLL1 leads to a rescue of the knockout

To test whether the effects of the knockout of *ttll1* are reversible, an add-back experiment was performed. Therefore, a C-terminal 2xmyc-tagged TTLL1 full-length was ectopically expressed in *ttll1*^{-/-} cells. Since the parental cell line (PC427) lacks the T7 polymerase and the Tet operator, which makes an inducible expression not possible, TTLL1-full-length^{c-term 2xmyc} was inserted in a tubulin locus.

Expression success was verified by qPCR (Figure 32A) and by western blot using an anti-myc antibody (Figure 32B).

A comparison of *ttll1*^{-/-} cells and *ttll1*^{-/-} cells that contain the rescue construct showed, that the expression of TTLL1-full-length^{c-term2xmyc} caused a regression of the observed morphological abnormalities that were detected after a depletion of TTLL1. After measuring the width of the posterior tip of the cells, the rescued cells had a significantly narrower posterior end ($P < 0.05$), which was again comparable to that of the WT⁴²⁷ cells (Figure 32C and D).

EB1 was analysed as a second indicator showing the regression of the blunt phenotype. Cells expressing TTLL1-full-length^{c-term2xmyc} showed an EB1 signal as a bundled signal at the posterior tip of the cells (Figure 32C).

Cells that were depleted of TTLL1 showed a significantly decreased glutamylation level. To investigate whether a rescue of the knockout causes an increase in the degree of microtubule glutamylation, cytoskeletal preparations of cells expressing TTLL1-full-length^{c-term2xmyc} were analysed by western blot and probed with the antibodies GT335 and PolyE (Figure 32B).

Comparing *ttll1*^{-/-} cells with cells that expressed the rescue construct a slight increase in the signal was shown, but there was no full recovery of the glutamylation levels.

It was also of interest to see if the observed growth defect, that was caused by the *ttll1* knockout, can be rescued.

The curves showed that after the expression of TTLL1-full-length^{c-term2xmyc} the cells had a normal growth (Figure 32E).

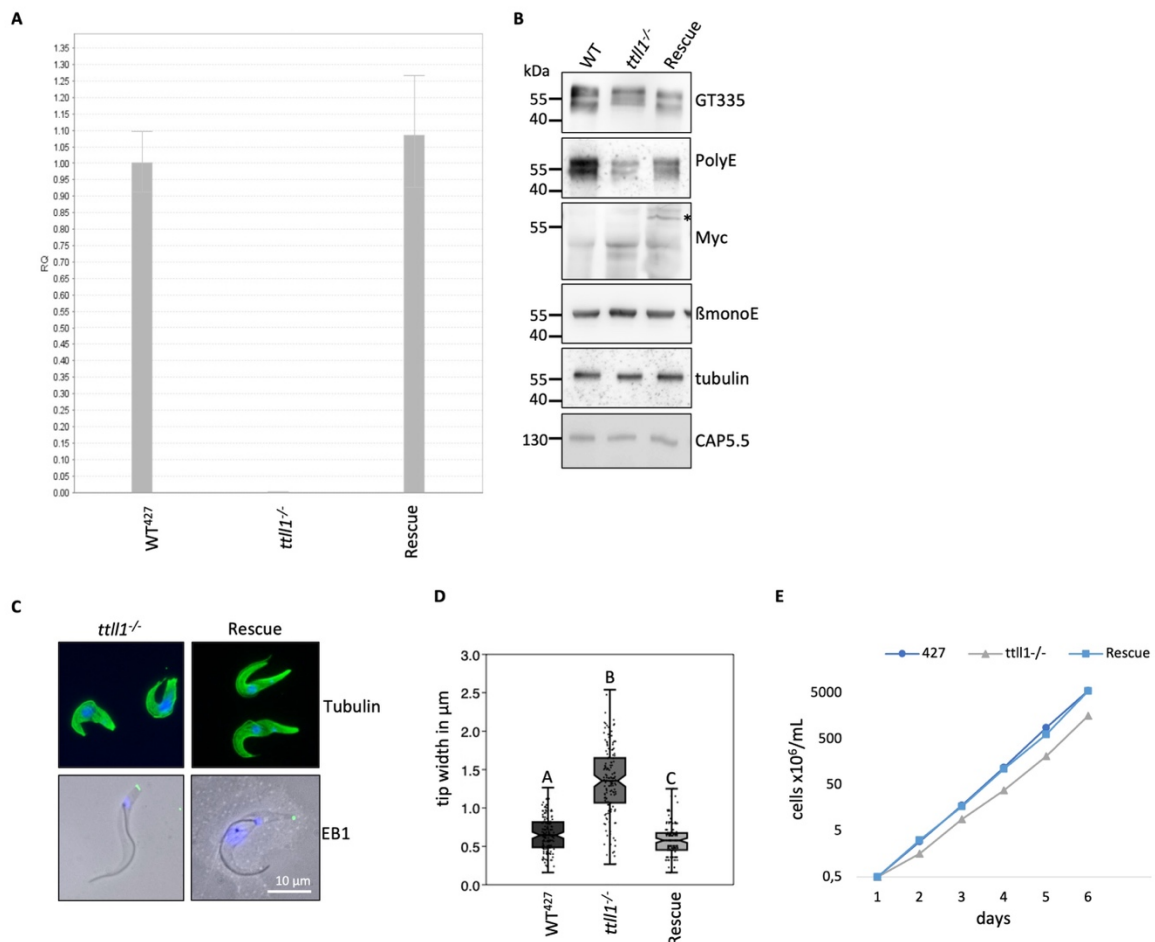


Figure 32: Rescue of *ttll1* knockout. (A) Quantification of mRNA levels by qPCR. Error bars represent the standard deviation. (B) Western blot of cytoskeletal preparations of the respective cell lines. Tubulin and CAP5.5 served as loading controls. Asterisks indicate the expressed TLL1-full-length^{C-term2xmyc}. (C) Immunofluorescence of cytoskeletons of *ttll1*^{-/-} cells knockout cells expressing TLL1-full-length^{C-term2xmyc}. Cells were stained with an anti-tubulin antibody (green, upper images) and anti-EB1 (green, lower images). DNA was stained with DAPI (blue). (D) Analysis of the width of the posterior end of the corresponding cell lines. Box and jitter plots show mean values and single data points respectively. Statistical significance between groups is indicated by different letters ($P < 0.05$). Error bars represent the standard deviation (E) Cumulative growth curves of the respective cell lines. Each data point corresponds to the mean of three biological replicates, each measured three times. The data were plotted logarithmically.

Overexpression of TLL1

Possible effects of an overexpression of TLL1 in cells was investigated. For this purpose, a C-terminal 2xmyc tagged TLL1-full length was ectopically overexpressed in a *T. brucei* cell line, which contain the T7 polymerase and the Tet-operator, thus capable of inducible expression (PC449).

First the success of TLL1^{myc}-overexpression was verified by qPCR (Figure 33A). The results showed that an induction of ectopic expression resulted in a significant increase of the mRNA levels. After the induction of TLL1^{myc} expression, it was clearly seen that the cells became significantly longer, in contrast to WT⁴⁴⁹ cells (Figure 33B and C, ***P<0.001). The tip of the posterior end was significantly wider with an average width of 1 μ m (Figure 33D, ***P<0.01). Because of that the cells were classified to the blunt phenotype.

Also, the length of the flagellum differed significantly from the WT⁴⁴⁹. The flagellum was not significantly longer, as seen in TLL1-depleted cells, instead the length was significantly more dispersed (Figure 33E).

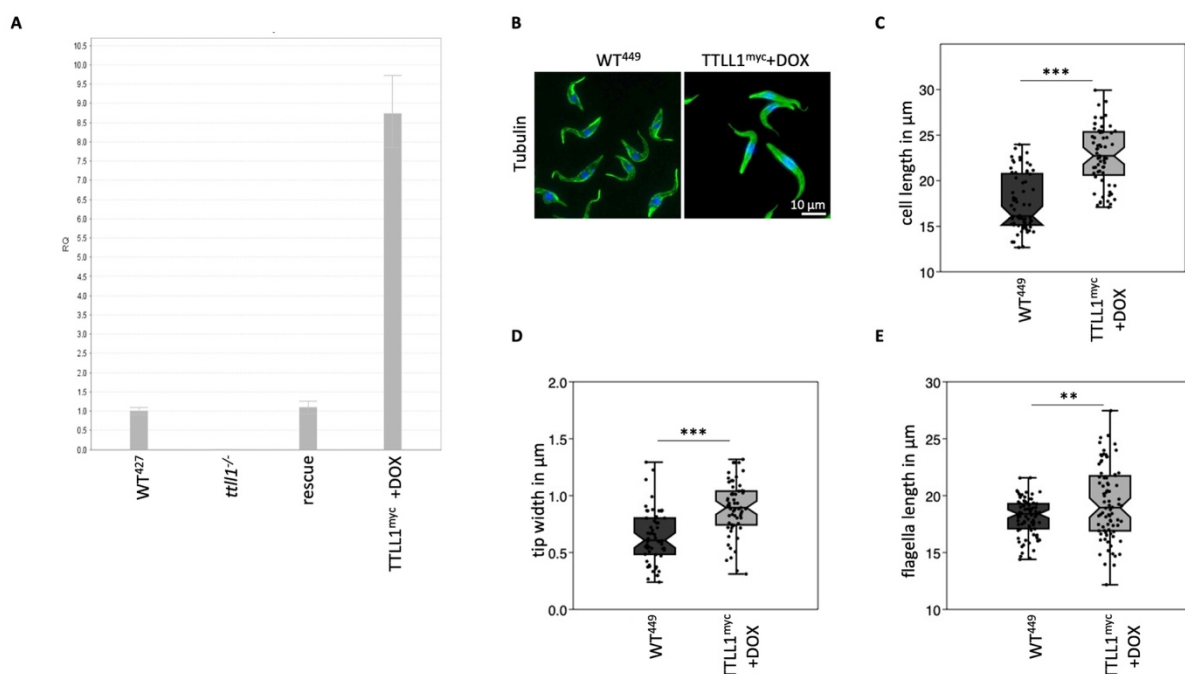


Figure 33: Morphological changes after overexpression of TLL1^{myc}. (A) Quantification of mRNA levels by qPCR. Error bars represent the standard deviation. (B) Immunofluorescence of WT⁴⁴⁹ cells and cells after induction of TLL1 expression for three days (C) cell length, (D) tip width and (E) flagella length. Box and jitter plots show mean values and single data points respectively. Statistical significance is shown by asterisks (***P<0.001, **P<0.01). Error bars represent the standard deviation.

Since it was shown in this work that TLL1 has a glutamylation activity it was of interest if there was an increase in the glutamylation level after the overexpression of TLL1^{myc}. Therefore, western blot analysis was performed and samples of cells that expressed TLL1^{myc} over a period of three days were probed with GT335 and PolyE.

The results showed that after three days of induction, the signal of GT335 and PolyE increased whereby PolyE increased strongly. The overexpression of $TLL1^{myc}$ was verified via the detection of the myc-tag (Figure 34A).

Cells overexpressing $TLL1^{myc}$ showed an inhibited growth (Figure 34B) and cytokinesis defects, as an increase of zoids and multinucleated cells was observed (Figure 34C).

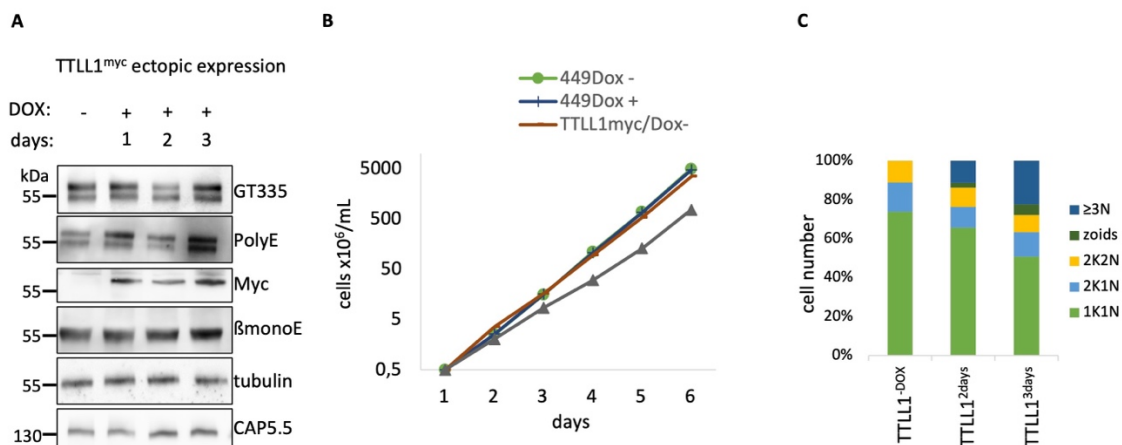


Figure 34: Increased glutamylation levels and inhibited growth of the cells after the overexpression of $TLL1^{myc}$. (A) Western blot of cytoskeletal preparations of cells overexpressing $TLL1^{myc}$. Tubulin and CAP5.5 served as loading controls. (B) Cumulative growth curves of the respective cell lines. Each data point corresponds to the mean of three biological replicates, each measured three times. Data were plotted logarithmically. (C) Percentages of different cell cycle stages of not-induced $TLL1^{DOX}$ cells and cells that overexpressed $TLL1^{myc}$ for two and three days. Zoids correspond to cells without nuclei (N) or kinetoplast DNA (K) and $\geq 3N$ corresponds to cells with more than two nuclei or kinetoplasts. $TLL1^{DOX}$ (n)= 245 cells; $TLL1^{2days}$ (n)=160 cells; $TLL1^{3days}$ (n)= 265 cells; 4(n)= 183 cells.

Swim velocity of *ttl1*^{-/-} and TTLL1-overexpressing cells

Reduced cell mobility was observed in both cell lines, the one that was depleted of TTLL1 and the one that ectopically overexpressed TTLL1. The corresponding motility analysis was performed in cooperation with Hannes Wunderlich (Experimental Physics I, University of Bayreuth).

While WT⁴²⁷ cells moved at a speed of 3.67 $\mu\text{m/s}$, cells lacking TTLL1 moved at a slower speed of 2.87 $\mu\text{m/s}$. A rescue of the *ttl1* knockout resulted in an increase in swimming speed to 4 $\mu\text{m/s}$, which was similar to the WT⁴²⁷. The effect of an overexpression of TTLL1^{+DOX}, however, had no effect in the motility of the cells compared to the corresponding WT⁴⁴⁹ and the non-induced TTLL1^{-DOX} cell line.

Table 3: Swim velocities of TTLL1-manipulated cells. Data were collected in collaboration with Hannes Wunderlich (Experimental Physics I, University of Bayreuth)

Cell line	velocity
WT ⁴²⁷	3.67 $\mu\text{m/s}$
<i>ttl1</i> ^{-/-}	2.87 $\mu\text{m/s}$
<i>ttl1</i> ^{-/-} rescue	4.05 $\mu\text{m/s}$
WT ⁴⁴⁹	5.07 $\mu\text{m/s}$
TTLL1 -DOX	5.26 $\mu\text{m/s}$
TTLL1 +DOX	4.99 $\mu\text{m/s}$

Discussion

The subpellicular cytoskeleton of *T. brucei* is a highly ordered array of parallel organised microtubules, that is localised underneath the plasma membrane. It is a key structure that gives the cell its shape and elasticity (Sinclair and de Graffenried, 2019). It differs from the highly dynamic microtubule cytoskeleton of mammalian cells in being extremely stable. This makes the cytoskeleton of the parasite unique.

However, during its life cycle, the parasite undergoes several morphological changes that require the new arrangement of the cytoskeleton, such as the semiconservative duplication of cytoskeletal microtubules during cell division, a change in the positioning of organelles, as well as a different movement of the cells (Sherwin and Gull, 1989; Robinson and Gull, 1991; Matthews, Sherwin and Gull, 1995; Robinson *et al.*, 1995). To allow such substantial changes, the very stable cytoskeleton must have a certain remodelling capacity. It is unclear how this interplay between stability and flexibility is regulated in *T. brucei*. Microtubule properties could be altered by the parasites unique set of cytoskeleton-associated proteins or by post-translational modifications (PTMs) (Westermann and Weber, 2003; Janke, 2014; Sinclair and de Graffenried, 2019).

Many enzymes involved in PTMs of tubulin are conserved in a variety of organisms including trypanosomes. One of the largest groups is represented by the tubulin tyrosine ligase-like (TTLL) enzymes (Janke *et al.*, 2005), which were originally defined by a conserved amino acid sequence domain that they share with the founding member of this family, the tubulin tyrosine-ligase (TTL) (Ersfeld *et al.*, 1993; van Dijk *et al.*, 2007).

As part of the detyrosination-tyrosination cycle, TTL catalyses the attachment of a tyrosine residue to the C-terminal end of α -tubulin, whereas the other proteins are either polyglycyclases or polyglutamylases (Janke, 2014). Glycylation has not been identified in *T. brucei*, however, using mass spectrometry it was shown that the cytoskeleton and the flagellum of trypanosomes are highly glutamylated (Schneider, Plessmann and Weber, 1997). Based on sequence homologies eight TTLLs were identified in the parasite (Casanova *et al.*, 2015).

In this study, three *T. brucei* homologs of the TTL family, TTL6A, TTL12B, and TTL1, were characterised. Enzymes of the TTL6 group have been identified as polyglutamylases in vitro and in vivo because they can increase the degree of polyglutamylation of microtubules in HeLa cells, whereas TTL12 showed negligible activity (van Dijk *et al.*, 2007).

Although the amino acid sequence of the TTL12 protein family exhibits the core TTL domain, it lacks the so-called 'extended TTL domain', which is common to most known TTLs but missing in the TTL (van Dijk *et al.*, 2007).

In my analysis I was able to demonstrate that *T. brucei* TTL12B has in vivo glutamylation activity. A depletion of the putative polyglutamylases TTL6A, TTL12B and TTL1 resulted in a strong decrease in the signal of GT335 and PolyE (Figure 10 and 22A), whereby the former antibody detects the branching point of glutamate side chains, and the latter long side chains with at least four glutamate residues (Figure 109).

In *Tetrahymena thermophila* (Ciliophora), TTL1 was also found to have polyglutamylase activity, but it seems to be an α -tubulin specific activity (Janke *et al.*, 2005). In my experiments a depletion of TTL1 resulted in a significant decrease in glutamylation levels when probed with GT335 or PolyE. A stronger reduction of glutamylation on α -tubulin was detected, suggesting a substrate specificity of TTL1 preferring α -tubulin (Figure 22A, upper protein bands). This was also confirmed by analysing protein samples with β -monoE, an antibody that specifically detects glutamate side chains on β -tubulin. There was no reduction of in the signal bands after a knockout of *ttl1* (Figure 22C). For TTL6A it was shown that both α - and β -tubulin are substrates. This was confirmed by Julia Bechthold, a master student of mine, who characterised a *ttl6 α* ^{-/-} cell line, that I had generated. In western blot she showed a strong reduction of GT335 and PolyE signal, which was similar to the results of TTL6A RNAi-depleted cells, and, additionally, she demonstrated a complete loss of the β -monoE signal (Figure 41) (Master thesis of Julia Bechthold, Molecular Parasitology, University of Bayreuth, 2022).

Furthermore, my results showed that the antibodies GT335 and PolyE in unpurified *T. brucei* whole cell extracts only detect α - and β -tubulin as substrates and had no cross-reactivity with other proteins (Figure 40). In immunopurified HeLa cell extracts it was shown, that the two known nucleosome assembly proteins NAP1 and NAP2 are target to polyglutamylation as well as several other proteins, that were recently discovered (Regnard *et al.*, 2000; van Dijk *et al.*, 2008).

Numerous studies in the past few years have been able to demonstrate the importance of a balance of PTMs at microtubule structures and their relevance for a normal physiological function. Imbalanced PTMs are linked to a series of human diseases, such as cilia- , neuronal- , blood- and muscle disorders as well as cell division abnormalities (Akhmanova and Hoogenraad, 2018; Magiera *et al.*, 2018b).

Most of the diseases affect the highly ordered microtubule structures of cilia and neurons, which is why there is an emerging role of PTMs in this field (He, Ling and Hu, 2020). The cell morphology of trypanosomes is also governed by two highly ordered microtubule structures: the subpellicular cytoskeleton and the axoneme of the flagellum. Since many tubulin PTMs are conserved in trypanosomes, it is suggested that they play an important role in regulating the function of these structures.

After a depletion of TLL6A or TLL12B a complete disruption of the posterior tip of the cells was observed (Figure 11A). Normally the cells have a highly ordered tip structure with the plus-ends of microtubules bundled into a pointed end, the so called 'open-pipe' (Hemphill, Lawson and Seebeck, 1991). The knockdown of either polyglutamylase resulted in approximately 30 % of the cell population that showed the recently described 'glove phenotype' (Figure 11B) (Jentsch *et al.*, 2020). This phenotype is characterised by the outgrowth of several lobes at the posterior end of the cells, whereby the anterior end remains unaffected.

An ultrastructural analysis using TEM showed that the microtubules in glove cells were still continuous within the cytoskeleton, but single microtubules were fanned out at the posterior ends (Figure 12A and B). The loss of the posterior microtubule-organisation of the cytoskeleton distinguishes this phenotype from the known 'nozzle' phenotype (Hammarton, Engstler and Mottram, 2004; Pasternack *et al.*, 2015). Cells exhibiting this morphology have an elongated posterior end with a bundled tip.

A loss of *ttll1* resulted in cells with an elongated posterior end. The tip, however, displayed a blunt end, which is different to both phenotypes described above (Figure 24 and Figure 25). Since there are no publications to date describing a blunt posterior end, this phenotype was termed as 'blunt cells' in this thesis. Blunt cells were characterised as such that had a posterior end that was wider than 0.8 μm . Cells depleted of TLL1 had an average width of

approximately 1.5 μm . Since more than 95 % of the cells exhibited a blunt end, this phenotype was analysed in more detail using TEM and U-ExM.

It was shown that the plus-ends of the microtubules were still somehow bundled, which was completely different to the fanned-out microtubules in TLL6A and TLL12B RNAi-depleted cells. However, the open-pipe structure in *ttl1*^{-/-} cells was much larger in diameter (Figure 25B).

To get a better idea of the correlation between the observed phenotypes of the TLL-depleted cells and the reduction in the glutamylation levels, the cells were analysed in immunofluorescence with GT335 and PolyE. In cells depleted of either TLL6A or TLL12B the decrease in the antibody signal was comparable to the reduction observed in western blot. Both TLL6A^{RNAi} and TLL12B^{RNAi} cells exhibited a strong reduction or even a complete loss of GT335 particularly at the posterior protrusions (Figure 13). The signal for PolyE was also reduced, but uniformly across the cell body.

The glutamylation in *ttl1*^{-/-} cells was strongly reduced (Figure 22 and Figure 23), but the posterior end of the cells was still ordered. The observed effects indicate that there is a link between glutamylation and the preservation of normal cell morphology. Specifically, it could be possible that the length of glutamate side chains has important functions in maintaining a normal posterior tip, as *ttl1*^{-/-} cells showed a strong reduction of long side chains (PolyE), whereas TLL6A- or TLL12B-depleted cells showed a strong reduction in the glutamylation including short side chains (GT335).

A different behaviour of microtubule polymerization was observed in TLL-depleted cells. Therefore, the cells were stained with YL1/2, an antibody that detects tyrosinated α -tubulin. Tyrosination is a commonly used marker for newly synthesized microtubules (Westermann and Weber, 2003). *T. brucei* consists of mostly long-lived microtubules, which is why detyrosination is dominant. Only a weak staining at the posterior ends, the basal bodies, and the new growing flagellum can be detected (Sherwin *et al.*, 1987).

It was previously shown that the knockout of VASH, the enzyme that mediates the detyrosination of microtubules in *T. brucei*, resulted in cells that were heavily tyrosinated. The cells exhibited a nozzle like phenotype and growth defects (van der Laan *et al.*, 2019).

In TLL6A- or TLL12B-RNAi-depleted cells a significant increase in tyrosination was detectable at the posterior gloves of the cells, supporting the fact that these cells have an impaired

microtubule organisation (Figure 15) and suggesting that there is a major imbalance in microtubule polymerization. A knockout of *ttl1* also resulted in an increase in tyrosination, but to a weaker extent compared to the RNAi cells (Figure 27).

Other results that demonstrated the disruption of the basic cytoskeletal architecture included the analysis of the binding behaviour of MAPs. Polyglutamylation has previously been shown to affect the motor activity of MAPs such as kinesin-I and TUBB3, resulting in differences in velocity and processivity as well as the binding of MAPs to neuronal microtubules like Tau (Sirajuddin, Rice and Vale, 2014; Hausrat *et al.*, 2022). I hypothesize that a controlled glutamylation pattern is required to recruit other functional proteins that maintain the integrity of the microtubule cytoskeleton. This is based on the analysis of three cytoskeleton-associated proteins: EB1, XMAP215, and TbAIR9.

EB1 normally bundles the plus-ends of microtubules at the posterior tip. In cells lacking either TLL6A or TLL12B, EB1 is mostly absent. This would be reasonable for cells with gloves since the tip structure is completely disturbed. However, in cells with an apparently normal cell structure EB1 was also partially absent (Figure 16A). This would support the assumption that polyglutamylation is important for the recruitment of EB1. Similar results were obtained when the binding of the endogenously mNG-XMAP215 was analysed. After RNAi of TLL6A, mNG-XMAP215 was 40 % less abundant at the cell tips (Figure 16C and Figure 42) (Master thesis of Mainus Thein, Molecular Parasitology, University of Bayreuth, 2022). It was previously shown that EB1 and XMAP215 interact to increase the polymerization rate of microtubules (Zanic *et al.*, 2013), leading to the suggestion that both proteins also interact in *T. brucei*. Interestingly, TbAIR9 was also lost in TLL6A- or TLL12B-depleted cells (Figure 17C). Since AIR9 appears to be important for the correct localisation of other MAPs (Sinclair *et al.*, 2021), it may be possible that the failed localisation of EB1 and XMAP215 is related to the loss of TbAIR9.

The loss of EB1 and XMAP215 are similar to observations made in mammals and yeast. The absence of a tyrosine residue on α -tubulin resulted in a loss of microtubule end-binding proteins, such as Bik1p, CLIP170 and p150Glued (Badin-Larçon *et al.*, 2004; Erck *et al.*, 2005; Peris *et al.*, 2006). For a proper localisation they require a binding site consisting of tyrosinated α -tubulin and the presence of EB1 (Bieling *et al.*, 2008). However, my results do not lead to

the suggestion that the localisation of EB1 and XMAP215 is affected by the observed tyrosination defect (Figure 15).

What effect polyglutamylation might have on the localisation of the investigated cytoskeleton-associated proteins has not been explored until now. An indication was provided by recent atomistic simulation showing that polyglutamylation could lead to slower diffusion rates of EB1 along microtubules (Bigman and Levy, 2020).

A loss of cytoskeleton-associated proteins could not be observed in cells depleted of TLL1, suggesting that it has other functions in *T. brucei*. However, in *tll1*^{-/-} cells an abnormal distribution of EB1 and XMAP215 was documented at the blunt tip structure of the cells (Figure 28). Although no drastic disruption of the cytoskeletal microtubules occurred, the cells displayed an inhibited growth and cytokinesis defects, that were also observed in the TLL6A- or TLL12-depleted cells (Figure 14 and Figure 26). A few publications have already shown that a loss or the overexpression of MAPs resulted in such defects, suggesting a higher relevance of the regulation of the investigated cytoskeleton-associated proteins (Vedrenne *et al.*, 2002; Olego-Fernandez *et al.*, 2009; May *et al.*, 2012; Portman and Gull, 2014; Hilton *et al.*, 2018).

As most cellular phenotypes of microtubule PTM deficiencies are associated with stable microtubule structures such as cilia, flagella and axons, it was of interest to examine the TLL-depleted *T. brucei* cells in more detail because they rely on these structures for their survival. In particular, a correct pattern of axonemal PTMs is known to be essential for flagellar and axonemal architecture and cell motility (Alper *et al.*, 2014; Gadadhar *et al.*, 2017; Hong *et al.*, 2018; Giordano *et al.*, 2019).

In collaboration with the group of Prof. Dr. Matthias Weiss (Chair of Experimental Physics I, University of Bayreuth), a deviant swimming behaviour of TLL-depleted cells was documented. This was characterised by a decrease in directional motion, slower movement, and a decrease in the straightness of the recorded trajectories (Figure 20 and Table 3). This indicates that an imbalance in the axonemal glutamylation correlates with a severe motility defect in *T. brucei*.

The effects of an impaired glutamylation on flagellar function have been previously demonstrated in mammalian cells. Mutations in glutamylases (TLL1, TLL9) and deglutamylases (CCP1, CCP5) cause aberrations in spermatogenesis and sperm motility

resulting in male infertility in mice (Mullen, Eicher and Sidman, 1976; Vogel *et al.*, 2010; Konno *et al.*, 2016; Wu, Wei and Morgan, 2017). In *ttl19^{-/-}* mice, abnormal sperm motility was attributed to the loss of doublet 7, which occurred selectively, and reduced polyglutamylation at doublet 5 (Konno *et al.*, 2016). It has been shown that a possible outcome of a disturbed axonemal glutamylation is a defective interaction between tubulin and proteins of the inner arm dynein (Kubo *et al.*, 2010). Structural deficiencies within the flagellum were also shown in mice depleted of two polycylases. Disruption of the structure of outer and inner arm dynein, caused by the depletion, resulted in an altered sperm flagellar beat pattern, leading to subfertile mice (Gadadhar *et al.*, 2021). In addition, mice lacking TLL1 showed a lost beat asymmetry in axonemes and tracheal epithelial cilia, resulting in impaired airway cilia function (Ikegami *et al.*, 2010). How polyglutamylation affects the flagellar function in trypanosomes still needs to be elucidated. Several studies have previously shown that *T. brucei* is a well-suited model-organism to study human ciliopathies such as infertility and hydrocephalus, a pathological enlargement of the fluid spaces of the brain filled with cerebrospinal fluid (Dawe *et al.*, 2005, 2007; Coutton *et al.*, 2018).

Knowing that the axoneme of *T. brucei* is extremely glutamylated (Schneider, Plessmann and Weber, 1997), it is reasonable to assume that TLL6A, TLL12B, and TLL1 are also active within the flagellum. Western blot of flagellar fractions of the corresponding TLL-depleted cells confirmed the reactivity of the polyglutamylases at the axoneme, as a decrease of the glutamylation levels was detected (Figure 18C and Figure 29B).

Not only was a reduction in the glutamylation observed, but also an altered distribution pattern of the glutamylation within the flagellum.

Normally the axoneme is uniformly stained with GT335 and PolyE, but *ttl1^{-/-}* cells showed an unusual accumulation of PolyE (Figure 30). Expansion microscopy and an evaluation of the staining intensities made it possible to get a better picture of the distribution of glutamylation within the flagellum. When expanded cells were stained together with an anti-tubulin antibody and PolyE, a significant shift in the PolyE signal was measured (Figure 30). The tubulin staining served as a control, as it should equally recognise the axoneme in WT⁴²⁷ and *ttl1^{-/-}* cells. Whereas in WT⁴²⁷ cells the peaks of tubulin and PolyE overlapped, implying tubulin and PolyE are evenly distributed across the flagella, cells lacking TLL1 exhibited a PolyE peak that was distinctly shifted to one flagella site. The tubulin signal was not affected by this (Figure

30B I-IV). Evaluation of the fluorescence signal showed that it was not an accumulation which was observed but a result of a reduction of PolyE on one side of the flagella.

This was also seen in cells stained with GT335 (detects the branching point of glutamate side chains) and PolyE (detects long glutamate side chains). Interestingly in TLL1-depleted cells a shift of the GT335 signal was observed, but in the opposite direction as it was shown for PolyE (Figure 30A I-IV). This would imply that a knockout of *tll1* results in a glutamylation pattern that is split between different sides of the flagella. On the one side of the flagella, there is a strong reduction of long glutamate side chains, while on the other side, there is a reduction of glutamylation including short side chains, but the long side chains are preserved.

To investigate on which side the PolyE signal was maintained an additional staining of the PFR was performed. The results showed that PolyE was located adjacent to the PFR signal (Figure 30C I-IV), indicating that only the microtubule doublets 4-7 remain to have long glutamate side chains (Figure 30D I-IV). An ultrastructural analysis of a cross section of TLL1-depleted cells did not reveal any infrequent alterations of the axoneme that could have explained the observed effects (Figure 31).

It was previously shown that the transport of 'intraflagellar trains', a process in which molecular motors run on microtubule doublets and transport large protein complexes (trains) (Ishikawa and Marshall, 2011), occurs preferentially on certain microtubule doublets demonstrating an asymmetric functionality (Bertiaux *et al.*, 2018). The PFR, a structure unique in kinetoplastids, is tightly associated to the axoneme and is essential for the motility of the cells (Bastin, Sherwin and Gull, 1998; Koyfman *et al.*, 2011). It could also be conceivable, that the PFR might be restricting to TLL1 being active on the remaining doublets.

Since *T. brucei* expresses eight different TLLs it would be reasonable to assume that they have different functions within the flagellum. It could be possible that the TLLs in *T. brucei* preferentially act on certain microtubule-doublets. This study gives indications that TLL1 would be active on the doublets 1-4 and 7-9. However, the relationship between a differential glutamylase activity of TLLs on the axoneme is currently not known.

In *tll1*^{-/-} cells, the effects of the depletion on the cellular integrity were shown to be reversible (Figure 32). It was previously shown that an overexpression of some polyglutamylases in the protozoan *Leishmania* induces apoptosis whereby an overexpression of deglutamylases inhibits regulated cell death (Basmacıyan *et al.*, 2019). Therefore, it was suggested, that a

balance of polyglutamylation/deglutamylation is needed to maintain a normal cell function. To test this hypothesis, cells overexpressing TLL1 were analysed. The ectopic expression of TLL1 resulted in elongated cells that also exhibited a blunt posterior tip and showed an inhibited cell growth associated with cytokinesis defects (Figure 33 Figure 34B and C). It was shown that the expression resulted in an increase of the glutamylation level. Interestingly mainly the PolyE signal was increased (Figure 34A). Comparing this with the results of TLL1-depleted cells, in which the PolyE signal was more reduced than the GT335 signal in immunofluorescence (Figure 22 and Figure 23), it could be suggested that TLL1 acts as an elongating enzyme. The observed effects of a TLL1 depletion within the flagellum, in which a pronounced decrease in long glutamylation sides was observed, would support this assumption (Figure 30).

Recently an active-site in TLLs was identified, it determines whether they have an initiating or an elongating function (Mahalingan *et al.*, 2020). They propose a division of TLLs according to the conserved residue Q180, according to which TLL1, 6, 9, 11 and 13 would belong to the elongases and TLL2, 4, 5 and 12 to the initiases. After screening the protein sequences of *T. brucei* TLL1, TLL6A and TLL12B for Q180, only TLL1 had a glutamine residue within this region (Figure 43) and thus would belong to the elongases, supporting my results.

According to this approach the polyglutamylases TLL6A and TLL12B would be classified among the initiating enzymes, which would also support my results. An important indication for this was the β -monoE specificity of TLL6A, since this antibody recognizes the linkage of glutamate side chains (Figure 41).

However, these are preliminary findings and indications of the ways in which the enzymes catalyse the attachment of glutamate residues. To gain a clear picture, the corresponding proteins need to be recombinantly expressed and tested in enzyme assays. Analysis by mass spectrometry would also provide more detailed results. However, our approaches for this analysis have been unsuccessful so far, as the terminal tails of tubulin are strongly negatively charged, which makes the detection difficult.

In this work, glutamylation was studied in the insect stage (procyclic cells) of *T. brucei*. They are suitable to analyse the impact of PTMs on the organisation of microtubule structures, because they undergo strong morphological changes during the life cycle in the tsetse fly (Sharma *et al.*, 2009). It would be interesting to address the impact of PTMs in bloodstream cells, since they are the causative form for diseases. My experiments have shown that

glutamylation has an important function in cell motility. Since procyclic and bloodstream cells have different motility patterns and circulate in different host environments, it would be of interest to see if a similar effect can be observed in these cells. Targeting such proteins that are important for cell locomotion could offer an approach for new drug development, as motility is essential for the parasite's survival.

In summary, this study showed that polyglutamylation is important for maintaining cell architecture, cellular integrity and motility of *T. brucei*. It was also shown that a balance of glutamylation must be sustained for a normal cell function. In addition, this work demonstrated that *T. brucei* is a well-suited model organism to analyse posttranslational modifications, especially in highly organised microtubule structures, such as the flagellum. Since the axonemal structure of trypanosomes is highly conserved, basic molecular mechanisms of various ciliopathies can be studied in this system, which are also relevant for human diseases.

Materials and methods

Materials

Hard- and software

This work was written on a MacBook Pro (Apple Inc., Germany) using Microsoft Word 2022. Microsoft Excel and PowerPoint 2022 were used for the design of Graphs and Figures. Additionally, figures were designed using BioRender.com (publication and licensing rights can be found in the supplements). Images have been edited in ImageJ (v1.53a) (Schindelin *et al.*, 2012). Statistics were done with Past4 (v3.24) (Hammer, Harper and Ryan, 2001).

DNA and protein sequences were obtained from the TriTryp database (<https://tritrypdb.org/tritrypdb/app>). Plasmids were virtually designed using the Gene Construction Kit (Textco BioSoftware, Inc., v2.5). Pairwise sequence alignments were done with EMBOSS needle (https://www.ebi.ac.uk/Tools/psa/emboss_needle/). Using the tool 'RNAit' (<https://dag.compbio.dundee.ac.uk/RNAit/>) RNAi constructs could be designed specifically for trypanosomes (Redmond, Vadivelu and Field, 2003).

Chemicals, reagents and kits

All reagents, chemicals and kits were purchased from the following companies: Roth (Karlsruhe), Merck (Darmstadt), Invitrogen via ThermoFisher Scientific (Schwerte), New England Biolabs (NEB, Frankfurt a. M.), Qiagen (Hilden), Macherey-Nagel (Düren).

Antibodies**Table 4: Primary antibodies.** WB = western blot, IF = immunofluorescence.

antibody	species	antigen	dilution	source
TAT	mouse monoclonal	α -tubulin	1:10.000 WB 1:7.000 IF	Molecular Parasitology, University of Bayreuth
GT335	mouse monoclonal	anti-glutamylation (EGEGE*EEG)	1:10.000 WB/IF	AdipoGen, Liestal, Switzerland
PolyE	rabbit polyclonal	polyglutamate peptide	1:10.000 WB/IF	AdipoGen, Liestal, Switzerland
β-monoE	rabbit monoclonal	anti-glutamylation specific for β -tubulin (glutamylated GEF motif)	1:5.000 WB 1:7.000 IF	kind gift from Carsten Janke, Institut Curie, Université PSL, France (Bodakuntla et al., 2021)
YL1/2	rat monoclonal	tyrosinated α -tubulin	1:250 WB 1:10 tip dye IF; 1:50 basal bodies IF	Molecular Parasitology, University of Bayreuth
L8C4	mouse monoclonal	paraflagellar rod (PFR)	1:1.000 WB/IF	Molecular Parasitology, University of Bayreuth
EB1	mouse monoclonal (IgM)	end-binding protein 1 (Tb927.9.2760)	1:50 IF 1:5 WB	Gertrud Lallinger-Kube, Molecular Parasitology, University of Bayreuth
CAP5.5	mouse monoclonal (IgG)	cytoskeleton associated protein 5.5 (Tb927.4.3950)	1:500 WB 1:1.000 IF	Jana Ritschar, Molecular Parasitology, University of Bayreuth
9E10	Mouse monoclonal (IgG)	myc	1:2.000 WB	SeraLab, London, UK
BiP	mouse monoclonal	luminal binding protein 1 (Tb927.11.7460)	1:3.000 WB	Gertrud Lallinger-Kube, Molecular Parasitology, University of Bayreuth

Table 5: Secondary antibodies. WB = western blot, IF = immunofluorescence.

antibody	antigen/species	dilution	source
mouse HRP	rabbit anti-mouse IgG (whole molecule), polyclonal	1:80.000 WB	Merck, Darmstadt
rabbit HRP	goat anti-rabbit IgG (H+L) conjugated, polyclonal	1:10.000 WB	Biozol, Eching
rat HRP	anti-rat	1:80.000 WB	Biozol, Eching
Atto 488 FITC labelled	goat anti-mouse IgG (whole molecule), polyclonal	1:500 IF	Sigma-Aldrich, Steinheim
Atto 550 Cy3 labelled	goat anti-mouse IgG (whole molecule), polyclonal	1:500 IF	Sigma-Aldrich, Steinheim
CF488A FITC labelled	goat anti-rabbit IgG (H+L)	1:1.000 IF	Sigma-Aldrich, Steinheim
Alexa Fluor 488	goat anti-rat IgG (H+L)	1:1.000 IF	Invitrogen by Thermo Fisher Scientific, Oregon USA

DNA oligonucleotides**Table 6: DNA oligonucleotides.** Underlined sequences represent restriction sites. All oligonucleotides were purchased from Microsynth, Balgach, Switzerland.

oligonucleotide	sequence 5'-3'	restriction endonuclease	purpose
TbTTLL6A_for	ATA <u>GGA TCC AAG CTT</u> CTC TTC TCG GCG CCA AGT GT	HindIII, BamHI	TTLL6A RNAi TTLL6A qPCR analysis
TbTTLL6A_rev	ATA <u>CTC GAG TCT AGA</u> AAC GCC TTA ACG TTG GCG AC	XhoI, XbaI	TTLL6A RNAi TTLL6A qPCR analysis
TbTTLL12B_for	ATA <u>GGA TCC AAG CTT</u> TCG GTG GAA GTT TGA AGC TA	HindIII, BamHI	TTLL12B RNAi TTLL12B qPCR analysis
TbTTLL12B_rev	ATA <u>CTC GAG TCT AGA</u> AAT GCT TCA AAG TCT TTC AT	XhoI, XbaI	TTLL12B RNAi TTLL12B qPCR analysis
Puro_for	ATA <u>TCT AGA</u> AGC TCA TGC AGG CTA GGG C	XbaI	generation of gene knockout vector puromycin (pALC14_puromycin)
Puro_rev	ATA <u>CTC GAG</u> AAT ACT GCA TAG ATA ACA	XhoI	generation of gene knockout vector puromycin (pALC14_puromycin)
BSD_for	ATA <u>TCT AGA</u> TGG GTC CCA TTG TTT GCC T	XbaI	generation of gene knockout vector blastidicin (pALC14_blasticidin)
BSD_rev	ATA <u>CTC GAG</u> ACT ATT TTC TTT GAT GAA AGG G	XhoI	generation of gene knockout vector blastidicin (pALC14_blasticidin)
TTLL1_5'UTR_for	ATA <u>AAG CTT</u> TAG GTT AGG TGA AGG A	HindIII	TTLL1 gene knockout
TTLL1_5'UTR_rev	ATA <u>TCT AGA</u> GTG TAA GTG AAT GTG T	XbaI	TTLL1 gene knockout

TTLL1_3'UTR_for	ATA <u>CTC GAG</u> CCT CAC TTC ATC TGT T	XhoI	TTLL1 gene knockout
TTLL1_3'UTR_rev	ATA <u>GGA TCC</u> TGT TGG CAT CAG AGA G	BamHI	TTLL1 gene knockout
TTLL1_analyse_for	TAC GCA CCG TTC CTT GCT CCA C	-	TTLL1 gene knockout PCR analysis
TTLL1_analyse_rev	GAG ATA GAC TAC GCT ACC ACC C	-	TTLL1 gene knockout PCR analysis
TTLL1_rescue_for	ATA <u>AAG CTT</u> ATG TTC CCT AAT ACA TCG CTG CGA CCC G	HindIII	TTLL1 rescue
TTLL1_rev	TAT <u>GGT ACC</u> TAA ATG GGC AGT GAT CTT TAC CTT GGC	KpnI	TTLL1 rescue
qTTLL1_for	CTC TCA GGG CCG TGG AAT TT	-	TTLL1 qPCR analysis
qTTLL1_rev	ACA TACA GGC GCA GGT CAA A	-	TTLL1 qPCR analysis
FA_TTLL1_for	ATA <u>GGC CGG CCT</u> ATA TGT TCC CTA ATA CAT CGC TGC	FseI	TTLL1 ectopic expression
FA_TTLL1_rev	TAT <u>GGC GCG CCG</u> GCA CTC TCC TAC TTG CAA	AscI	TTLL1 ectopic expression
qPFR_for	CGT TGG AGA TGT TTG GAC CT	-	PFR qPCR analysis (endogenous control)
qPFR_rev	GCA CGG TAC TCC ACC ATC TT	-	PFR qPCR analysis (endogenous control)

Plasmids**Table 7: Vectors.**

vector	description
pALC14	stem loop vector, inducible RNA interference with doxycycline, procyclin promotor, puromycin resistance, ampicillin resistance for molecular cloning (kind gift from A. Schneider)
pFC4	stem loop vector, inducible RNA interference with doxycycline, procyclin promotor, blasticidin resistance, ampicillin resistance for molecular cloning (kind gift from A. Schneider)
pALC14_puromycin	modified in this thesis, parental vector: pALC14, stuffer was replaced by a puromycin resistance cassette, ampicillin resistance for molecular cloning, vector was used for generation of gene knockout cell lines
pALC14_blasticidin	modified in this thesis, parental vector: pALC14, stuffer was replaced by a blasticidin resistance cassette, ampicillin resistance for molecular cloning, vector was used for generation of gene knockout cell lines
pTag8-tub	vector with homologous regions for insertion to a tubulin locus, was used for ectopic expression of <i>tll1</i> ^{-/-} rescue
pEnGOP	was used as template for the amplification of the puromycin resistance cassette, necessary for the generation of pALC14_puromycin
pNAT_BSD_6Myc_X	Alsford & Horn (2008), was used as template for the amplification of the blasticidin resistance cassette, necessary for the generation of pALC14_blasticidin
pHD1800	origin pHD1700 (kindly provided by F. Voncken), modified by Gertrud Lallinger-Kube (Molecular Parasitology, University of Bayreuth), used for inducible expression with doxycycline, procyclin promotor, 2x c-terminal myc tag, hygromycin resistance, ampicillin resistance for molecular cloning

Table 8: Plasmids generated in this study.

plasmid	parental vector	insert	description
TTLL6A_RNAi	pALC14	a 266 bp fragment of the genomic sequence of TTLL6A	RNA interference targeting TTLL6A (Tb927.3.5380)
TTLL12B_RNAi	pFC4	a 180 bp fragment of the genomic sequence of TTLL12B	RNA interference targeting TTLL12B (Tb927.11.2420)
TTLL1_Puro	pALC14_puromycin	5'UTR and 3'UTR of TTLL1	gene knockout targeting TTLL1 (Tb927.5.3860) using homologous recombination
TTLL1_BSD	pALC14_blasticidin	5'UTR and 3'UTR of TTLL1	gene knockout targeting TTLL1 using homologous recombination
TTLL1_rescue	pTag8-tub	TTLL1 full-length	add-back experiment of TTLL1 full-length in TTLL1 knockout cells, 2x C-terminal myc tag
TTLL1_OE	pHD1800	TTLL1 full-length	ectopic expression of TTLL1 2x C-terminal myc tag

Microbiological techniques

E. coli strains and media

For molecular cloning *E. coli* XL1-blue was used. Cells were grown in LB-media or on LB-agar plates containing 100 µg/mL ampicillin.

LB-medium

1 % (w/v) tryptone

0.5 % (w/v) yeast extract

0.5 % (w/v) NaCl

LB-agar

LB-medium plus 1.5 % (w/v) agar

Transformation of Plasmid DNA in *E. coli*

Chemically competent *E. coli* XL1-blue were thawed on ice. 3 µL (or 300 ng) plasmid DNA were added to the cells and incubated on ice for 30 min. Heat shock was then performed at 42°C for 45 sec. 1 mL LB-medium was added, and the cells recovered for 1 h at 37°C while shaking. Cells were plated on LB-agar (containing 100 µg/mL ampicillin) and transformants were grown at 37°C for 16 h.

Molecular biological methods

Polymerase chain reaction

The amplification of DNA was performed according to standard protocols for S7 Fusion High-Fidelity DNA Polymerase (Biozym, Hessisch Oldendorf) and Taq-Polymerase (NEB, Frankfurt a. M.). 250 ng of genomic *T. brucei* DNA was used as template.

Isolation of plasmid DNA from *E. coli*

To identify transformants that contain the correct plasmid after molecular cloning, single colonies were picked and grown in 3 mL LB-medium (containing 100 µg/mL ampicillin) at 37°C for 16 h while shaking. Cells were harvested by centrifugation (30 sec, 13.500 rcf; 5424, rotor FA-45-24-11, Eppendorf, Hamburg) and pellets were resuspended in 150 µL cold GTER buffer.

Then 200 μL lysis buffer was added, reaction tubes were inverted eight times and incubated for 3 min on ice. 150 μL neutralization buffer was added and incubated for 3 min on ice. Precipitated chromosomal *E. coli* DNA was pelleted via centrifugation for 5 min at 13.500 rcf (5424, rotor FA-45-24-11, Eppendorf, Hamburg). 450 μL of the supernatant was mixed with 900 μL 100 % ethanol to precipitate plasmid DNA.

After centrifugation for 15 min at 13.500 rcf (5424, rotor FA-45-24-11, Eppendorf, Hamburg) the pellet was washed in 70 % ethanol and air-dried at room temperature. DNA was dissolved in 30 μL 1x TE buffer.

GTER buffer	lysis buffer	1x TE buffer
50 mM glucose	0.2 N NaOH	10 mM Tris-HCl, pH 7.4
25 mM Tris-HCl, pH 8.0	1 % (v/v) SDS	1 mM EDTA
10 mM EDTA, pH 8.0		
100 $\mu\text{g}/\text{mL}$ RNase		

To isolate high amounts of plasmid DNA, 50 mL LB-medium (containing 100 $\mu\text{g}/\text{mL}$ ampicillin) were inoculated with verified transformants and cultivated for 16 h at 37°C while shaking.

Determination of DNA and RNA concentration

Nucleic acid concentrations were determined with a 'ND-1000 Spectrophotometer' (Peqlab, Erlangen). DNA and RNA concentrations were measured by their absorbance at 260 nm.

Restriction hydrolysis of DNA

Site specific endonucleases were purchased from NEB (Frankfurt a.M.). The enzymes were used according to the manufacturer's instructions. 1 μg DNA was hydrolysed with 1 unit of the corresponding enzyme for 1 h 30 min at 37°C. For a subsequent buffer exchange, the reaction was purified using the 'NucleoSpin Gel and PCR Clean-up' kit (Macherey-Nagel, Düren). The purified DNA was separated and analysed on a 1 % agarose gel before being used for subsequent ligation.

Separation of DNA fragments by agarose gel electrophoresis

For the analysis of DNA it was mixed with Loading Dye (to 1x concentration) and loaded onto a 1-2 % agarose gel (SeaKem LE agarose, Lonza, Rockland, ME, USA). Following DNA ladders were used: SPP1 ladder for larger DNA fragments (hydrolysis of SPP1 bacteriophage DNA with EcoRI, Karin Angermann, Molecular Parasitology, University of Bayreuth) and LMW ladder for separating small DNA fragments (low molecular weight ladder, kindly provided by Prof. Olaf Stemmann, Genetics, University of Bayreuth).

The gels ran at 120 V for 20-30 min ('HU6 Mini Horizontal', Scie-Plas Limited, Cambridge, UK) in 1x TAE running buffer and were stained afterwards with ethidium bromide for 15 min. After another 15 min of destaining in deionised water, the DNA could be visualized under a UV light source ('GenoSmart Compact Imaging System', VWR, Darmstadt).

1x TAE

0.04 M Tris

0.1142 % (v/v) acetic acid

1.3 mM EDTA

pH 8.0 with acetic acid

6x Loading dye

10 mM Tris-HCl, pH 7.6

0.03 % (w/v) bromphenol blue

0.03 % (w/v) xylene cyanol FF

60 % (v/v) glycerin

60 mM EDTA

Ligation of DNA fragments

To insert the hydrolysed fragments into the plasmids, they were ligated with 5 units of a T4 DNA ligase (ThermoFisher Scientific, Schwerte) in the appropriate buffer (1x concentration). Ligation occurred either for 2 h at room temperature or overnight at 18°C. For the calculation of a molar vector to fragment ratio of 1:3 the NEBioCalculator (<https://international.neb.com>) was used.

Isolation of RNA

RNA from 4×10^7 cells of the corresponding cell lines were isolated with the 'RNeasy Plus Mini Kit' (Qiagen) after the manufacturer's instructions. RNAi cells were treated with doxycycline 24 h prior to the isolation. Additionally, DNA hydrolysis was performed to remove any

remaining genomic DNA. For this purpose, 1 μL rDNaseI (2 units) and 5 μL 10x DNaseI-Reaction buffer (Invitrogen) were added to the 50 μL isolated RNA and then incubated at 37°C for 30 min. For DNaseI inactivation 5 μL inactivation beads were mixed with the reaction and incubated for another 5 min at room temperature. After centrifugation for 1 min at high speed (5424, rotor FA-45-24-11, Eppendorf, Hamburg), the supernatant was collected in a new reaction tube and the RNA concentration was determined photometrically.

400 ng of the measured RNA was mixed with RNA-sample buffer (1:1) and incubated at 65°C for 10 min. The entire sample was loaded onto a 1 % agarose gel and run at 100 V for 1 h in 1xTAE buffer treated with 0.1 % DEPC. Before use, all utensils for the gel were cleaned with 5% H_2O_2 and washed with deionized water (treated with 0.1 % DEPC) to eliminate possible RNase contaminations. RNA was visualized after staining in ethidium bromide and destaining in deionized water (treated with 0.1 % DEPC) for 15 min each using a UV light source ('GenoSmart Compact Imaging System', VWR, Darmstadt). RNA was stored at -80°C.

Revers transcription of RNA in cDNA

The generation of cDNA was performed using the 'RevertAid First Stand cDNA Synthesis Kit' (ThermoScientific) according to the manufacturer's instructions. Therefore, 500 ng isolated RNA was reversely transcribed. Random Hexamer Primer was used for synthesis. As a negative control a reaction was performed lacking the reverse transcriptase. The cDNA was stored at -20°C.

Quantitative real time PCR (qPCR)

qPCR was carried out to quantify mRNA levels. Reactions consisted of 10 μL of SYBR Green Mix ('Maxima SYBR Green/ROX qPCR Master Mix (2x)', ThermoScientific), 0.6 μL each of the corresponding forward and reverse primer (10 μM), 5 ng of cDNA, and nuclease-free water in a total volume of 20 μL . As controls, reactions with negative cDNA as template were performed as well as reactions with nuclease-free water as template.

The qPCR analysis was performed in 48-well plates ('MicroAmp Fast Optical 48-Well Reaction Plate (0.1mL), Applied Biosystems by Life Technologies) on a Step One real time PCR system

(Applied Biosystems by Life Technologies). Four replicates were measured for each tested cDNA. PCR-cycling protocol was performed as described in Table 9.

The tested mRNA levels were calculated using the $\Delta\Delta\text{CT}$ -method (Pfaffl, 2004). It determines the expression levels of a target gene via the normalization to an endogenous control (in this study: PFR).

Table 9: qPCR protocol.

	time	temperature	cycles
initial denaturation	10 min	95°C	1x
denaturation	15 sec	95°C	40x
annealing	30 sec	55°C	
extension	30 sec	72°C	
dissoziation	15 sec	95°C	1x

Protein biochemical methods

Denaturing sodium dodecyl sulfate polyacrylamide gel electrophoresis (SDS-PAGE)

Separation of proteins by SDS-PAGE was performed according to Banerjee, Bovenzi and Bane (2010). This method is based on the standard procedure of Laemmli (Laemmli, 1970). Simple modifications, such as the use of low-grade sodium dodecyl sulfate and a Tris-HCl buffer with a pH of 9.8 of the stacking gel, can achieve a high separation of alpha- and beta-tubulin (Table 10).

Samples were mixed with hot Laemmli (to 1x) and boiled for 10 min. After vortexing and centrifugation for 5 min at high-speed (5424, rotor FA-45-24-11, Eppendorf, Hamburg), they were loaded on a polyacrylamide gel or stored at -20°C.

Samples that were probed with the antibodies TAT, GT335 and PolyE after immunoblotting were diluted in 1x Laemmli (1:80) and loaded onto a SDS Gel. Gels run in 1x SDS-PAGE buffer for 40 min at 25 mA per gel.

2x Laemmli

125 mM Tris-HCl, pH 6.8
 5 % (v/v) glycerol
 4 % (v/v) SDS
 5 % (v/v) β -mercaptoethanol
 crystals of bromphenol blue

1x SDS-PAGE buffer

25 mM Tris
 0.2 M glycine
 0.001 % (v/v) SDS (L5750, Sigma-Aldrich, Taufkirchen)

Table 10: Components of SDS-gels.

component	resolving gel (7.5 %)	stacking gel
ddH₂O	12.8 mL	10.8 mL
30 % acrylamide-bisacrylamide	8 mL	4 mL
1.5 M Tris-HCl, pH 9.8	8 mL	-
0.5 M Tris-HCl, pH 6.8	-	5 mL
10 % SDS (L5750, Sigma-Aldrich)	320 μ L	200 μ L
10 % APS	400 μ L	100 μ L
Temed	25.6 μ L	20 μ L

Methanol-chloroform precipitation of protein samples

Samples treated with high salt concentrations were precipitated with methanol-chloroform. For this purpose, four times the volume of 100 % methanol and one volume of 100 % chloroform were added to the samples and mixed by vortexing. Afterwards, three volumes of deionized water were added and mixed again by vortexing. Centrifugation for 5 min at 14.200 rcf (5424, rotor FA-45-24-11, Eppendorf, Hamburg) resulted in phase separation, with the interphase containing the precipitated protein.

The upper aqueous phase was discarded, and three volumes of 100 % methanol were added. After vortexing and centrifugation (14.200 rcf, 5 min, 5424, rotor FA-45-24-11, Eppendorf, Hamburg), the methanol was completely removed, and the pellets were air-dried. The pellets were then resuspended in hot 1x Laemmli and boiled for 10 min. Samples were stored at -20°C.

Immunoblot

For the detection of proteins by immunoblot, they were first separated by SDS-PAGE and then transferred to a nitrocellulose membrane (Roti-NC Transfermembran, Carl Roth, Karlsruhe) using the tank blot technique ('Mini Trans-Blot cell', BioRad, Munich). The transfer was performed either for 2 h at 250 mA on ice or overnight at 100 mA at room temperature.

The membrane was stained in ponceau S for 1 min to reversibly stain the proteins. Unspecific staining was removed by swirling the membrane several times in ddH₂O. The brief staining of the proteins served as a loading control.

Unspecific binding sites were saturated with blocking buffer for 1 h. The membrane was incubated with the primary antibody for 1 h. After washing the membrane three times for 5 min in PBS-T it was incubated with the secondary antibody for 1 h. The membrane was washed three times for 5 min. Both the primary and secondary antibodies were diluted in blocking buffer.

Protein bands were detected by chemiluminescence. The horseradish peroxidase which is coupled to the secondary antibody converted the HRP reaction components A and B (Takara Western Blot Ultra-Sensitive HRP Substrate, BIO INC., Japan; added in a 1:1 ratio) into light signal that were detected and documented with the LAS-4000-Imaging System (Fujifilm Europe, GmbH, Düsseldorf).

1x Blotting buffer

25 mM Tris
190 mM glycerol
20 % (v/v) methanol

Ponceau S

3.3 mM ponceau S
40 % (v/v) methanol
15 % (v/v) acetic acid

1x PBS

0.14 M NaCl
2.7 mM KCl
8.5 mM Na₂HPO₄ x 2H₂O
pH 7.4

PBS-T

0.1 % (v/v) Tween-20
in 1x PBS

Blocking buffer

5 % milk powder (Magermilchpulver, Sucofin, TSI, Zeven) in 1x PBS-T

Microscopy

Microscopy of cells was performed using an 'Axio Imager 2' (Zeiss, Oberkochen) microscope, a 'SPOT Pursuit' camera (SPOT Imaging, Sterling Heights, MI, USA) and the 'VisiView' software (Visitron Systems, Puchheim). When using the 100x oil objective (Plan-Apochromat 100x/1.40 Oil Ph3 M27, Zeiss, Oberkochen), it was necessary to apply immersion oil ('Immersol™ 518F, Zeiss, Oberkochen) to the samples.

Immunofluorescence

For immunostaining of *T. brucei* cells, 2×10^6 cells were centrifuged (3.400 rcf, 1 min, 5424, rotor FA-45-24-11, Eppendorf, Hamburg). The pellet was washed once with 1x PBS and then resuspended in 1 mL 1x PBS and placed on poly-L-lysine coated slides. Prior to this, small squares were drawn on the slides with a 'ImmEdge Hydrophobic Barrier Pen' (Vector Laboratories, Burlingame, CA, USA) to keep the cells in a confined area. The cells attached to the slides for 10 min in a humidified chamber. Afterwards the slides were washed in 1x PBS to remove unattached cells.

For the preparation of whole cells, cells were fixed in ice-cold 100 % methanol for at least 30 min. For preparation of cytoskeletons, cells were treated with a detergent for 2 min (1x PBS +1 % NP40) prior fixation in methanol. Subsequently, the detergent was washed off with 1x PBS and cells were incubated in ice-cold 100 % methanol as described previously.

After fixation cells were rehydrated in 1x PBS for one minute. The primary antibody was added to the cells, which were incubated for 1 h in a humidified chamber. The slides were washed three times for 5 min in PBS-T in a coplin jar while shaking gently. The secondary antibody was added to the cells and incubated for 1 h in a humidified chamber.

The slides were washed once in PBS-T and stained with DAPI (1 µg/mL in 1x PBS). DNA staining occurred for 5 min in a humidified chamber and then the slides were washed a final time in PBS-T. As a final step, 5 µL of 'Vectashield mounting medium' (Vector Laboratories, Burlingame, CA, USA) was added to the cells and sealed with a cover slip. The slides could either be analysed directly or stored at 4°C in the dark for several weeks.

Ultrastructural expansion microscopy (U-ExM)

The expansion of *T. brucei* cells was performed as previously described in Kalichava and Ochsenreiter (2021).

For the microscopic analysis of the expanded gels, small gene-frames with a thickness of 0,25 mm (Gene Frame, 1,5 x 1,6 cm, ThermoScientific, Schwerte) were put on a slide and a small piece of gel was placed inside the frame. Areas that were not covered with gel were filled with small amounts of 1 % low melting agarose. A coverslip was then placed on top of the gel and firmly, but carefully, adhered to the gene frame. Excess gel and liquid that was squeezed out was removed with a tissue. The sample was immediately examined after its preparation.

Electron microscopy

For the ultrastructural analysis of the cells, whole mount electron microscopy was performed. For this purpose, 1×10^7 cells were centrifuged (400 rcf, 10 min, 5702 R, rotor A-4-38, Eppendorf, Hamburg) and washed once in PEME.

The cells were resuspended in 50 μ L PEME. Next, 5 μ L of the cell suspension was placed on pioloform-coated mesh copper grids (size 100, Plano GmbH, Wetzlar, Germany), and they were incubated for 20 min to allow attachment. Unattached cells were first removed by aspiration with a filter paper and then by adding 5 μ L PEME and aspirating again.

Then 5 μ L PEM + 1 % NP40 was added to the grids and incubated for 5 min. Again, the grids were washed with PEME before they were treated with 5 μ L of 2 % uranyl acetate for exactly 1 min. A final time the grids were washed with deionized water and then they were placed on a filter paper to dry.

Samples were imaged with a JEM-1400 Plus electron microscope (JEOL, Germany) with a Ruby CCD camera (JEOL, Germany).

PEME

1 M PIPES

2 mM EGTA

1 mM MgSO₄

0.1 mM EDTA

pH 6.9

PEM

1 M PIPES

2 mM EGTA

1 mM MgSO₄

Isolation of flagella from *T. brucei*

To analyse flagella separately from the cytoskeleton at the protein level, 5×10^7 cells were harvested (2.500 rcf, 10 min, 5702 R, rotor A-4-38, Eppendorf, Hamburg) and washed in 1x PBS. The cell-pellet was resuspended in 500 μ L PMN + 0.5 % Triton. After incubation on ice for 10 min, the pellet was washed twice in the same buffer.

This was followed by the treatment with PMN + 1 M NaCl. The suspension was mixed well and incubated on ice for another 10 min. By centrifugation at 16.000 rcf for 10 min at 4°C (Mikro 200R, type 2495, rotor 2424, Hettich Zentrifugen, Tuttlingen) the flagella were pelleted, and the disrupted cytoskeleton was in the soluble fraction.

The supernatant was removed and precipitated with methanol/chloroform. The pellet was washed in PMN and then taken up in hot 1x Laemmli.

PMN

10 mM Na₃PO₄

150 mM NaCl

1 mM MgCl₂

Cell biological methods

T. brucei cell lines, cultivation and storage

Procyclic *T. brucei* cells were maintained in SDM-79 medium (Life Technologies, UK) supplemented with 10 % fetal bovine serum, 7.5 mg/L hemin and the corresponding selection antibiotics (Table 11) at 27°C. Cells were transferred every three to five days, as needed. Cell growth was measured using a CASY cell counter (Roche innovates AG, Germany). For storage logarithmically grown cells were centrifuged (10 min, 400 rcf; 5702 R, rotor A-4-38, Eppendorf, Hamburg) and resuspended in 0.5 mL cryomedium. Cells were first cooled down to -80°C and then stored in liquid nitrogen.

Cryomedium

SDM-79

corresponding antibiotics

10 % (v/v) FBS

7 % (v/v) glycerol

sterile filtered

Table 11: Procyclic T. brucei cell lines.

cell line	description
427	procyclic wild-type
29-13	inducible with doxycycline; selection with 15 µg/ml G418 (TetR), 50 µg/ml hygromycin (T7RNAP); suitable for RNA interference; reference: Wirt and Clayton, 1995
449	inducible with doxycycline; selection with 50 µg/ml phleomycin (TetR); suitable for ectopic expression; reference: Biebinger et al., 1997

Transfection of *T. brucei*

Prior to transfection, 10 µg of plasmid DNA were linearised overnight with the corresponding enzymes and buffers in a total volume of 50 µL at 37°C. For the linearization of RNAi constructs, the plasmids were treated with two units NotI. For the linearization of gene knockout constructs, the plasmids were hydrolysed with one unit HindIII and on one unit BamHI.

2 µL of the reactions were analysed on a 1 % agarose gel. Successfully linearized DNA was then precipitated with 0.1 volumes of 3 M Na-acetate and two volumes of ice cold 100 % ethanol and was incubated on ice for at least 30 min. After centrifugation at 24.100 rcf for 15 min at 4°C (Mikro 200R, type 2495, rotor 2424, Hettich Zentrifugen, Tuttlingen) the DNA was washed in ice cold 70 % ethanol. The ethanol was removed under sterile conditions and the pellet was dried in the laminar flow hood (ScanLaf, Mars Safety Class, LaboGene, Lynge, DK). The DNA was then dissolved in 10 µL sterile water.

For the transfection $1-2 \times 10^7$ cells were pelleted for 10 min at 400 rcf (5702 R, rotor A-4-38, Eppendorf, Hamburg) and cells were resuspended in 100 μ L transfection buffer (TF buffer). The cell suspension was added to the 10 μ L of DNA and homogenised well by resuspending. 105 μ L of this mixture was transferred to a transfection cuvette (732-1136, VWR, Radnor, PA, USA). The transfection was carried out via electroporation on a 'Nucleofector II' (Amaxa biosystems, via Lonza, Basel, Switzerland).

TF buffer

90 mM sodium phosphate

5 mM KCl

0.15 mM CaCl_2

50 mM HEPES, pH 7.3

sterile filtered

Generation of gene knockout cell lines

For a successful gene knockout, a suitable vector for homologous recombination was needed. For this purpose, the RNAi stem-loop vector pALC14 served as a template.

The included stuffer was replaced by either a puromycin resistance with a size of 1.000 bp (template: pEnG0P) or by a blasticidin resistance with a size of 900 bp (template: pNAT_BSD-6Myc_X). PCR products of the 5'UTR (286 bp) and 3'UTR (360 bp) of the target gene *ttll1* (Tb927.5.3860, 3.579 bp) were cloned into the modified vectors containing the antibiotic resistances (pALC14_puromycin and pALC14_blasticidin) via the restriction sites HindIII/XbaI and XhoI/BamHI. This resulted in two gene knockout vectors, each flanked by homologous regions of the target gene.

The final constructs were introduced into the cells in two transfection steps (Figure 35). After each transfection positive clones were confirmed by PCR.

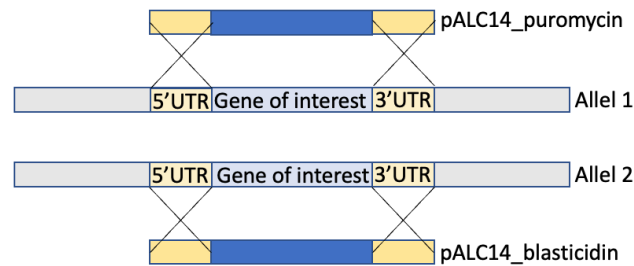


Figure 35: Schematic representation of the gene knockout by homologous recombination in *T. brucei*.

RNA interference in *T. brucei*

To successfully knockdown TTLL6A (Tb927.3.5380) and TTLL12B (Tb927.11.2420) it was necessary to create RNAi constructs. For this purpose, the stem-loop vector 'pFC4' (kindly provided by André Schneider) was used for molecular cloning. It allows the doxycycline-inducible expression of a hairpin dsRNA. To avoid off-target effects, RNAi fragments were generated with the tool 'RNAit' (Redmond, Vadivelu and Field, 2003).

A 266 bp PCR product for TTLL6A and a 180 bp PCR product for TTLL12B were amplified and cloned in the vector pFC4 using the restriction sites HindIII, XbaI, XhoI and BamHI. This vector contains an element, called 'PDF 260' (Figure 36), which was removed by a restriction hydrolysis with HindIII and XbaI followed by gel extraction of the vector bone prior to insertion of the PCR amplifiants.

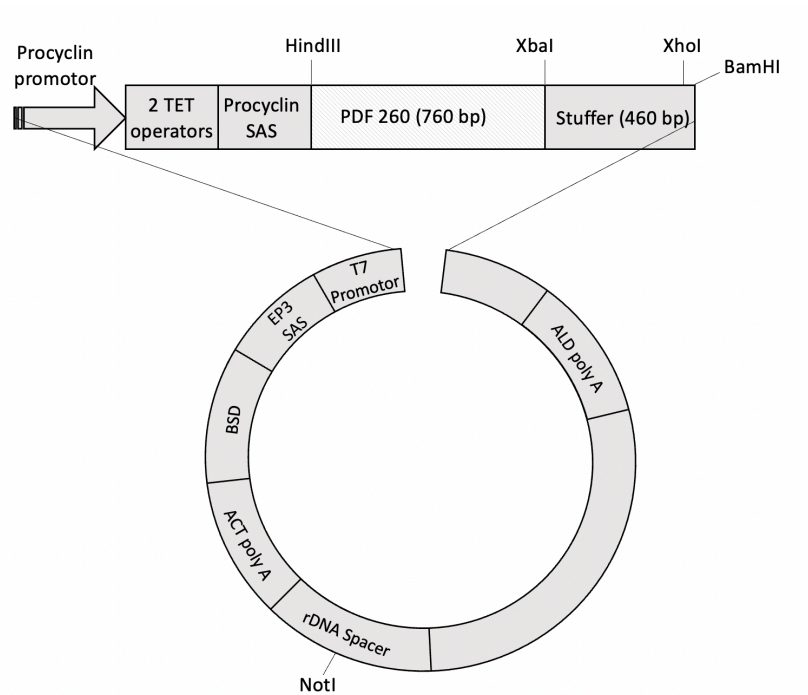


Figure 36: Schematic representation of the stem loop vector pFC4 (kindly provided by André Schneider).

The corresponding PCR products were first introduced in the coding direction via the HindIII and XbaI restriction sites, then, the same PCR products were introduced in the non-coding direction via the interfaces XhoI and BamHI. Both PCR fragments were separated by a stuffer (Figure 37).

Through the single doxycycline-inducible promoter, the formation of the hairpin-structure occurs through the pairing of the homologous cloned PCR amplicons. Cellular degradation is initiated once the homologous dsRNA is present.

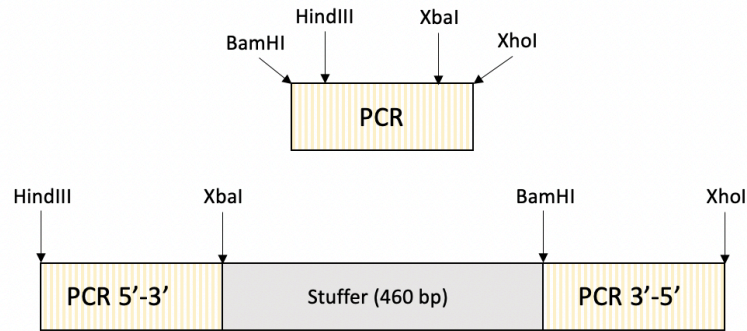


Figure 37: Schematic representation of the RNAi cloning strategy. First a 150 – 250 bp PCR product was amplified containing the restriction sites BamHI, HindIII, XbaI and XhoI. In a first cloning step, the PCR product was inserted left of the stuffer into the modified stem loop vector pFC4 (modification: removal of the PDF 260 fragment). In a second cloning step the PCR product and the vector containing the first PCR fragment was hydrolysed with the enzymes BamHI and XhoI. This allows the integration of the same PCR fragment to the right of the stuffer and in a 3'-5' direction, enabling the formation of a dsRNA hairpin after a doxycycline mediated induction.

Ectopic expression in *T. brucei*

To study possible effects of an overexpression of TTLL1 a plasmid that inducibly expressed the protein was generated. For this purpose, a PCR product of the open reading-frame (except the stop codon) of TTLL1 was amplified. Using the restriction sites FseI and AscI the product was inserted into the expression vector pHD1800. A 2x C-terminal myc tag allowed the detection of the expressed TTLL1^{myc}.

Growth curves

Cell growth was measured and documented over a period of five days with a CASY cell counter (Roche Innovatis AG, Germany). 5×10^5 cells/mL in a volume of 5 mL were seeded in 6 well plates. Three biological replicates were prepared for each treatment. Once the cells reached a density of $5-6 \times 10^6$ cells/mL, they were diluted to their initial concentration. The dilution factor was later included in the data analysis, therefore generating cumulative growth curves.

Flow cytometry analysis

Possible effects on the cell cycle of *T. brucei* RNAi-depleted and knockout cells were examined by flow cytometry. 6×10^6 cells of a logarithmically grown culture were harvested (10 min, 2.500 rcf, 5702 R, rotor A-4-38, Eppendorf, Hamburg) and washed in 1x PBS.

The cell-pellet was resuspended in 250 μ L of 0.5 % formaldehyde (diluted in 1xPBS), transferred into a 15 mL falcon tube and then incubated on ice for 5 min. 2.5 mL of 70 % ice-cold ethanol was slowly added to the cells while vortexing. After 1 h of rotation at 4°C the cell suspension was centrifuged for 5 min (1.400 rcf, 5702 R, rotor A-4-38, Eppendorf, Hamburg). The cells were resuspended in staining solution and incubated at for 30 min 37°C.

The analysis was done with the 'Cytomics FC 500' (Beckman Coulter, Krefeld) and the associated 'CXP' software.

Staining solution

950 μ L PBS

2 μ L RNase A (stock 10mg/mL)

50 μ L propidium iodide (stock 1mg/mL)

Motility analysis of *T. brucei*

The analysis of the swimming behaviour of the cells was performed as described in (Jentzsch *et al.*, 2020).

Quantification of western blot signal and fluorescence intensities

Quantification of western blots and fluorescence images was performed with ImageJ (v1.53a). For western blots the tool 'Analyse Gels' was used. To quantify images the tool 'Analyse measure' was used. Data were normalised to the signal from the anti-tubulin antibody signal.

Statistics

For statistical analysis the software Past4 (v3.24) (Hammer, Harper and Ryan, 2001) was used. For comparison of differences of two groups the data was first tested for normal distribution using the Shapiro-Wilk test. If normality was validated, means were compared with a t-test (Student, 1908), if normality was not met, groups were compared using the two-sample Kolmogorov Smirnov test (Pratt and Gibbons, 1981). If more than two groups were compared a normal distribution was tested using the Shapiro-Wilk test and homogeneity of variances was tested using Levene's test. (Levene, 1961). If the assumptions were met, groups were compared with an Anova (Girden, 1992) and Tukey-HSD. If the assumptions were violated a Kruskal-Wallis test (Kruskal and Wallis, 1952) with a Mann-Whitney pairwise test was performed.

Editing of images

Fluorescence images were edited with ImageJ (v1.53a). Deconvolution of expansion microscopy images was done using the plug-in 'DeconvolutionLab2 2.1.2' and the algorithm 'Richardson-Lucy (RL)' (Sage *et al.*, 2017). PSF image (point spread function) was generated with the plug-in 'Diffraction PSF 3D'.

References

Aillaud, C. *et al.* (2017) 'Vasohibins/SVBP are tubulin carboxypeptidases (TCPs) that regulate neuron differentiation', *Science*, 358(6369), pp. 1448–1453. Available at: <https://doi.org/10.1126/science.aao4165>.

Akhmanova, A. (2015) 'Control of microtubule organization and dynamics: two ends in the limelight', *Nature Reviews Molecular Cell Biology*, 16(12), pp. 711–726. Available at: <https://doi.org/10.1038/nrm4084>.

Akhmanova, A. and Hoogenraad, C.C. (2018) 'More is not always better: hyperglutamylation leads to neurodegeneration', *The EMBO Journal*, 37(23). Available at: <https://doi.org/10.15252/embj.2018101023>.

Akhmanova, A. and Steinmetz, M.O. (2008) 'Tracking the ends: a dynamic protein network controls the fate of microtubule tips', *Nature Reviews Molecular Cell Biology*, 9(4), pp. 309–322. Available at: <https://doi.org/10.1038/nrm2369>.

Alper, J.D. *et al.* (2014) 'The Motility of Axonemal Dynein Is Regulated by the Tubulin Code', *Biophysical Journal*, 107(12), pp. 2872–2880. Available at: <https://doi.org/10.1016/j.bpj.2014.10.061>.

Alushin, G.M. *et al.* (2014) 'High-Resolution Microtubule Structures Reveal the Structural Transitions in $\alpha\beta$ -Tubulin upon GTP Hydrolysis', *Cell*, 157(5), pp. 1117–1129. Available at: <https://doi.org/10.1016/j.cell.2014.03.053>.

Angelopoulos, E. (1970) 'Pellicular Microtubules in the Family Trypanosomatidae', *The Journal of Protozoology*, 17(1), pp. 39–51. Available at: <https://doi.org/10.1111/j.1550-7408.1970.tb05157.x>.

Badin-Larçon, A.C. *et al.* (2004) 'Suppression of nuclear oscillations in *Saccharomyces cerevisiae* expressing Glu tubulin', *Proceedings of the National Academy of Sciences*, 101(15), pp. 5577–5582. Available at: <https://doi.org/10.1073/pnas.0307917101>.

Banerjee, A., Bovenzi, F.A. and Bane, S.L. (2010) 'High-resolution separation of tubulin monomers on polyacrylamide minigels', *Analytical Biochemistry*, 402(2), pp. 194–196. Available at: <https://doi.org/10.1016/j.ab.2010.03.035>.

Basmacıyan, L. *et al.* (2019) '(De)glutamylation and cell death in *Leishmania* parasites', *PLOS Neglected Tropical Diseases*. Edited by A. Jardim, 13(4), p. e0007264. Available at: <https://doi.org/10.1371/journal.pntd.0007264>.

Bastin, P., Sherwin, T. and Gull, K. (1998) 'Paraflagellar rod is vital for trypanosome motility', *Nature*, 391(6667), pp. 548–548. Available at: <https://doi.org/10.1038/35300>.

Bechthold, J. (2022) 'The effect of unbalanced tubulin glutamylation on the cytoskeleton of *Trypanosoma brucei*'. Master Thesis, Molecular Parasitology, University of Bayreuth.

- Berezniuk, I. *et al.* (2012) 'Cytosolic Carboxypeptidase 1 Is Involved in Processing α - and β -Tubulin', *Journal of Biological Chemistry*, 287(9), pp. 6503–6517. Available at: <https://doi.org/10.1074/jbc.M111.309138>.
- Bertiaux, E. *et al.* (2018) 'Bidirectional intraflagellar transport is restricted to two sets of microtubule doublets in the trypanosome flagellum', *Journal of Cell Biology*, 217(12), pp. 4284–4297. Available at: <https://doi.org/10.1083/jcb.201805030>.
- Bhabha, G. *et al.* (2016) 'How Dynein Moves Along Microtubules', *Trends in Biochemical Sciences*, 41(1), pp. 94–105. Available at: <https://doi.org/10.1016/j.tibs.2015.11.004>.
- Bieling, P. *et al.* (2008) 'CLIP-170 tracks growing microtubule ends by dynamically recognizing composite EB1/tubulin-binding sites', *Journal of Cell Biology*, 183(7), pp. 1223–1233. Available at: <https://doi.org/10.1083/jcb.200809190>.
- Bigman, L.S. and Levy, Y. (2020) 'Tubulin tails and their modifications regulate protein diffusion on microtubules', *Proceedings of the National Academy of Sciences*, 117(16), pp. 8876–8883. Available at: <https://doi.org/10.1073/pnas.1914772117>.
- Bramblett, G.T., Chang, S.L. and Flavin, M. (1987) 'Periodic crosslinking of microtubules by cytoplasmic microtubule-associated and microtubule-corset proteins from a trypanosomatid.', *Proceedings of the National Academy of Sciences*, 84(10), pp. 3259–3263. Available at: <https://doi.org/10.1073/pnas.84.10.3259>.
- Briggs, L.J. *et al.* (2004) 'The flagella connector of *Trypanosoma brucei*: an unusual mobile transmembrane junction', *Journal of Cell Science*, 117(9), pp. 1641–1651. Available at: <https://doi.org/10.1242/jcs.00995>.
- Brun, R. *et al.* (2010) 'Human African trypanosomiasis', *The Lancet*, 375(9709), pp. 148–159.
- Buschmann, H. *et al.* (2007) 'Homologues of Arabidopsis Microtubule-Associated AIR9 in Trypanosomatid Parasites: Hints on Evolution and Function', *Plant Signaling & Behavior*, 2(4), pp. 296–299. Available at: <https://doi.org/10.4161/psb.2.4.4041>.
- Casanova, M. *et al.* (2015) 'Characterisation of polyglutamylases in trypanosomatids', *International Journal for Parasitology*, 45(2–3), pp. 121–132. Available at: <https://doi.org/10.1016/j.ijpara.2014.09.005>.
- Choudhary, C. *et al.* (2009) 'Lysine Acetylation Targets Protein Complexes and Co-Regulates Major Cellular Functions', *Science*, 325(5942), pp. 834–840. Available at: <https://doi.org/10.1126/science.1175371>.
- Chu, C.-W. *et al.* (2011) 'A novel acetylation of β -tubulin by San modulates microtubule polymerization via down-regulating tubulin incorporation', *Molecular Biology of the Cell*. Edited by E.L.F. Holzbaaur, 22(4), pp. 448–456. Available at: <https://doi.org/10.1091/mbc.e10-03-0203>.

- Coutton, C. *et al.* (2018) 'Mutations in CFAP43 and CFAP44 cause male infertility and flagellum defects in Trypanosoma and human', *Nature Communications*, 9(1), p. 686. Available at: <https://doi.org/10.1038/s41467-017-02792-7>.
- Dawe, H.R. *et al.* (2005) 'The Parkin co-regulated gene product, PACRG, is an evolutionarily conserved axonemal protein that functions in outer-doublet microtubule morphogenesis', *Journal of Cell Science*, 118(23), pp. 5421–5430. Available at: <https://doi.org/10.1242/jcs.02659>.
- Dawe, H.R. *et al.* (2007) 'The hydrocephalus inducing gene product, Hydin, positions axonemal central pair microtubules', *BMC Biology*, 5(1), p. 33. Available at: <https://doi.org/10.1186/1741-7007-5-33>.
- DeJesus, E. *et al.* (2013) 'A Single Amino Acid Substitution in the Group 1 Trypanosoma brucei gambiense Haptoglobin-Hemoglobin Receptor Abolishes TLF-1 Binding', *PLoS Pathogens*. Edited by K.L. Hill, 9(4), p. e1003317. Available at: <https://doi.org/10.1371/journal.ppat.1003317>.
- Desai, A. and Mitchison, T.J. (1997) 'Microtubule polymerization dynamics', *Annual Review of Cell and Developmental Biology*, 13(1), pp. 83–117. Available at: <https://doi.org/10.1146/annurev.cellbio.13.1.83>.
- van Dijk, J. *et al.* (2007) 'A Targeted Multienzyme Mechanism for Selective Microtubule Polyglutamylolation', *Molecular Cell*, 26(3), pp. 437–448. Available at: <https://doi.org/10.1016/j.molcel.2007.04.012>.
- van Dijk, J. *et al.* (2008) 'Polyglutamylolation Is a Post-translational Modification with a Broad Range of Substrates', *Journal of Biological Chemistry*, 283(7), pp. 3915–3922. Available at: <https://doi.org/10.1074/jbc.M705813200>.
- Erck, C. *et al.* (2005) 'A vital role of tubulin-tyrosine-ligase for neuronal organization', *Proceedings of the National Academy of Sciences*, 102(22), pp. 7853–7858. Available at: <https://doi.org/10.1073/pnas.0409626102>.
- Ersfeld, K. *et al.* (1993) 'Characterization of the tubulin-tyrosine ligase.', *Journal of Cell Biology*, 120(3), pp. 725–732. Available at: <https://doi.org/10.1083/jcb.120.3.725>.
- Ersfeld, K., Asbeck, K. and Gull, K. (1998) 'Direct visualisation of individual gene organisation in Trypanosoma brucei by high-resolution in situ hybridisation', *Chromosoma*, 107(4), pp. 237–240. Available at: <https://doi.org/10.1007/s004120050302>.
- Fenn, K. and Matthews, K.R. (2007) 'The cell biology of Trypanosoma brucei differentiation', *Current Opinion in Microbiology*, 10(6), pp. 539–546. Available at: <https://doi.org/10.1016/j.mib.2007.09.014>.
- Gadadhar, S. *et al.* (2017) 'The tubulin code at a glance', *Journal of Cell Science* 130(8) pp. 1347-1353. Available at: <https://doi.org/10.1242/jcs.199471>.

- Gadadhar, S. *et al.* (2021) 'Tubulin glycylation controls axonemal dynein activity, flagellar beat, and male fertility', *Science*, 371(6525), p. eabd4914. Available at: <https://doi.org/10.1126/science.abd4914>.
- Galjart, N. (2010) 'Plus-End-Tracking Proteins and Their Interactions at Microtubule Ends', *Current Biology*, 20(12), pp. R528–R537. Available at: <https://doi.org/10.1016/j.cub.2010.05.022>.
- Gard, D.L. and Kirschner, M.W. (1987) 'A microtubule-associated protein from *Xenopus* eggs that specifically promotes assembly at the plus-end.', *Journal of Cell Biology*, 105(5), pp. 2203–2215. Available at: <https://doi.org/10.1083/jcb.105.5.2203>.
- Giordano, T. *et al.* (2019) 'Loss of the deglutamylase CCP5 perturbs multiple steps of spermatogenesis and leads to male infertility', *Journal of Cell Science*, p. jcs.226951. Available at: <https://doi.org/10.1242/jcs.226951>.
- Girden, E.R. (1992) *ANOVA: Repeated measures*. Sage Publications.
- Gluezn, E. *et al.* (2011) 'The Kinetoplast Duplication Cycle in *Trypanosoma brucei* Is Orchestrated by Cytoskeleton-Mediated Cell Morphogenesis', *Molecular and Cellular Biology*, 31(5), pp. 1012–1021. Available at: <https://doi.org/10.1128/MCB.01176-10>.
- Gudimchuk, N.B. and McIntosh, J.R. (2021) 'Regulation of microtubule dynamics, mechanics and function through the growing tip', *Nature Reviews Molecular Cell Biology*, 22(12), pp. 777–795. Available at: <https://doi.org/10.1038/s41580-021-00399-x>.
- Guedes-Dias, P. and Holzbaur, E.L.F. (2019) 'Axonal transport: Driving synaptic function', *Science*, 366(6462), p. eaaw9997. Available at: <https://doi.org/10.1126/science.aaw9997>.
- Gull, K. (1999) 'The Cytoskeleton of Trypanosomatid Parasites', *Annual Review of Microbiology*, 53(1), pp. 629–655. Available at: <https://doi.org/10.1146/annurev.micro.53.1.629>.
- Hammarton, T.C. *et al.* (2003) 'Stage-specific Differences in Cell Cycle Control in *Trypanosoma brucei* Revealed by RNA Interference of a Mitotic Cyclin', *Journal of Biological Chemistry*, 278(25), pp. 22877–22886. Available at: <https://doi.org/10.1074/jbc.M300813200>.
- Hammarton, T.C., Engstler, M. and Mottram, J.C. (2004) 'The *Trypanosoma brucei* Cyclin, CYC2, Is Required for Cell Cycle Progression through G1 Phase and for Maintenance of Procyclic Form Cell Morphology', *Journal of Biological Chemistry*, 279(23), pp. 24757–24764. Available at: <https://doi.org/10.1074/jbc.M401276200>.
- Hammer, O., Harper, D.A.T. and Ryan, P.D. (2001) 'PAST: Paleontological Statistics Software Package for Education and Data Analysis', p. 9.

- Hausrat, T.J. *et al.* (2022) 'Disruption of tubulin-alpha4a polyglutamylation prevents aggregation of hyper-phosphorylated tau and microglia activation in mice', *Nature Communications*, 13(1), p. 4192. Available at: <https://doi.org/10.1038/s41467-022-31776-5>.
- He, K., Ling, K. and Hu, J. (2020) 'The emerging role of tubulin posttranslational modifications in cilia and ciliopathies', *Biophysics Reports*, 6(4), pp. 89–104. Available at: <https://doi.org/10.1007/s41048-020-00111-0>.
- Hemphill, A., Lawson, D. and Seebeck, T. (1991) 'The Cytoskeletal Architecture of *Trypanosoma brucei*', *The Journal of Parasitology*, 77(4), p. 603. Available at: <https://doi.org/10.2307/3283167>.
- Hilton, N.A. *et al.* (2018) 'Identification of TOEFAZ1-interacting proteins reveals key regulators of *Trypanosoma brucei* cytokinesis: TOEFAZ1 interactors in *T. brucei*', *Molecular Microbiology*, 109(3), pp. 306–326. Available at: <https://doi.org/10.1111/mmi.13986>.
- Hirokawa, N. *et al.* (2009) 'Kinesin superfamily motor proteins and intracellular transport', *Nature Reviews Molecular Cell Biology*, 10(10), pp. 682–696. Available at: <https://doi.org/10.1038/nrm2774>.
- Hong, S.-R. *et al.* (2018) 'Spatiotemporal manipulation of ciliary glutamylation reveals its roles in intraciliary trafficking and Hedgehog signaling', *Nature Communications*, 9(1), p. 1732. Available at: <https://doi.org/10.1038/s41467-018-03952-z>.
- Howard, W.D. and Timasheff, S.N. (1986) 'GDP state of tubulin: stabilization of double rings', *Biochemistry*, 25(25), pp. 8292–8300. Available at: <https://doi.org/10.1021/bi00373a025>.
- Ikegami, K. *et al.* (2010) 'Tubulin polyglutamylation is essential for airway ciliary function through the regulation of beating asymmetry', *Proceedings of the National Academy of Sciences*, 107(23), pp. 10490–10495. Available at: <https://doi.org/10.1073/pnas.1002128107>.
- Ishikawa, H. and Marshall, W.F. (2011) 'Ciliogenesis: building the cell's antenna', *Nature Reviews Molecular Cell Biology*, 12(4), pp. 222–234. Available at: <https://doi.org/10.1038/nrm3085>.
- Ishikawa, T. (2012) 'Structural biology of cytoplasmic and axonemal dyneins', *AAA + Proteins*, 179(2), pp. 229–234. Available at: <https://doi.org/10.1016/j.jsb.2012.05.016>.
- Janke, C. *et al.* (2005) 'Tubulin Polyglutamylase Enzymes Are Members of the TTL Domain Protein Family', *Science*, 308(5729), pp. 1758–1762. Available at: <https://doi.org/10.1126/science.1113010>.
- Janke, C. (2014) 'The tubulin code: Molecular components, readout mechanisms, and functions', *Journal of Cell Biology*, 206(4), pp. 461–472. Available at: <https://doi.org/10.1083/jcb.201406055>.

- Janke, C. and Bulinski, J. C. (2011) 'Post-translational regulation of the microtubule cytoskeleton: mechanisms and functions', *Nature Reviews Molecular Cell Biology*, 12(12), pp. 773–786. Available at: <https://doi.org/10.1038/nrm3227>.
- Janke, C. and Magiera, M.M. (2020) 'The tubulin code and its role in controlling microtubule properties and functions', *Nature Reviews Molecular Cell Biology*, 21(6), pp. 307–326. Available at: <https://doi.org/10.1038/s41580-020-0214-3>.
- Jentzsch, J. *et al.* (2020) 'Microtubule polyglutamylation is important for regulating cytoskeletal architecture and motility in *Trypanosoma brucei*', *Journal of Cell Science*, p. jcs.248047. Available at: <https://doi.org/10.1242/jcs.248047>.
- Kalichava, A. and Ochsenreiter, T. (2021) 'Ultrastructure expansion microscopy in *Trypanosoma brucei*', *Open Biology*, 11(10), p. 210132. Available at: <https://doi.org/10.1098/rsob.210132>.
- Kargbo, A. *et al.* (2022) 'Epizootiology and Molecular Identification of Trypanosome Species in Livestock Ruminants in the Gambia', *Acta Parasitologica*, 67(1), pp. 130–142. Available at: <https://doi.org/10.1007/s11686-021-00442-z>.
- Kelliher, M.T., Saunders, H.A. and Wildonger, J. (2019) 'Microtubule control of functional architecture in neurons', *Current Opinion in Neurobiology*, 57, pp. 39–45. Available at: <https://doi.org/10.1016/j.conb.2019.01.003>.
- Kennedy, P.G. (2013) 'Clinical features, diagnosis, and treatment of human African trypanosomiasis (sleeping sickness)', *The Lancet Neurology*, 12(2), pp. 186–194. Available at: [https://doi.org/10.1016/S1474-4422\(12\)70296-X](https://doi.org/10.1016/S1474-4422(12)70296-X).
- Kennedy, P.G.E. and Rodgers, J. (2019) 'Clinical and Neuropathogenetic Aspects of Human African Trypanosomiasis', *Frontiers in Immunology*, 10, p. 39. Available at: <https://doi.org/10.3389/fimmu.2019.00039>.
- Kimura, Y. *et al.* (2010) 'Identification of Tubulin Deglutamylase among *Caenorhabditis elegans* and Mammalian Cytosolic Carboxypeptidases (CCPs)', *Journal of Biological Chemistry*, 285(30), pp. 22936–22941. Available at: <https://doi.org/10.1074/jbc.C110.128280>.
- Kohl, L., Robinson, D. and Bastin, P. (2003) 'Novel roles for the flagellum in cell morphogenesis and cytokinesis of trypanosomes', *The EMBO Journal*, 22(20), pp. 5336–5346. Available at: <https://doi.org/10.1093/emboj/cdg518>.
- Konno, A. *et al.* (2016) 'Doublet 7 shortening, doublet 5-preferential poly-Glu reduction, and beating stall of sperm flagella in *Ttll9* $-/-$ mice', *Journal of Cell Science*, p. jcs.185983. Available at: <https://doi.org/10.1242/jcs.185983>.
- Koyfman, A.Y. *et al.* (2011) 'Structure of *Trypanosoma brucei* flagellum accounts for its bihelical motion', *Proceedings of the National Academy of Sciences*, 108(27), pp. 11105–11108. Available at: <https://doi.org/10.1073/pnas.1103634108>.

- Kruskal, W.H. and Wallis, W.A. (1952) 'Use of Ranks in One-Criterion Variance Analysis', *Journal of the American Statistical Association*, 47(260), pp. 583–621. Available at: <https://doi.org/10.1080/01621459.1952.10483441>.
- Kubo, T. *et al.* (2010) 'Tubulin Polyglutamylation Regulates Axonemal Motility by Modulating Activities of Inner-Arm Dyneins', *Current Biology*, 20(5), pp. 441–445. Available at: <https://doi.org/10.1016/j.cub.2009.12.058>.
- van der Laan, S. *et al.* (2019) 'Evolutionary Divergence of Enzymatic Mechanisms for Tubulin Detyrosination', *Cell Reports*, 29(12), pp. 4159–4171.e6. Available at: <https://doi.org/10.1016/j.celrep.2019.11.074>.
- Lacomble, S. *et al.* (2010) 'Basal body movements orchestrate membrane organelle division and cell morphogenesis in *Trypanosoma brucei*', *Journal of Cell Science*, 123(17), pp. 2884–2891. Available at: <https://doi.org/10.1242/jcs.074161>.
- LaCount, D.J., Barrett, B. and Donelson, J.E. (2002) 'Trypanosoma brucei FLA1 Is Required for Flagellum Attachment and Cytokinesis', *Journal of Biological Chemistry*, 277(20), pp. 17580–17588. Available at: <https://doi.org/10.1074/jbc.M200873200>.
- Laemmli, U.K. (1970) 'Cleavage of Structural Proteins during the Assembly of the Head of Bacteriophage T4', *Nature*, 227(5259), pp. 680–685. Available at: <https://doi.org/10.1038/227680a0>.
- Lallinger-Kube, G. (2017) *Characterization of the single end-binding protein homologue TbEB1 in Trypanosoma brucei*. Dissertation, Universität Bayreuth (Germany).
- Landskron, L. *et al.* (2022) 'Posttranslational modification of microtubules by the MATCAP detyrosinase', *Science*, 376(6595), p. eabn6020. Available at: <https://doi.org/10.1126/science.abn6020>.
- Levene, H. (1961) 'Robust tests for equality of variances', *Contributions to probability and statistics. Essays in honor of Harold Hotelling*, pp. 279–292.
- López-Escobar, L. *et al.* (2022) 'Stage-specific transcription activator ESB1 regulates monoallelic antigen expression in *Trypanosoma brucei*', *Nature Microbiology*, 7(8), pp. 1280–1290. Available at: <https://doi.org/10.1038/s41564-022-01175-z>.
- Magiera *et al.* (2018a) 'Excessive tubulin polyglutamylation causes neurodegeneration and perturbs neuronal transport', *The EMBO Journal*, 37(23), e100440. Available at: <https://doi.org/10.15252/embj.2018100440>.
- Magiera *et al.* (2018b) 'Tubulin Posttranslational Modifications and Emerging Links to Human Disease', *Cell*, 173(6), pp. 1323–1327. Available at: <https://doi.org/10.1016/j.cell.2018.05.018>.

- Mahalingan, K.K. *et al.* (2020) 'Structural basis for polyglutamate chain initiation and elongation by TLL family enzymes', *Nature Structural & Molecular Biology*, 27(9), pp. 802–813. Available at: <https://doi.org/10.1038/s41594-020-0462-0>.
- Matthews, K.R., Ellis, J.R. and Paterou, A. (2004) 'Molecular regulation of the life cycle of African trypanosomes', *Trends in Parasitology*, 20(1), pp. 40–47. Available at: <https://doi.org/10.1016/j.pt.2003.10.016>.
- Matthews, K.R., Sherwin, T. and Gull, K. (1995) 'Mitochondrial genome repositioning during the differentiation of the African trypanosome between life cycle forms is microtubule mediated', *Journal of Cell Science*, 108(6), pp. 2231–2239.
- May, S.F. *et al.* (2012) 'The *Trypanosoma brucei* AIR9-like protein is cytoskeleton-associated and is required for nucleus positioning and accurate cleavage furrow placement', *Molecular Microbiology*, 84(1), pp. 77–92. Available at: <https://doi.org/10.1111/j.1365-2958.2012.08008.x>.
- McCulloch, R. (2004) 'Antigenic variation in African trypanosomes: monitoring progress', *Trends in Parasitology*, 20(3), pp. 117–121. Available at: <https://doi.org/10.1016/j.pt.2003.12.004>.
- McKean, P.G. (2003) 'Coordination of cell cycle and cytokinesis in *Trypanosoma brucei*', *Current Opinion in Microbiology*, 6(6), pp. 600–607. Available at: <https://doi.org/10.1016/j.mib.2003.10.010>.
- McNally, F.J. and Roll-Mecak, A. (2018) 'Microtubule-severing enzymes: From cellular functions to molecular mechanism', *Journal of Cell Biology*, 217(12), pp. 4057–4069. Available at: <https://doi.org/10.1083/jcb.201612104>.
- Mitchison, T. and Kirschner, M. (1984) 'Dynamic instability of microtubule growth', *Nature*, 312(5991), pp. 237–242. Available at: <https://doi.org/10.1038/312237a0>.
- Moreira-Leite, F.F. *et al.* (2001) 'A Trypanosome Structure Involved in Transmitting Cytoplasmic Information during Cell Division', *Science*, 294(5542), pp. 610–612.
- Mukai, M., Ikegami, K., Sugiura, Y., Takeshita, K., Nakagawa, A., & Setou, M. (2009). Recombinant mammalian tubulin polyglutamylase TLL7 performs both initiation and elongation of polyglutamylation on β -tubulin through a random sequential pathway. *Biochemistry*, 48(5), 1084–1093. Available at: <https://doi.org/10.1021/bi802047y>
- Mullen, R.J., Eicher, E.M. and Sidman, R.L. (1976) 'Purkinje cell degeneration, a new neurological mutation in the mouse.', *Proceedings of the National Academy of Sciences*, 73(1), pp. 208–212. Available at: <https://doi.org/10.1073/pnas.73.1.208>.
- Nachury, M.V. and Mick, D.U. (2019) 'Establishing and regulating the composition of cilia for signal transduction', *Nature Reviews Molecular Cell Biology*, 20(7), pp. 389–405. Available at: <https://doi.org/10.1038/s41580-019-0116-4>.

- Nehlig, A. *et al.* (2017) 'Regulation of end-binding protein EB1 in the control of microtubule dynamics', *Cellular and Molecular Life Sciences*, 74(13), pp. 2381–2393. Available at: <https://doi.org/10.1007/s00018-017-2476-2>.
- Nett, I.R.E. *et al.* (2009) 'Identification and Specific Localization of Tyrosine-Phosphorylated Proteins in *Trypanosoma brucei*', *Eukaryotic Cell*, 8(4), pp. 617–626. Available at: <https://doi.org/10.1128/EC.00366-08>.
- Neuteboom, L.W. *et al.* (1999) 'Isolation and characterization of cDNA clones corresponding with mRNAs that accumulate during auxin-induced lateral root formation', *Plant Molecular Biology*, 39(2), pp. 273–287. Available at: <https://doi.org/10.1023/A:1006104205959>.
- Nieuwenhuis, J. and Brummelkamp, T.R. (2019) 'The Tubulin Detyrosination Cycle: Function and Enzymes', *Trends in Cell Biology*, 29(1), pp. 80–92. Available at: <https://doi.org/10.1016/j.tcb.2018.08.003>.
- Nogales, E., Wolf, S.G. and Downing, K.H. (1998) 'Erratum: Structure of the $\alpha\beta$ tubulin dimer by electron crystallography', *Nature*, 393(6681), pp. 191–191. Available at: <https://doi.org/10.1038/30288>.
- Odiit, M., Kansiime, F. and Enyaru, J. (1997) 'Duration of symptoms and case fatality of sleeping sickness caused by *Trypanosoma brucei rhodesiense* in Tororo, Uganda', *East African medical journal*, 74(12), pp. 792–795.
- Ogbadoyi, E. *et al.* (2000) 'Architecture of the *Trypanosoma brucei* nucleus during interphase and mitosis', *Chromosoma*, 108(8), pp. 501–513. Available at: <https://doi.org/10.1007/s004120050402>.
- Ogbadoyi, E.O., Robinson, D.R. and Gull, K. (2003) 'A High-Order *Trans* -Membrane Structural Linkage Is Responsible for Mitochondrial Genome Positioning and Segregation by Flagellar Basal Bodies in Trypanosomes', *Molecular Biology of the Cell*, 14(5), pp. 1769–1779. Available at: <https://doi.org/10.1091/mbc.e02-08-0525>.
- Olego-Fernandez, S. *et al.* (2009) 'Cell Morphogenesis of *Trypanosoma brucei* Requires the Paralogous, Differentially Expressed Calpain-related Proteins CAP5.5 and CAP5.5V', *Protist*, 160(4), pp. 576–590. Available at: <https://doi.org/10.1016/j.protis.2009.05.003>.
- Pasternack, D.A. *et al.* (2015) 'Sphingosine Kinase Regulates Microtubule Dynamics and Organelle Positioning Necessary for Proper G₁/S Cell Cycle Transition in *Trypanosoma brucei*', *mBio*. Edited by L.M. Weiss, 6(5), pp. e01291-15. Available at: <https://doi.org/10.1128/mBio.01291-15>.
- Pays, E., Vanhamme, L. and Pérez-Morga, D. (2004) 'Antigenic variation in *Trypanosoma brucei*: facts, challenges and mysteries', *Current Opinion in Microbiology*, 7(4), pp. 369–374. Available at: <https://doi.org/10.1016/j.mib.2004.05.001>.
- Pepin, J. and Meda, H. (2001) 'The epidemiology and control of human African

- trypanosomiasis', in *Advances in Parasitology*. Elsevier, pp. 71–132. Available at: [https://doi.org/10.1016/S0065-308X\(01\)49038-5](https://doi.org/10.1016/S0065-308X(01)49038-5).
- Peris, L. *et al.* (2006) 'Tubulin tyrosination is a major factor affecting the recruitment of CAP-Gly proteins at microtubule plus ends', *Journal of Cell Biology*, 174(6), pp. 839–849. Available at: <https://doi.org/10.1083/jcb.200512058>.
- Pfaffl, M.W. (2004) 'Real-time RT-PCR: Neue Ansätze zur exakten mRNA Quantifizierung', *BIOspektrum*, 1(04), pp. 92–95.
- Ploubidou, A. *et al.* (1999) 'Evidence for novel cell cycle checkpoints in trypanosomes: kinetoplast segregation and cytokinesis in the absence of mitosis', *Journal of Cell Science*, 112(24), pp. 4641–4650.
- Portman, N. and Gull, K. (2014) 'Identification of Paralogous Life-Cycle Stage Specific Cytoskeletal Proteins in the Parasite *Trypanosoma brucei*', *PLoS ONE*. Edited by Z. Li, 9(9), p. e106777. Available at: <https://doi.org/10.1371/journal.pone.0106777>.
- Portran, D. *et al.* (2017) 'Tubulin acetylation protects long-lived microtubules against mechanical ageing', *Nature Cell Biology*, 19(4), pp. 391–398. Available at: <https://doi.org/10.1038/ncb3481>.
- Pratt, J.W. and Gibbons, J.D. (1981) 'Kolmogorov-Smirnov Two-Sample Tests', in J.W. Pratt and J.D. Gibbons (eds) *Concepts of Nonparametric Theory*. New York, NY: Springer New York, pp. 318–344. Available at: https://doi.org/10.1007/978-1-4612-5931-2_7.
- Prota, A.E. *et al.* (2013) 'Structural basis of tubulin tyrosination by tubulin tyrosine ligase', *Journal of Cell Biology*, 200(3), pp. 259–270. Available at: <https://doi.org/10.1083/jcb.201211017>.
- Ralston, K.S. *et al.* (2009) 'The *Trypanosoma brucei* Flagellum: Moving Parasites in New Directions', *Annual Review of Microbiology*, 63(1), pp. 335–362. Available at: <https://doi.org/10.1146/annurev.micro.091208.073353>.
- Raper, J. *et al.* (1999) 'Characterization of a Novel Trypanosome Lytic Factor from Human Serum', *Infection and immunity*, 67(4), pp. 1910–1916.
- Redemann, S. *et al.* (2019) 'Current approaches for the analysis of spindle organization', *Current opinion in structural biology*, 58, pp. 269–277. Available at: <https://doi.org/10.1016/j.sbi.2019.05.023>.
- Redmond, S., Vadivelu, J. and Field, M.C. (2003) 'RNAit: an automated web-based tool for the selection of RNAi targets in *Trypanosoma brucei*', *Molecular and Biochemical Parasitology*, 128(1), pp. 115–118. Available at: [https://doi.org/10.1016/S0166-6851\(03\)00045-8](https://doi.org/10.1016/S0166-6851(03)00045-8).

- Regnard, C. *et al.* (2000) 'Polyglutamylation of Nucleosome Assembly Proteins', *Journal of Biological Chemistry*, 275(21), pp. 15969–15976. Available at: <https://doi.org/10.1074/jbc.M000045200>.
- Robinson, D. *et al.* (1991) '[25] Microtubules, tubulin, and microtubule-associated proteins of trypanosomes', in *Methods in Enzymology*. Elsevier, pp. 285–299. Available at: [https://doi.org/10.1016/0076-6879\(91\)96027-0](https://doi.org/10.1016/0076-6879(91)96027-0).
- Robinson, D.R. *et al.* (1995) 'Microtubule polarity and dynamics in the control of organelle positioning, segregation, and cytokinesis in the trypanosome cell cycle.', *Journal of Cell Biology*, 128(6), pp. 1163–1172. Available at: <https://doi.org/10.1083/jcb.128.6.1163>.
- Robinson, D.R. and Gull, K. (1991) 'Basal body movements as a mechanism for mitochondrial genome segregation in the trypanosome cell cycle', *Nature*, 352(6337), pp. 731–733. Available at: <https://doi.org/10.1038/352731a0>.
- Rogowski, K. *et al.* (2010) 'A Family of Protein-Deglutamylating Enzymes Associated with Neurodegeneration', *Cell*, 143(4), pp. 564–578. Available at: <https://doi.org/10.1016/j.cell.2010.10.014>.
- Roostalu, J. and Surrey, T. (2017) 'Microtubule nucleation: beyond the template', *Nature Reviews Molecular Cell Biology*, 18(11), pp. 702–710. Available at: <https://doi.org/10.1038/nrm.2017.75>.
- Rotureau, B. *et al.* (2012) 'A new asymmetric division contributes to the continuous production of infective trypanosomes in the tsetse fly', *Development*, 139(10), pp. 1842–1850. Available at: <https://doi.org/10.1242/dev.072611>.
- Rotureau, B. *et al.* (2014) 'Forward motility is essential for trypanosome infection in the tsetse fly: Trypanosome motility is essential in tsetse flies', *Cellular Microbiology*, 16(3), pp. 425–433. Available at: <https://doi.org/10.1111/cmi.12230>.
- Rotureau, B. and Van Den Abbeele, J. (2013) 'Through the dark continent: African trypanosome development in the tsetse fly', *Frontiers in Cellular and Infection Microbiology*, 3. Available at: <https://doi.org/10.3389/fcimb.2013.00053>.
- Ryan, K.A. *et al.* (1988) 'Replication of Kinetoplast DNA in Trypanosomes', *Annual Review of Microbiology*, 42(1), pp. 339–358. Available at: <https://doi.org/10.1146/annurev.mi.42.100188.002011>.
- Sage, D. *et al.* (2017) 'DeconvolutionLab2: An open-source software for deconvolution microscopy', *Methods*, 115, pp. 28–41. Available at: <https://doi.org/10.1016/j.ymeth.2016.12.015>.
- mondiale de la Santé, O. and World Health Organization (2021) 'Elimination of Human African Trypanosomiasis as public health problem—Élimination de la trypanosomiase humaine africaine comme problème de santé publique', *Weekly Epidemiological Record=Relevé épidémiologique hebdomadaire*, 96(21), pp. 196–196.

- Sasse, R. and Gull, K. (1988) 'Tubulin post-translational modifications and the construction of microtubular organelles in *Trypanosoma brucei*', *Journal of Cell Science*, 90(4), pp. 577–589.
- Schindelin, J. *et al.* (2012) 'Fiji: an open-source platform for biological-image analysis', *Nature Methods*, 9(7), pp. 676–682. Available at: <https://doi.org/10.1038/nmeth.2019>.
- Schneider, A., Plessmann, U. and Weber, K. (1997) 'Subpellicular and flagellar microtubules of *Trypanosoma brucei* are extensively glutamylated', *Journal of Cell Science*, 110(4), pp. 431–437.
- Schock, M., Schmidt, S. and Ersfeld, K. (2021) 'Novel Cytoskeleton-Associated Proteins in *Trypanosoma brucei* Are Essential for Cell Morphogenesis and Cytokinesis', *Microorganisms*, 9(11), p. 2234. Available at: <https://doi.org/10.3390/microorganisms9112234>.
- Schuster, S. *et al.* (2021) 'Unexpected plasticity in the life cycle of *Trypanosoma brucei*', *eLife*, 10, p. e66028. Available at: <https://doi.org/10.7554/eLife.66028>.
- Seebeck, Th. *et al.* (1988) 'The cytoskeleton of *Trypanosoma brucei*-the beauty of simplicity', *Protoplasma*, 145(2–3), pp. 188–194. Available at: <https://doi.org/10.1007/BF01349358>.
- Shapiro, T.A. and Englund, P.T. (1995) 'THE STRUCTURE AND REPLICATION OF KINETOPLAST DNA', *Annual Review of Microbiology*, 49(1), pp. 117–143. Available at: <https://doi.org/10.1146/annurev.mi.49.100195.001001>.
- Sharma, R. *et al.* (2009) 'The heart of darkness: growth and form of *Trypanosoma brucei* in the tsetse fly', *Trends in Parasitology*, 25(11), pp. 517–524. Available at: <https://doi.org/10.1016/j.pt.2009.08.001>.
- Shashi, V. *et al.* (2018) 'Loss of tubulin deglutamylase CCP 1 causes infantile-onset neurodegeneration', *The EMBO Journal*, 37(23). Available at: <https://doi.org/10.15252/embj.2018100540>.
- Sherwin, T. *et al.* (1987) 'Distinct localization and cell cycle dependence of COOH terminally tyrosinolated alpha-tubulin in the microtubules of *Trypanosoma brucei brucei*.' , *The Journal of Cell Biology*, 104(3), pp. 439–446. Available at: <https://doi.org/10.1083/jcb.104.3.439>.
- Sherwin, T. and Gull, K. (1989) 'Visualization of detyrosination along single microtubules reveals novel mechanisms of assembly during cytoskeletal duplication in trypanosomes', *Cell*, 57(2), pp. 211–221. Available at: [https://doi.org/10.1016/0092-8674\(89\)90959-8](https://doi.org/10.1016/0092-8674(89)90959-8).
- Siegel, T.N., Hekstra, D.R. and Cross, G.A.M. (2008) 'Analysis of the *Trypanosoma brucei* cell cycle by quantitative DAPI imaging', *Molecular and Biochemical Parasitology*, 160(2), pp. 171–174. Available at: <https://doi.org/10.1016/j.molbiopara.2008.04.004>.
- Sinclair, A.N. *et al.* (2021) 'The *Trypanosoma brucei* subpellicular microtubule array is organized into functionally discrete subdomains defined by microtubule associated proteins', *PLoS Pathogens*, 17(5), p. e1009588. Available at: <https://doi.org/10.1371/journal.ppat.1009588>.

- Sinclair, A.N. and de Graffenried, C.L. (2019) 'More than Microtubules: The Structure and Function of the Subpellicular Array in Trypanosomatids', *Trends in Parasitology*, 35(10), pp. 760–777. Available at: <https://doi.org/10.1016/j.pt.2019.07.008>.
- Sirajuddin, M., Rice, L.M. and Vale, R.D. (2014) 'Regulation of microtubule motors by tubulin isotypes and post-translational modifications', *Nature Cell Biology*, 16(4), pp. 335–344. Available at: <https://doi.org/10.1038/ncb2920>.
- Smith, T. *et al.* (2017) 'Metabolic reprogramming during the *Trypanosoma brucei* life cycle', *F1000Research*, 6(683). Available at: <https://doi.org/10.12688/f1000research.10342.2>.
- Song, Y. and Brady, S.T. (2015) 'Post-translational modifications of tubulin: pathways to functional diversity of microtubules', *Trends in Cell Biology*, 25(3), pp. 125–136. Available at: <https://doi.org/10.1016/j.tcb.2014.10.004>.
- Stephens, N.A. and Hajduk, S.L. (2011) 'Endosomal Localization of the Serum Resistance-Associated Protein in African Trypanosomes Confers Human Infectivity', *Eukaryotic Cell*, 10(8), pp. 1023–1033. Available at: <https://doi.org/10.1128/EC.05112-11>.
- Student (1908) 'The Probable Error of a Mean', *Biometrika*, 6(1), pp. 1–25. Available at: <https://doi.org/10.2307/2331554>.
- Tetley, L. and Vickerman, K. (1985) 'Differentiation in *Trypanosoma brucei*: host-parasite cell junctions and their persistence during acquisition of the variable antigen coat', *Journal of Cell Science*, 74(1), pp. 1–19.
- Thein, M. (2022) 'The effects of polyglutamylase deficiency on microtubule-associated proteins in *Trypanosoma brucei*'. Master Thesis, Molecular Parasitology, University of Bayreuth.
- Thomashow, L.S. *et al.* (1983) 'Tubulin genes are tandemly linked and clustered in the genome of *trypanosoma brucei*', *Cell*, 32(1), pp. 35–43. Available at: [https://doi.org/10.1016/0092-8674\(83\)90494-4](https://doi.org/10.1016/0092-8674(83)90494-4).
- Tyler, K.M., Matthews, K.R. and Gull, K. (1997) 'The bloodstream differentiation–division of *Trypanosoma brucei* studied using mitochondrial markers', *Proceedings of the Royal Society of London. Series B: Biological Sciences*, 264(1387), pp. 1481–1490. Available at: <https://doi.org/10.1098/rspb.1997.0205>.
- Urwyler, S. *et al.* (2007) 'A family of stage-specific alanine-rich proteins on the surface of epimastigote forms of *Trypanosoma brucei*', *Molecular Microbiology*, 63(1), pp. 218–228. Available at: <https://doi.org/10.1111/j.1365-2958.2006.05492.x>.
- Uzureau, P. *et al.* (2013) 'Mechanism of *Trypanosoma brucei* gambiense resistance to human serum', *Nature*, 501(7467), pp. 430–434. Available at: <https://doi.org/10.1038/nature12516>.

- Vanhamme, L. *et al.* (2003) 'Apolipoprotein L-I is the trypanosome lytic factor of human serum', *Nature*, 422(6927), pp. 83–87.
- Vanhollebeke, B. *et al.* (2008) 'A Haptoglobin-Hemoglobin Receptor Conveys Innate Immunity to *Trypanosoma brucei* in Humans', *Science, New Series*, 320(5876), pp. 677–681.
- Vanhollebeke and Pays, E. (2010) 'The trypanolytic factor of human serum: many ways to enter the parasite, a single way to kill', *Molecular Microbiology*, 76(4), pp. 806–814.
- Vassella, E. *et al.* (1997) 'Differentiation of African trypanosomes is controlled by a density sensing mechanism which signals cell cycle arrest via the cAMP pathway', *Journal of Cell Science*, 110(21), pp. 2661–2671.
- Vaughan, S. *et al.* (2008) 'A Repetitive Protein Essential for the Flagellum Attachment Zone Filament Structure and Function in *Trypanosoma brucei*', *Protist*, 159(1), pp. 127–136. Available at: <https://doi.org/10.1016/j.protis.2007.08.005>.
- Vedrenne, C. *et al.* (2002) 'Two Related Subpellicular Cytoskeleton-associated Proteins in *Trypanosoma brucei* Stabilize Microtubules', *Molecular Biology of the Cell*, 13(3), pp. 1058–1070. Available at: <https://doi.org/10.1091/mbc.01-06-0298>.
- Venturelli, A. *et al.* (2022) 'Current Treatments to Control African Trypanosomiasis and One Health Perspective', *Microorganisms*, 10(7), p. 1298.
- Vicente, J.J. and Wordeman, L. (2019) 'The quantification and regulation of microtubule dynamics in the mitotic spindle', *Cell Dynamics*, 60, pp. 36–43. Available at: <https://doi.org/10.1016/j.ceb.2019.03.017>.
- Vickerman, K. (1985) 'Developmental cycles and biology of pathogenic Trypanosomes', *British Medical Bulletin*, 41(2), pp. 105–114. Available at: <https://doi.org/10.1093/oxfordjournals.bmb.a072036>.
- Vogel, P. *et al.* (2010) 'Tubulin Tyrosine Ligase–Like 1 Deficiency Results in Chronic Rhinosinusitis and Abnormal Development of Spermatid Flagella in Mice', *Veterinary Pathology*, 47(4), pp. 703–712. Available at: <https://doi.org/10.1177/0300985810363485>.
- Wall, K.P. *et al.* (2020) 'C-Terminal Tail Polyglycylation and Polyglutamylation Alter Microtubule Mechanical Properties', *Biophysical Journal*, 119(11), pp. 2219–2230. Available at: <https://doi.org/10.1016/j.bpj.2020.09.040>.
- Westermann, S. and Weber, K. (2003) 'Post-translational modifications regulate microtubule function', *Nature Reviews Molecular Cell Biology*, 4(12), pp. 938–948. Available at: <https://doi.org/10.1038/nrm1260>.
- Wheeler, R.J., Gull, K. and Sunter, J.D. (2019) 'Coordination of the Cell Cycle in Trypanosomes', *Annual Review of Microbiology*, 73(1), pp. 133–154. Available at: <https://doi.org/10.1146/annurev-micro-020518-115617>.

Woodward, R. and Gull, K. (1990) 'Timing of nuclear and kinetoplast DNA replication and early morphological events in the cell cycle of *Trypanosoma brucei*', *Journal of Cell Science*, 95(1), pp. 49–57.

Wu, H.-Y., Wei, P. and Morgan, J.I. (2017) 'Role of Cytosolic Carboxypeptidase 5 in Neuronal Survival and Spermatogenesis', *Scientific Reports*, 7(1), p. 41428. Available at: <https://doi.org/10.1038/srep41428>.

Zanic, M. *et al.* (2009) 'EB1 Recognizes the Nucleotide State of Tubulin in the Microtubule Lattice', *PLoS ONE*. Edited by R.C. May, 4(10), p. e7585. Available at: <https://doi.org/10.1371/journal.pone.0007585>.

Zanic, M. *et al.* (2013) 'Synergy between XMAP215 and EB1 increases microtubule growth rates to physiological levels', *Nature Cell Biology*, 15(6), pp. 688–693. Available at: <https://doi.org/10.1038/ncb2744>.

List of all own publications

1) Al Nasr, I., Jentzsch, J., Winter, I., Schobert, R., Ersfeld, K., Koko, W., Mujawah, A., Khan, T., Biersack, B. Antiparasitic activities of new lawsone Mannich bases. Arch Pharm Chem Life Sci., 352, doi:10.1002/ardp.201900128 (2019).

2) Jentzsch, J., Koko, W., Al Nasr, I., Khan, T., Schobert, R., Ersfeld, K., Biersack, B. New antiparasitic bis-naphthoquinone derivatives. Chem. Biodiversity, 17, doi:10.1002/cbdv.201900597 (2020).

3) Koko, W., Jentzsch, J., Kalie, H., Schobert, R., Ersfeld, K., Al Nasr, I., Khan, T., Biersack, B. Evaluation of the antiparasitic activities of imidazol-2-ylidene-gold(I) complexes. Arch Pharm Chem Life Sci, doi:10.1002/ardp.201900363 (2020).

4) Al Nasr, I., Jentzsch, J., Shaikh, A., Shuveksh, P., Koko, W., Khan, T., Ahmed, K., Schobert, R., Ersfeld, K., Biersack, B.
New Pyrano-4H-benz[g]chromene-5,10-diones with Antiparasitic and Antioxidant Activities. Chem. Biodiversity 17, doi:10.1002/cbdv.202000839 (2020).

5) Jentzsch, J., Sabri, A., Speckner, K., Lallinger-Kube, G., Weiss, M., Ersfeld, K.
Microtubule polyglutamylation is important for regulating cytoskeletal architecture in *Trypanosoma brucei*. Journal of Cell Science 133, doi:10.1242/jcs.248047 (2020).
This article has an associated first-person interview with the first author of the paper.

Nur Publikation 5) "Microtubule polyglutamylation is important for regulating cytoskeletal architecture in *Trypanosoma brucei*" steht in Verbindung mit der vorliegenden Dissertation.

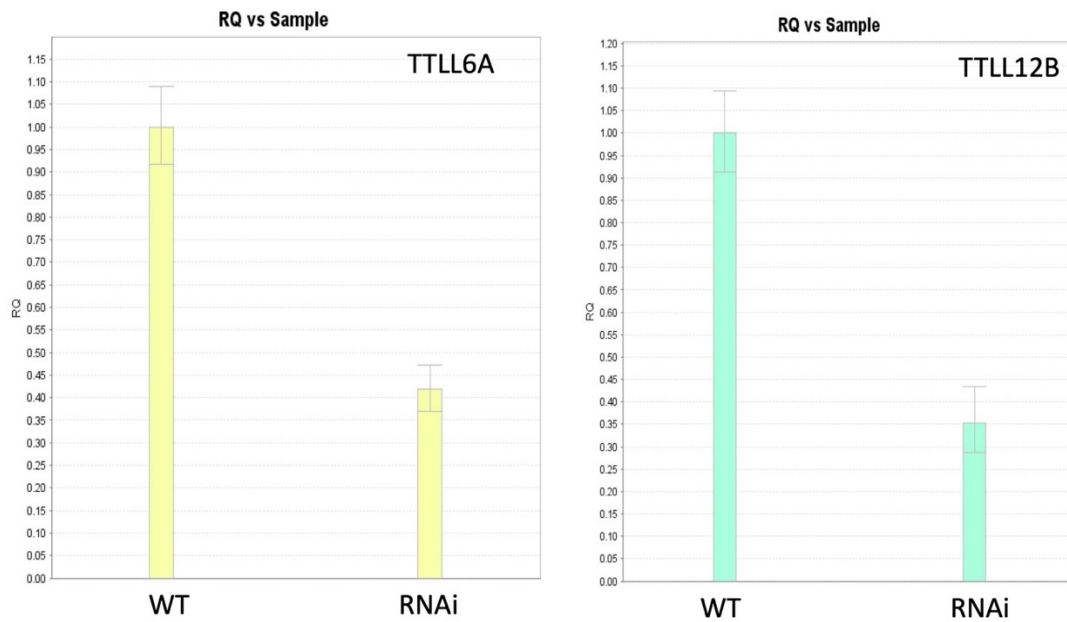
Supplementary figures

Figure 38: qPCR analysis of TTLL-RNAi depleted cells. The tested mRNA levels were calculated using the $\Delta\Delta CT$ -method. PFR was used as the endogenous control. Error bars represent the standard error.

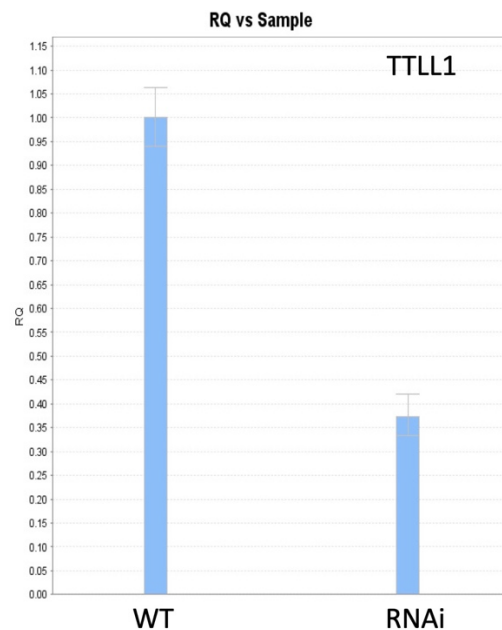


Figure 39: qPCR analysis of TTLL1-RNAi cells. The tested mRNA levels were calculated using the $\Delta\Delta CT$ -method. PFR was used as the endogenous control. Error bars represent the standard error.

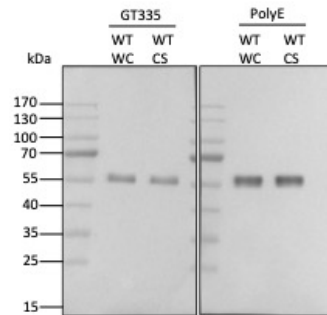


Figure 40: Western blot of WT cell extracts. Whole cells (WC) and cytoskeletal preparations (CS) were probed with GT335 and PolyE.

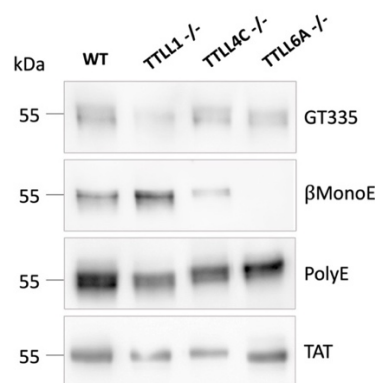


Figure 41: Western blot analysis of WT, *ttll1*^{-/-} and *ttll6a*^{-/-} cells. Cytoskeletal preparations were stained with GT335, β -monoE and PolyE. TAT (tubulin) served as a loading control. Figure taken from Julia Bechthold (Master thesis of Julia Bechthold, Molecular Parasitology, University of Bayreuth 2022)

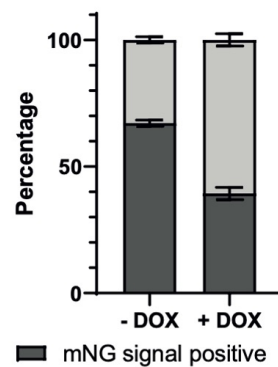


Figure 42: Proportion of *TLL6A*^{RNAi} cells showing a mNG-XMAP215 signal. Cytoskeletal preparations of RNAi cells that were not-induced (-DOX) and cells that were depleted of *TLL6A* (+DOX) were analysed in immunofluorescence. Figure was taken from Marinus Thein (Master thesis of Marinus Thein, Molecular Parasitology, University of Bayreuth, 2022).

>Tb927.5.3860_TTLL1

MFPNTSLRPGGAANIGLRKTELYGGARGAKPLSSASSVYGMMSGNSNLPHAIGGSGRITNVGSGSP
 ISQVLPVGGNSQLSSLRDGDVAKSNPVRYRTPQMVMIVAELSGARQDGPMLRYRTDLDKHVIHFARFR
 PRSVEIVEDEEITAGDWHFFWMSVGRVRSLSFSSEYRLSDS**Q**IINHFPNHYELTRKDLMYKNIKKYIKDPN
 NVQLRMPYSLPEQLANGGDNVTYLRFADCVPITYNIPNDLAMFEEEFRRQPGSTWIVKPTSRSQGRGIFLI
 NRLSQLKKWLKERKELDEFEGVMMMNSFVVSKEYIRDPLLIGGKKFDLRLYVLVTSFKPLVAYLHDQGFARF
 CATRYVANALSDEDLCSHLTNVALQKGEKEYNASHGGKWTLANLLLFIQGRFGAAAADWLMHGIEFVIY
 HSLRALESVMFNDRHCFELYGYDILVDSQLRPHLIEVNSSPSLSTTTVSDRLLKEEVLQDVLQVVFPPDFPS
 NNAMPYWEYRLRADLTTALPTGFRLQVGE

>Tb927.3.5380_TTLL6A

MITDVTSTKRPVESRKCIVVMCADTRYHVVRTAAVSLGWHVEDGERDDVPSSFHGISLNKDMNSLSETIS
 LLGAKCNAALNPQIIWLDKSVLSSRVAALSCFHRVNHFPGMHVIARKATLFKRLMRIRRHDLSPTLRSL
 DAFPWSFSPSTELLQLERFISDGREGEIFILKPNKGCEG**K**GIITAEPHVVVERMTDEERNECLVQQYVPHPL
 CIDRKKFDLRIYVLVTSVVVGKPPRKGFRGAAPPKETHGGSSFPLNGLQLFVHKEGLVRICTEDYATPNASN
 CKRQGMHLTNYAVNKRAQGFSGVDLNTDDSSNGICEGNKRDFKLEHYINGLVGCKSDTTEDDVS
 GETTSRWERVLHRIDRCILLTVLSGLENLRREFIGTGASRGRSDGRNCFELGVDILLTEDLKPVLMEVNHS
 PSFCDSDFDRTKHRVLMDFRLLPEYVPSLENCNDAAYATLQESITAGGNMSSTGFRQISPLRVGGDD
 WADEEMQMFEEMLRHANGLR

>Tb927.11.2420_TTLL12B

MMKDFEAFSRVLADWFVVSVPQHLQRSLFEKLVNDVFDAGTSFSLAVVAREDEDEVEDAEDQSSETAG
 NYVLVASKNLKANDDIWLIDHCCTFRLRDFRAHLEANEALRTRLGRVLAVNLSGADNRHGAQLIFDHMW
 NKVGSYRLPTSADGDDSQYESYWFHDEVGSAITTVNEKANM**K**LEPIPICFPEKGGVFSAMWCVEDM
 EEEVATRAASTLEATSGKEILSLIYNTRHEEETEEDPYRSAQLLCVEAWRRLVKRLESVPGRRAREQSA
 LAPVERCPSGPLRVFTDSQQLSQNLTDANHFVVVDLPQEAHIVWVHHSIEGLNDYGHAQYISQFPEESE
 FTSKQGLLRLIQETYGYVDWYQTSYDSTTQLKELIGDFIVRKAALDKKIDTDPLVTYEDIGKLRSDGTNLW
 ISKPTNLARSIDMTLSSNLTELLRAVETGPKVICKYIANTATLRKRKFDLRFIVAVNSFTSEHSSSMEAYVYNT
 FWTRFALKEYSLDDFDCYEKHWVMNYTNPEALLQLHDHDFVKEFNEEYASSGYGEAAWEKIAYPKI
 LKMLREAFGMVVTRGGDHSRCRAMYGVDVMLRTERCVETGALTLEPSLLEITFSPDCRRACKYHPTFFN
 DIFHTLFLRDPTNMTPL

Figure 43: Amino-acid sequences of TTLL1, TTLL6A and TTLL12B. Bold letters show residues at the position 180. Q180 could be a critical active site to classify TTLL1 as an elongase. Sequences were taken from TriTrypDB. (Mahalingan et al., 2020)

Publication and Licensing Rights for created Figures



49 Spadina Ave. Suite 200
Toronto ON M5V 2J1 Canada
www.biorender.com

Confirmation of Publication and Licensing Rights

October 26th, 2022
Science Suite Inc.

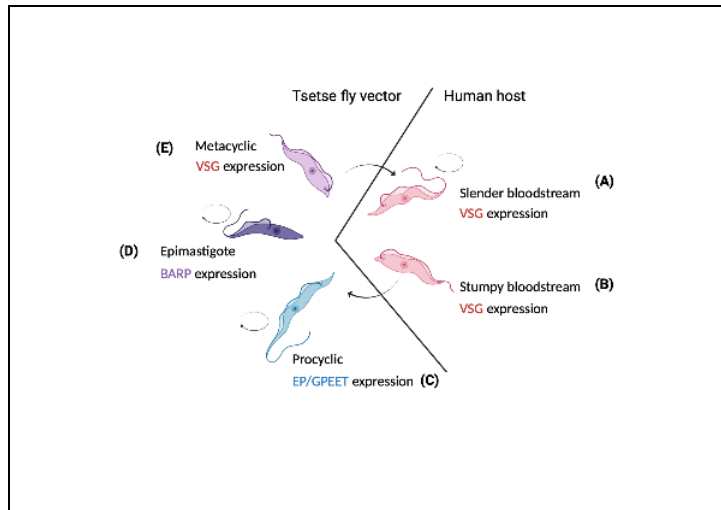
Subscription: Individual
Agreement number: DD24KK3RGU
Journal name: Disseration

To whom this may concern,

This document is to confirm that Jana Jentzsch has been granted a license to use the BioRender content, including icons, templates and other original artwork, appearing in the attached completed graphic pursuant to BioRender's [Academic License Terms](#). This license permits BioRender content to be sublicensed for use in journal publications.

All rights and ownership of BioRender content are reserved by BioRender. All completed graphics must be accompanied by the following citation: "Created with BioRender.com".

BioRender content included in the completed graphic is not licensed for any commercial uses beyond publication in a journal. For any commercial use of this figure, users may, if allowed, recreate it in BioRender under an Industry BioRender Plan.



For any questions regarding this document, or other questions about publishing with BioRender refer to our [BioRender Publication Guide](#), or contact BioRender Support at support@biorender.com.



49 Spadina Ave. Suite 200
Toronto ON M5V 2J1 Canada
www.biorender.com

Confirmation of Publication and Licensing Rights

October 23rd, 2022
Science Suite Inc.

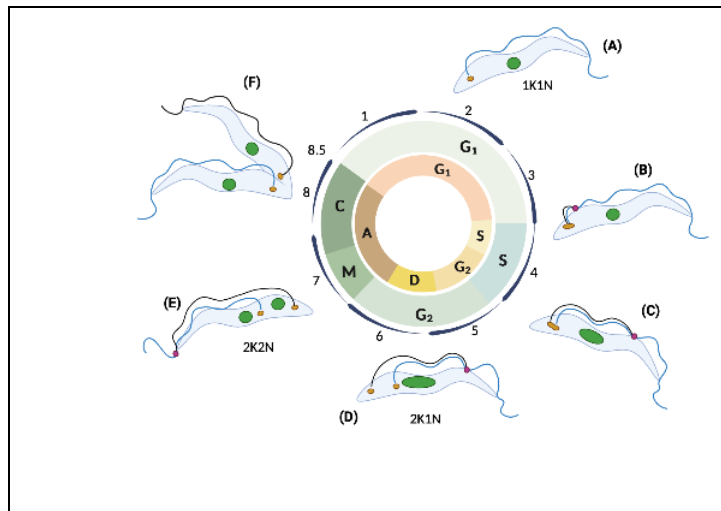
Subscription: Individual
Agreement number: TH24K5P2ZK
Journal name: Dissertation

To whom this may concern,

This document is to confirm that Jana Jentzsch has been granted a license to use the BioRender content, including icons, templates and other original artwork, appearing in the attached completed graphic pursuant to BioRender's [Academic License Terms](#). This license permits BioRender content to be sublicensed for use in journal publications.

All rights and ownership of BioRender content are reserved by BioRender. All completed graphics must be accompanied by the following citation: "Created with BioRender.com".

BioRender content included in the completed graphic is not licensed for any commercial uses beyond publication in a journal. For any commercial use of this figure, users may, if allowed, recreate it in BioRender under an Industry BioRender Plan.



For any questions regarding this document, or other questions about publishing with BioRender refer to our [BioRender Publication Guide](#), or contact BioRender Support at support@biorender.com.



49 Spadina Ave. Suite 200
Toronto ON M5V 2J1 Canada
www.biorender.com

Confirmation of Publication and Licensing Rights

October 23rd, 2022
Science Suite Inc.

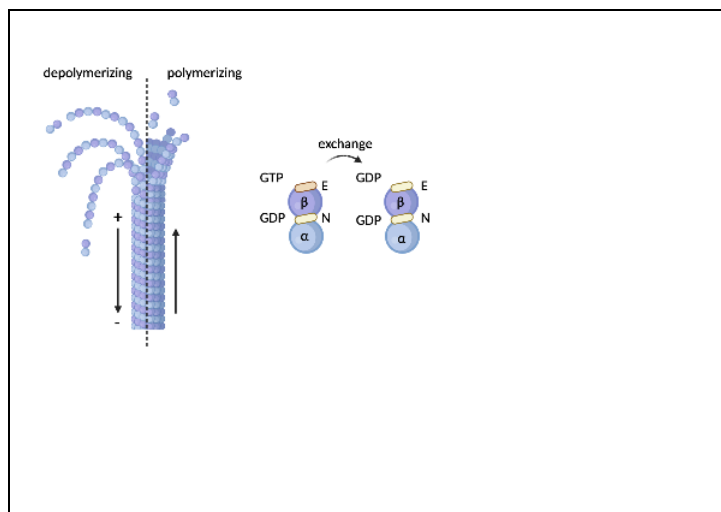
Subscription: Individual
Agreement number: EK24K5PMTTC
Journal name: Dissertation

To whom this may concern,

This document is to confirm that Jana Jentzsch has been granted a license to use the BioRender content, including icons, templates and other original artwork, appearing in the attached completed graphic pursuant to BioRender's [Academic License Terms](#). This license permits BioRender content to be sublicensed for use in journal publications.

All rights and ownership of BioRender content are reserved by BioRender. All completed graphics must be accompanied by the following citation: "Created with BioRender.com".

BioRender content included in the completed graphic is not licensed for any commercial uses beyond publication in a journal. For any commercial use of this figure, users may, if allowed, recreate it in BioRender under an Industry BioRender Plan.



For any questions regarding this document, or other questions about publishing with BioRender refer to our [BioRender Publication Guide](#), or contact BioRender Support at support@biorender.com.



49 Spadina Ave. Suite 200
Toronto ON M5V 2J1 Canada
www.biorender.com

Confirmation of Publication and Licensing Rights

October 23rd, 2022
Science Suite Inc.

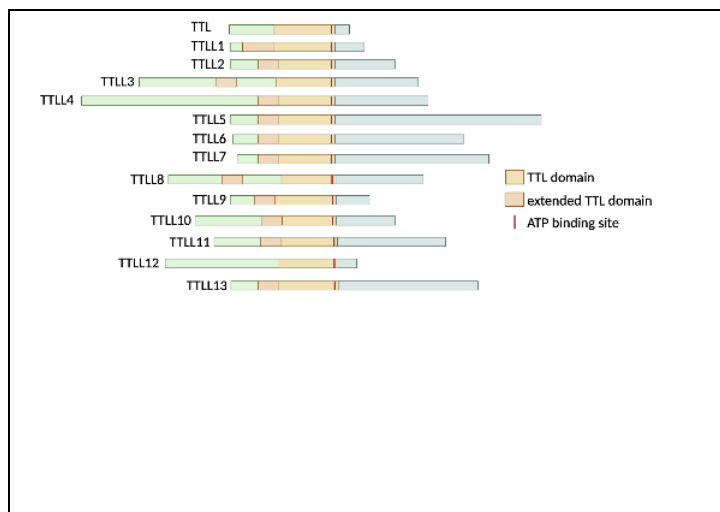
Subscription: Individual
Agreement number: VR24K5PUJV
Journal name: Dissertation

To whom this may concern,

This document is to confirm that Jana Jentzsch has been granted a license to use the BioRender content, including icons, templates and other original artwork, appearing in the attached completed graphic pursuant to BioRender's [Academic License Terms](#). This license permits BioRender content to be sublicensed for use in journal publications.

All rights and ownership of BioRender content are reserved by BioRender. All completed graphics must be accompanied by the following citation: "Created with BioRender.com".

BioRender content included in the completed graphic is not licensed for any commercial uses beyond publication in a journal. For any commercial use of this figure, users may, if allowed, recreate it in BioRender under an Industry BioRender Plan.



For any questions regarding this document, or other questions about publishing with BioRender refer to our [BioRender Publication Guide](#), or contact BioRender Support at support@biorender.com.



49 Spadina Ave. Suite 200
Toronto ON M5V 2J1 Canada
www.biorender.com

Confirmation of Publication and Licensing Rights

October 23rd, 2022
Science Suite Inc.

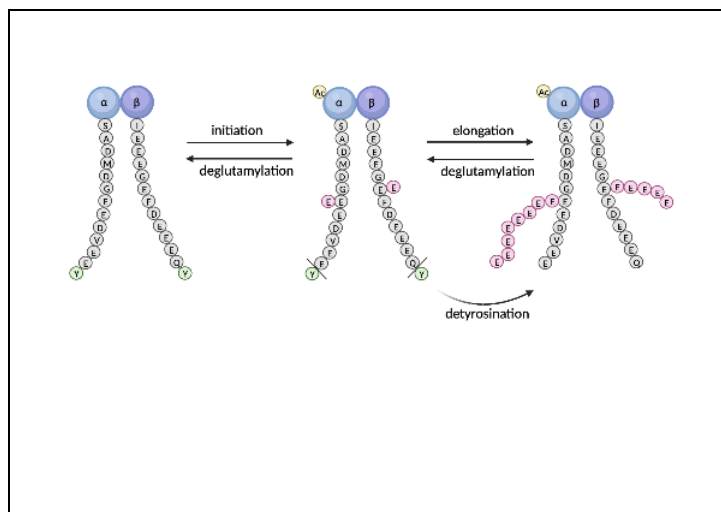
Subscription: Individual
Agreement number: HV24K5PZ4F
Journal name: Dissertation

To whom this may concern,

This document is to confirm that Jana Jentzsch has been granted a license to use the BioRender content, including icons, templates and other original artwork, appearing in the attached completed graphic pursuant to BioRender's [Academic License Terms](#). This license permits BioRender content to be sublicensed for use in journal publications.

All rights and ownership of BioRender content are reserved by BioRender. All completed graphics must be accompanied by the following citation: "Created with BioRender.com".

BioRender content included in the completed graphic is not licensed for any commercial uses beyond publication in a journal. For any commercial use of this figure, users may, if allowed, recreate it in BioRender under an Industry BioRender Plan.



For any questions regarding this document, or other questions about publishing with BioRender refer to our [BioRender Publication Guide](#), or contact BioRender Support at support@biorender.com.



49 Spadina Ave. Suite 200
Toronto ON M5V 2J1 Canada
www.biorender.com

Confirmation of Publication and Licensing Rights

October 23rd, 2022
Science Suite Inc.

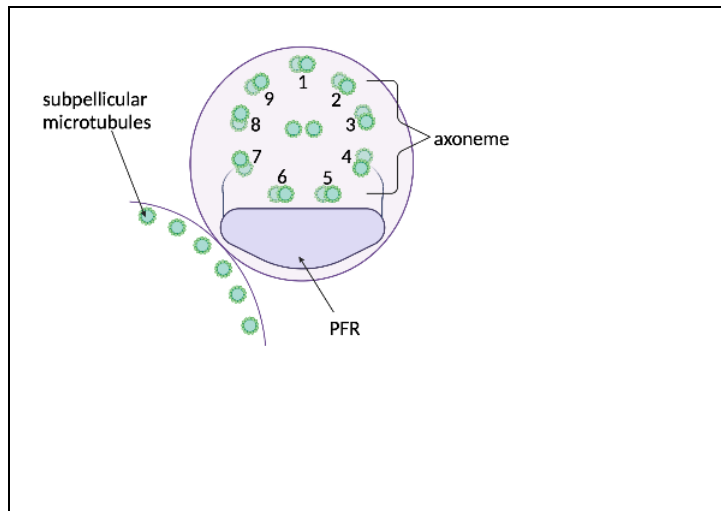
Subscription: Individual
Agreement number: AM24K5Q2K4
Journal name: Dissertation

To whom this may concern,

This document is to confirm that Jana Jentzsch has been granted a license to use the BioRender content, including icons, templates and other original artwork, appearing in the attached completed graphic pursuant to BioRender's [Academic License Terms](#). This license permits BioRender content to be sublicensed for use in journal publications.

All rights and ownership of BioRender content are reserved by BioRender. All completed graphics must be accompanied by the following citation: "Created with BioRender.com".

BioRender content included in the completed graphic is not licensed for any commercial uses beyond publication in a journal. For any commercial use of this figure, users may, if allowed, recreate it in BioRender under an Industry BioRender Plan.



For any questions regarding this document, or other questions about publishing with BioRender refer to our [BioRender Publication Guide](#), or contact BioRender Support at support@biorender.com.

Acknowledgments

Diese Seite möchte ich nutzen, um mich bei unserem großartigen Team zu bedanken! Dabei gilt mein größter Dank meinem Doktorvater Prof. Dr. Klaus Ersfeld. Es hat mir viel Spaß gemacht an dem Thema zu arbeiten. Ich habe so vieles im Labor gelernt, das kann man gar nicht in ein paar Sätzen zusammenfassen. Vielen Dank für die tolle Zeit!

Auch Prof. Dr. Matthias Weiß und seinem Team möchte ich für die Zusammenarbeit danken. Durch euren Input während unserer Meetings kamen immer wieder neue Fragestellungen zustande. Die vielen Vorschläge und Verbesserungen waren sehr hilfreich. Vielen lieben Dank auch für die Geduld, wenn die Biologen mal wieder einen Crash Kurs in Physik gebraucht haben. Auch Prof. Dr. Olaf Stemmann und meinen zwei Mentoren Prof. Dr. Stefan Heidmann und Prof. Dr. Benedikt Westermann möchte ich für die hilfreichen Anregungen während unserer Labmeetings bzw. das Feedback geben und Korrekturlesen unseres bereits veröffentlichten Papers danken.

Ein ganz großer Dank gilt auch Karin Angermann. Die Zusammenarbeit mit dir hat so viel Spaß gemacht. Wir konnten nicht nur über Probleme im Laboralltag grübeln, sondern auch über privates immer mal wieder quatschen. Du standest immer mit Rat und Tat zur Seite! Vielen Dank für diese großartige Zeit!

Ich möchte mich auch bei meinen Studenten bedanken. Mich hat es so sehr gefreut euch durch die einzelnen Projekte zu begleiten und zu sehen, wie ihr euch alle weiterentwickelt habt! Ganz besonders möchte ich dem harten Kern danken: Nina, Julia, Thomas, David, Sven, Lucas und Marinus! Mit dem ein oder anderen Bierchen haben wir einige brainstorm sessions verbracht. Das Feiern von kleinen und natürlich auch den großen Erfolgen war dabei ganz besonders wichtig, auch außerhalb des Labors. Wir sind zu einem großartigen Team zusammengewachsen! Dafür werde ich immer dankbar sein.

Sven möchte ich danken für seine wahnsinnige Geduld! Du konntest mir so viele Ratschläge geben und hast auch immer wieder neuen Input zu meinem Projekt gegeben. Deine Unterstützung hat so vieles leichter gemacht!

(Eidesstattliche) Versicherungen und Erklärungen

(§ 9 Satz Nr. 3 PromO BayNAT)

Hiermit versichere ich eidesstattlich, dass ich die Arbeit selbstständig verfasst und keine anderen als die von mir angegebenen Quellen und Hilfsmittel benutzt habe (vgl. Art. 64 Abs. 1 Satz 6 BayHSchG).

(§ 9 Satz 2 Nr. 3 PromO BayNAT)

Hiermit erkläre ich, dass ich die Dissertation nicht bereits zur Erlangung eines akademischen Grades eingereicht habe und dass ich nicht bereits diese oder eine gleichartige Doktorprüfung endgültig nicht bestanden habe.

(§ 9 Satz 2 Nr. 4 PromO BayNAT)

Hiermit erkläre ich, dass ich Hilfe von gewerblichen Promotionsberatern bzw. -vermittlern oder ähnlichen Dienstleitern weder bisher in Anspruch genommen habe noch künftig in Anspruch nehmen werde.

(§ 9 Satz 2 Nr. 7 PromO BayNAT)

Hiermit erkläre ich mein Einverständnis, dass die elektronische Fassung meiner Dissertation unter Wahrung meiner Urheberrechte und des Datenschutzes einer gesonderten Überprüfung unterzogen werden kann.

(§ 9 Satz 2 Nr. 8 PromO BayNAT)

Hiermit erkläre ich mein Einverständnis, dass bei Verdacht wissenschaftlichen Fehlverhaltens Ermittlungen durch universitätsinterne Organe der wissenschaftlichen Selbstkontrolle stattfinden können.

.....

Ort, Datum, Unterschrift